TECHNISCHE UNIVERSITÄT MÜNCHEN

Department Chemie

Lehrstuhl für Biotechnologie

Structural and functional characterization of small Heat shock proteins of the nematode *Caenorhabditis elegans*

Maike Krause

Vollständiger Abdruck der vom Department Chemie der Technischen Universität München zur Erlangung des akademischen Grades eines Dr. rer. nat. genehmigten Dissertation.

Vorsitzender:		Univ.-Prof. Dr. Aymelt Itzen
Prüfer der Dissertation:	1.	Univ.-Prof. Dr. Johannes Buchner
	2.	Univ.-Prof. Dr. Bernd Reif

Die Dissertation wurde am 03.09.2013 bei der Technischen Universität München eingereicht und durch das Department Chemie am 14.10.2013 angenommen.

ABSTRACT

Higher eukaryotes have several small Heat shock proteins (sHsps), which form a complex protein network. For instance, *Caenorhabditis elegans* has 16 different sHsps, which are only partially characterized concerning their function, localization, and regulation.

The aim of this thesis was to characterize the Hsp12-family of *C. elegans in vivo* and *in vitro*. Furthermore, Hsp25 and ZK1128.7 – which was not described closer until now – were analyzed *in vivo*. Multiple approaches were used for the investigations, i.e. CD spectropolarimetry, absorption spectrosopy, analytical ultracentrifugation, and quantitative Reverse Transcriptase-PCR (qRT-PCR).

In the *in vitro* studies, the Hsp12-family was examined with respect to the typical features of sHsps. All members showed a characteristic β-sheet rich secondary structure and a high thermal stability. The oligomeric states were tetramers and monomers, which is unusual for sHsps. In fact, only one member of the family, Hsp12.1, revealed chaperone activity.

In vivo, the expression patterns of the Hsp12 proteins regarding age, RNAi, knock-out, and stress were analyzed. Three of the four Hsp12 proteins showed a high expression during the L1 larval stage. In the adult stage, a further upregulation of Hsp12.3 and Hsp12.6 was observed. Under stress conditions, only Hsp12.6 showed a slight increase of expression, while all other members of the Hsp12-family were not inducable. These findings suggest development specific expression of all Hsp12-family members. In addition, the male frequency of the knock-out strain of Hsp12.6 (VC281) increased remarkably when a higher growth temperature was employed. This phenotype indicates that Hsp12.6's function is either important for the integrity of the nematodes' X-chromosomes or the development of the sex specific tissues.

Expression of Hsp25 peaked during the third larval stage and was afterwards reduced to a constant level. This expression pattern corresponds to the development and maintenance of muscles in *C. elegans*. Hence, this supports the suggestion that Hsp25 is expressed development and tissue specifically. ZK1128.7's expression was at its maximum during the adult stage of the nematode. Similar to the Hsp12-family, ZK1128.7 was not inducible by stress, which classifies this protein to be development specific, too.

ZUSAMMENFASSUNG

Höhere Eukaryoten haben mehrere kleine Hitzeschock Proteine (sHsps), welche ein komplexes Proteinnetzwerk bilden. *Caenorhabditis elegans* hat zum Beispiel 16 unterschiedliche sHsp, die bisher nur partiell in ihrer Funktion, Lokalisation und Regulation charakterisiert sind.

Die *in vitro* und *in vivo* Charakterisierung der Hsp12-Familie von *C. elegans* war Ziel dieser Dissertation. Weiterhin wurden Hsp25 und ZK1128.7 – ein bisher nicht beschriebenes sHsp – *in vivo* untersucht. Für die Untersuchungen wurden vielfältige Verfahren, wie etwa CD-Spektropolarimetrie, Absorptionsspektroskopie, analytische Ultrazentrifugation und quantitative Reverse Transkriptase-PCR (qRT-PCR) angewandt.

In den *in vitro* Studien wurde die Hsp12-Familie im Hinblick auf die typischen Eigenschaften der sHsps untersucht. Alle Mitglieder zeigten charakteristische β-Faltblatt reiche Sekundärstrukturen und hohe thermische Stabilitäten. Die Oligomerisierungszustände waren Tetramere und Monomere, was untypisch für sHsps ist. Tatsächlich zeigte nur ein Mitglied der Hsp12-Familie, Hsp12.1, Chaperonaktivität.

In vivo wurden die Expressionsmuster der Hsp12-Familie bezüglich Alter, RNAi, Knockout und Stress untersucht. Drei der vier Hsp12 Proteine zeigten eine hohe Expression im ersten Larvenstadium. Im adulten Stadium konnte eine weitere Hochregulation für Hsp12.3 und Hsp12.6 festgestellt werden. Unter Stressbedingungen zeigte nur Hsp12.6 eine leichte Erhöhung der Expression, während alle anderen Mitglieder der Hsp12-Familie nicht induziert wurden. Diese Ergebnisse lassen auf eine entwicklungsspezifische Expression der Hsp-Familie schließen. Zusätzlich konnte eine Zunahme der Männchenrate im Hsp12.6-Knockoutstamm (VC281) bei erhöhter Wachstumstemperatur festgestellt werden. Dieser Phänotyp impliziert, dass die Funktion von Hsp12.6 entweder für die Integrität der X-Chromosome des Nematoden oder für die Entwicklung geschlechtsspezifischer Merkmale wichtig ist.

Die Expression von Hsp25 zeigte ein Maximum im dritten Larvenstadium und fällt anschließend auf ein konstantes Level zurück. Dieses Expressionsmuster entspricht der Entwicklung und Aufrechterhaltung von Muskeln in *C. elegans*. Dies unterstreicht somit die Vermutung, dass Hsp25 enwicklungs- und gewebsspezifisch exprimiert wird. ZK1128.7 zeigte die höchste Expression im adulten Stadium des Nematoden. Wie die Hsp12-Familie ist auch ZK1128.7 nicht durch Stress induziert, wodurch dieses Protein ebenfalls als entwicklungsspezifisch klassifiziert wird.

CONTENTS

1 INTRODUCTION

In the last decades the improving conditions of life in respect to hygienics, nourishment and health care allowed people, especially in the Western World, to extend their lifespans. In Germany the life expectancy for every second man and every second women is larger than 80 and 85 years, respectively, corresponding to a doubling of the average life span in the last 130 years [1]. Latest statistics suggest a 60 % increase of people who will reach an age of more than 80 years until 2030 in Germany [2].

This is why age-related diseases like adult-onset diabetes (Type II) and senile dementia occur more frequently. Especially neurodegenerative diseases are often linked to protein misfolding, which appear more often in aged individuals. Additionally many other factors, as behavioral and environmental parameters, have a strong influence on age-related ailments. To improve the living conditions of all elderly and aging people it is necessary to analyze and investigate all contributing factors for disease patterns at old age [3]. In connection to neurodegenerative diseases, progress in the mentioned research field is of special interest.

Many of the neurodegenerative diseases are associated to the function/dysfunction of small Heat shock proteins (sHsp) [216, 163]. Analyzes of the general function and characterization of sHsp networks in organism is needed to acquire a better understanding of these correlations.

1.1 PROTEINS AND FOLDING THEORY

Proteins are the essential building blocks of every living organism and are synthesized at the ribosome as a linear polypeptide chain with an alternating order of the 20 proteinogenic amino acids. In general, proteins can be divided into two main classes - the natively unfolded and folded proteins. Folded proteins adopt their 3D-structure after their synthesis, the class of natively unfolded proteins transform into the folded state after binding of a ligand [70].

1 http://www.bbsr.bund.de/cln_032/nn_1051708/BBSR/DE/Raumbeobachtung/UeberRaumbeobachtung/Komponenten/Raumordnungsprognose/Downloads/DL__uebersicht.html#doc1178082bodyText1 (visited 15th July 2013)

2 http://www.ftd.de/wissen/leben/studie-durchschnittsalter-der-deutschen-steigt-abermals/60106560.html (visited 15th July 2013)

3 http://www.mpg.de/1020169/W000_Zur-Sache_014_019.pdf (visited 15th July 2013)

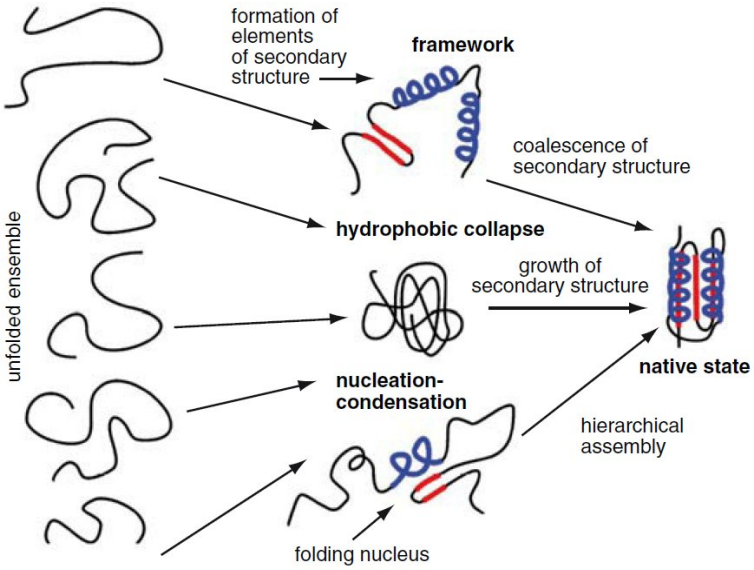

Figure 1.1: Mechanisms of protein folding showing the key differences in the hierarchical assembly of the native state following the three principal folding models: framework model, hydrophobic collapse model, and nucleation-condensation model. The entropy decreases from left to right as the structural complexity increases. The different models emphasize different dependencies on the relative timing of formation of secondary structure and tertiary interactions. Figure and caption taken from [164].

Most proteins are able to reach their native form, which represents a thermodynamical stable state and consequentially a minimum in the multidimensional energy landscape, from an unfolded state on their own. The native form of a protein is characterized by defined secondary structure elements (e.g. α-helices and β-strands), their relative orientation called tertiary structure, and the possibly quaternary structure, if more than one polypeptide chain is present. Anfinsen postulated that the native structure of a protein is exclusively determined by its amino acid sequence and solvent conditions [7]. However, folding of proteins cannot be achieved by testing every amino acid in every possible orientation; statistical reasons would require such a mechanism to proceed in timescales way beyond the lifespan of any organism (*Levinthal paradoxon*). On the contrary, the folding has to be accelerated at some point. According to this consideration, different hypotheses were proposed to explain spontaneous folding. Figure 1.1 gives an overview of the folding models described below.

According to the 'nuclear-growth model', established in 1973 by Wetlaufer et al., proteins form a secondary structure core on rather slow timescales which then leads to rapid growth of the missing structural elements of the protein [242]. The model describes protein folding as an all-or-none process and proteins that populate intermediate states during folding are not described by it [164].

For proteins with intermediate folding states the models of Kim/Baldwin and Karplus/Weaver are more convenient.

The 'framework model' of Kim and Baldwin is a modified variant of the 'nuclear-growth' model [124]. Karplus and Weaver proposed the 'diffusion-collision model' in 1979, which is an extension of the 'framework model' of Kim and Baldwin. According to the 'framework model', the folding strategy starts with the

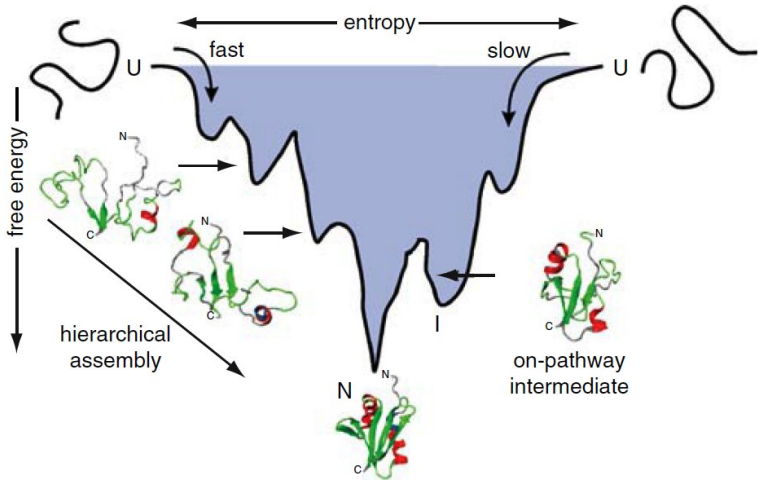

Figure 1.2: Rugged folding funnel landscape showing a two-dimensional cross-section illustrating two possible routes from the unfolded ensemble of structures to the native state. The entropy is reduced as the polypeptide chain descends the funnel, corresponding to the gradual restriction of the number of possible conformational states. at the same time, the hierarchical assembly leads to a decrease in free energy. For molecules randomly sampling the left-hand route, folding is fast and associated with no major free energy barriers (two-state). The alternative route from the right results in molecules becoming trapped in a low-energy conformation representing a populated I-state, which becomes a bottle-neck for folding to the native state (three-state model). The image and caption is taken from [164].

formation of intermediates which later assemble to the final tertiary structure [164]. In the 'diffusion-collision model', the formation of the final structure after preforming secondary structure features is triggered by diffusion [164]. All models that were mentioned above are classified as hierarchical folding models, since the formation of secondary structure patterns are the initial step of folding (fig. 1.1).

In contrast, the folding mechanism following the 'hydrophobic collapse' hypothesis is triggered by the formation of hydrophobic, tertiaric interaction between different residues of the polypeptide chain. After the first interactions are formed, the final arrangement of the peptide chain in secondary structures occur [219].

For the folding of small single domain proteins, the 'nucleation-condensation' model has spread in recent years. It combines different aspects of all folding models above. The folding starts at a nucleus and the formation of secondary and tertiary structures proceeds in parallel.

All folding processes can be visualized by the use of a folding funnel landscape [53]. The further the folding process thrives, the lower the total internal energy. Intermediates occur as local minima in the total folding funnel energy landscape. Figure 1.2 gives an example of a two dimensional folding funnel. Two different ways of folding are depicted: on the left side the folding of a protein with randomly sampling is shown, folding via intermediate states is presented on the right side of the folding funnel.

Nevertheless, not all proteins are able to adopt their native structure by autonomous folding. The aggregation of unfolded proteins, mediated by the exposure of hydrophobic residues, is the natural competition to folding [121]. To

reduce the amount and to prevent the misfolding of newly synthesized proteins, cells have a protein class of folding assistants, named molecular chaperones, at disposal [217].

1.2 MOLECULAR CHAPERONES

Molecular chaperones build the folding machinery, which is defined by its interaction with non-native polypeptide chains and their prevention of unspecific folding [64, 65]. They can be divided into two main classes, first, the ATP-dependent 'foldases', and second, the ATP-independent 'holdases' [87, 13]. Besides their function in protein folding and maturation, molecular chaperones are also important for the cell response to different stressors [64, 78]. Generally, five broadly conserved families can be distinguished; the Hsp100-, Hsp90-, Hsp70-, Hsp60-, and the small Heat shock protein (sHsp)-family [27, 185]. Representatives of the former four families are ATP-dependent in their function, the latter sHsp-family is not. A summary of the mechanisms of molecular chaperones is shown in figure 1.3. From left to right, starting in the upper left corner, the general mechanism of all chaperones are depicted, followed by the GroE-, Hsp70-, Hsp90- and ClpB/Hsp104-system. The lower left pattern represents the function of sHsps and the link to other chaperone systems. Other members of the huge class of molecular chaperones, such as the disordered and membrane function meditating Hsp12 of *S. cerevisiae* and the redox-regulated Hsp33 of *E. coli* are not allocated to one of the mentioned families [241, 107]. This indicates that the class of molecular chaperones unite many different functionalities and uncharacterized proteins, as well [166].

CHAPERONINS are large protein complexes with a size of approximately 800 - 900 kDa. The GroEL/GroES system from bacteria is one of the best characterized chaperonins [87]. It forms a cylindrical structure of fourteen GroEL subunits, which is capped after substrate binding with GroES in an ATP-dependent manner [88]. Since only one substrate molecule is encapsulated at a time, the folding occurs in total isolation from the crowded environment of the cytosol [185]. With the dissociation of GroES the substrate release is enabled and the cycle can start again [87].

HSP70 is one of the most conserved chaperones throughout all kingdoms of life. The prokaryotic homologue DnaK shares 60 % sequence identity with the eukaryotic Hsp70 protein [158]. All representatives of the Hsp70 family are involved in *de novo* folding and assembly of proteins, refolding of aggregated and misfolded proteins, the membrane translocation of organellar and secretory proteins, and the control of regulatory proteins [179, 88]. They prevent aggregation of unfolding proteins under stress conditions. The wide range of activity is based on the amplification and diversity of Hsp70 evolution, selectively recruited co-chaperones, and the cooperation with other chaperone systems [158]. Via the co-chaperone Sti1, the Hsp70 cycle is linked to the Hsp90 cycle. This allows Hsp70 to transfer client proteins, e.g. steroid hormone receptors, to Hsp90. Binding of clients is ATP-dependent and occurs with high affinity in the post-

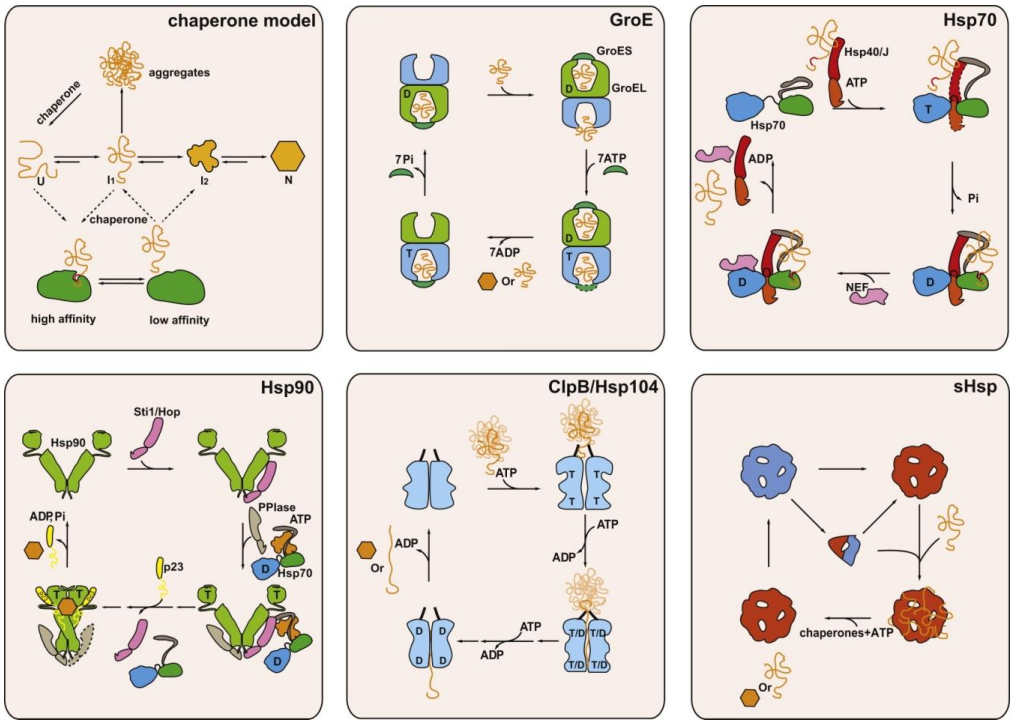

Figure 1.3: Molecular chaperone mechanisms. Chaperone model: In general, proteins fold via increasingly structured intermediates (I1, I2) from the unfolded state (U) to the folded state (N). Under stress conditions, this process can be reversed. Molecular chaperones bind proteins in non-native conformations. The shift from the high-affinity binding state to the low-affinity release state is often triggered by ATP binding and hydrolysis. GroE: The GroE machinery in bacteria, mitochondria, and chloroplasts consists of two identical rings that enclose a central cavity each. Non-native protein is bound by the apical domains of the rings, and upon binding of ATP and the co-chaperone GroES, the protein is encapsulated and released into the cavity. ATP hydrolysis in one ring results in the release of GroES and substrate protein from the opposite ring. During encapsulation the protein may fold partially or completely, depending on the characteristics of the respective substrate protein. Hsp70: The Hsp70 system comprises two co-chaperones, an activating protein (Hsp40/J-protein) and a nucleotide exchange factor (NEF). The activating protein can bind the non-native protein and delivers it to Hsp70. It forms a complex with Hsp70 and stimulates its ATPase. Hsp70 binds a stretch of seven amino acids in the substrate protein. The NEF will induce the exchange of nucleotide. This further accelerates the ATPase cycle. The substrate protein is released presumably in a non-native form. Hsp90: In this chaperone system a large number of proteins work together. First, for a number of substrate proteins, Hsp70 delivers the substrates to Hsp90. It is not clear whether this is true for all substrates. More than a dozen co-chaperones of Hsp90 exist in eukaryotes, which seem to modulate the system. One of them, Sti1/Hop, binds both Hsp70 and Hsp90 and at the same time inhibits Hsp90s ATPase (in yeast). In this complex, which also contains an additional PPIase co-chaperone, the substrate protein is transferred from Hsp70 to Hsp90. Sti1/Hop is released once Hsp90 binds nucleotide and a further co-chaperone (p23). ClpB/Hsp104: In bacteria and yeast, this chaperone is able to dissolve aggregates by actively pulling proteins through a central channel of the hexameric structure. Each protomer contains two ATPase sites, which have quite distinct characteristics concerning turnover and function. During passage through the chaperone complex, the substrate protein is unfolded. Refolding can occur upon release, and, to some extent, it can also occur in cooperation with other chaperones. sHsps: sHps are oligomeric complexes that are often activated, e.g., by heat or modifications. Many are believed to dissociate into smaller oligomers to become active. sHsps can bind many non-native proteins per complex. Release requires cooperation with other ATP-dependent chaperones such as Hsp70. Figure taken from [185].

hydrolysis ADP state [185]. The activity of Hsp70 is regulated by cofactors. J-domain containing proteins or Hsp40s are the major class of Hsp70 regulating cofactors [115]. They deliver previously bound clients to Hsp70 and stimulate the ATPase activity. The release of substrate and hydrolyzed nucleotides is further accelerated by the interaction of Hsp70 with nucleotide-exchange factors [185].

CLPB/HSP100 The family of Hsp100 chaperones is characterized by a conserved AAA ATPase group. They are divided into two classes according to the number of AAA domains. Class 1 Hsp100 family members have two independent nucleotide binding sites in each monomer [156]. Prominent members of this class are ClpA, ClpB, ClpC, and ClpE from bacteria. Hsp100s with only one AAA domain are forming the second class. ClpX and ClpY from bacteria are examples for this class [195]. The exact mechanism of the Hsp100 chaperone is still unclear. Representatives of the first class are thought to be involved in the disassembly of protein aggregates and their refolding (fig. 1.3) [81].

Since interactions with the Hsp90 and its cycle are analyzed with analytical ultracentrifugation in this thesis; this molecular chaperone is described in more detail in the following subsection.

1.2.1 HSP90 AND ITS CYCLE

Hsp90 is a highly abundant protein and essential for viability in eukaryotic organisms [226]. It is necessary for folding and maturation of a wide range of client proteins like transcription factors, e.g. p53, kinases and steroid hormone receptors [173, 178, 207, 184]. Furthermore, Hsp90 is involved in cellular processes like protein degradation, intracellular transport, and signal transduction [143].

STRUCTURE Hsp90 is a V-shaped dimer, which consists of two equivalent monomers and is a structural homologue to other ATPases of the GHKL (gyrase, Hsp90, histidine kinase and MutL) superfamily [217]. Every monomer can be divided into three domains: N-terminal, middle (M-) and C-terminal domain. In yeast, the middle and N-terminal domain are connected via a flexible, charged linker [143]. The N-terminal domain contains the ATP-lid with the ATP binding site and is necessary for the ATP turnover [237]. Interactions with clients and some co-chaperones are conducted by the middle domain. The C-terminal domain is essential for dimerization [235, 181]. Additionally, the C-terminal domain contains five conserved residues which are forming the MEEVD-motive and serve as binding site for co-chaperones containing a tetratricopeptide repeat (TPR) domain [217, 249].

ATPASE CYCLE OF HSP90 For Hsp90 it is crucial to undergo large conformational changes to conduct its functions [180, 186], as shown in figure 1.4. Upon ATP binding on the N-terminal domain, the ATP lid closes over the binding pocket and leads to dimerization of both N-terminal domains. In the next step of the ATPase cycle the M- and N-domain perform a compact twist, whereby

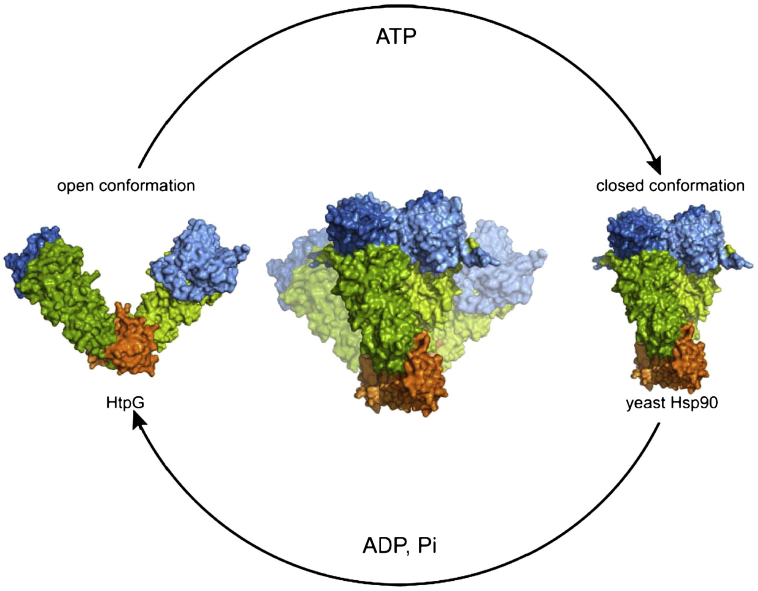

Figure 1.4: Hsp90 crystal structures of full length Hsp90 of *E. coli* (HtpG) in the open conformation (left, PDB 2IOQ) and nucleotide-bound yeast Hsp90 in the closed conformation (right, PDB 2CG9). The N-domain is depicted in blue, the M-domain in green and the C-domain in orange. Taken from [144].

the contact sides of both domains change and the closed state is adopted [187, 3]. After ATP hydrolysis and release of ADP and inorganic phosphate, the open conformation is restored (fig. 1.4). In contrast to what could be expected, binding of nucleotides does not lead to a specific conformation. Rather, in the case of Hsp90, the equilibrium of different possible conformations is shifted to the more favoured one [93].

EFFECTS OF CO-CHAPERONES In addition to nucleotide-mediated conformational changes, the Hsp90 cycle is modulated by co-chaperones. The co-chaperones can be divided into TPR-containing proteins as Hop, PP5, FKBPs and Cpr6/7 and others like p23, Aha1 and Cdc37. Dependent on the client, different co-chaperons are needed. For example Cdc37 is specific for interactions of Hsp90 with kinases and slows down the ATPase cycle [218]. In contrast, Aha1 accelerates the cycle via an asymmetric interaction that stabilizes the closed state [183, 217]. The interaction of Hsp90 with its clients has been most extensively studied in case of the steroid hormone receptor (SHR) and the co-chaperone p23.

THE GLUCOCORTICOID RECEPTOR AS HSP90 CLIENT As mentioned above, the activity of Hsp90 is triggered by several co-chaperones, which meditate the interaction with different client proteins. The interaction of the progesterone and the glucocorticoid receptor were intensively analyzed for the effect of the Hsp90 machinery [58, 128].

The glucocorticoid receptor (GR) is a transcription factor which is activates upon binding of steroid hormones. It regulates several genes which are involved in development, reproduction, and immune response [188, 10]. The receptor

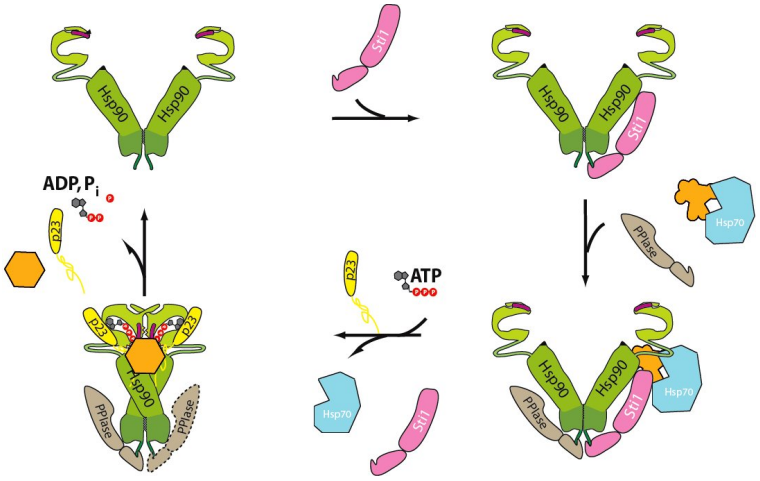

Figure 1.5: Schematic description of the Hsp90 cycle with the adaptor protein Sti1. The interaction of Hsp70 and Hsp90 is triggered via Sti1 and the transfer of a client protein, e.g. GR, is facilitated. After the release of Sti1 and Hsp70, p23 can bind to the Hsp90:client complex. Following ATP-hydrolysis the client, co-chaperones, ADP and inorganic phosphate are released and the cycle can start again. (Picture taken from Jing Li)

needs Hsp90 to gain a high affinity state for hormone binding and its translocation to the nucleus [178, 50, 233]. It is composed of three functional domains: the N-terminal regulatory domain, the DNA-binding domain (DBD) in the center, and the C-terminal ligand-binding domain (LBD), which is critical for the interaction with Hsp90 [234].

In its inactive form, the GR is localized in the cytoplasm [234]. The maturation of the GR starts with binding to Hsp70 in a co-chaperone independent manner [165]. With the help of the adaptor protein Sti1 GR is transferred to the Hsp90 cycle. Sti1 itself is replaced later on by a TPR containing co-chaperone of the Hsp90 cycle (fig. 1.5). Additionally, p23 binds to the GR:Hsp90 complex and inhibits the ATPase activity of Hsp90 [36, 179]. Thus, the turnover rate of Hsp90 is reduced, which allows an improved binding of the client protein [178].

1.2.2 SMALL HEAT SHOCK PROTEINS

Small Heat shock proteins (sHsps) form a diverse group of ATP-independent chaperones which bind partially unfolded proteins and can be found almost in all kingdoms of life [89, 134, 13]. Exceptions are some pathogenic bacteria, such as *Mycoplasma genitalium* and *Heliobacter pylori*. Single cell eukaryotes, most bacteria and archaea typically have one or two sHsps whereas higher organisms contain up to nineteen (*Arabidopsis thaliana*) different sHsp. *Drosophila melanogaster* has four, humans ten, and *Caenorhabditis elegans* contains sixteen different sHsps (fig. 1.6)[89, 240].

CHARACTERISTICS OF SHSPS Even if the sequence identity between all sHsp is very low, all members of the super-family feature several typical characteristics: i) all sHsp have a monomeric size between 12 − 43 kDa [89, 44], ii) a conserved α-crystallin domain of 80 - 100 amino acids [134, 116], iii) a dy-

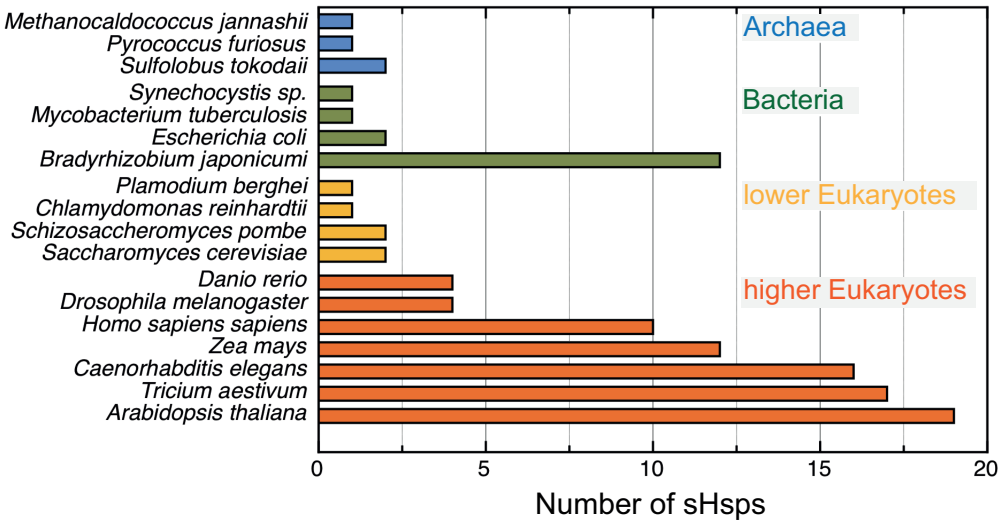

Figure 1.6: Numbers of sHsps in different organisms. In general, the number of sHsps are increasing from prokaryotes to higher eukaryotes. *Rhizobia* seem to be the only described exception. Modified according to [240].

namic quaternary structure, which allows sHsp to form high oligomers up to 50 subunits (iv) and v) the ability to be induced by stress conditions and act as chaperones in suppression of protein aggregation processes [89, 134].

The human α-crystallin is considered as the best analyzed and characterized member of the small Heat shock protein family and is eponymous for the conserved α-crystallin domain. It is a main component of the human eye lens and reaches a concentration of 450 mg/mL [67]. Two isoforms of α-crystallin (αA-crystallin and αB-crystallin) are responsible for the suppression of protein aggregation in the highly crowded environment present in the human eye [100]. Mutations or depletion of these proteins lead to the early formation of cataracts subsequently causing blindness [99, 24].

STRUCTURAL FEATURES Typically, sHsps are composed of three regions, the N-terminal region, the α-crystallin domain, and a C-terminal domain. The N-terminal region shows the highest variability in length and sequence, for example, Hsp12.2 of *Caenorhabditis elegans* has a 24 amino acid long N-terminal domain [33], whereas the N-terminus of Hsp42 of *Saccharomyces cerevisiae* has a length of 247 amino acids [90, 166]. For Hsp16.5 from *Methanocaldococcus jannashii* (MjHsp16.5) and Hsp16.9 from *Tricium aestivum* - wheat (TaHsp16.9) it could be shown that parts of the N-termini are enclosed in the oligomeric superstructure, where they form strong hydrophobic interactions and contribute to the total stability of the molecule [227, 123]. For the αB-crystallin oligomer, Jehle et al. described different orientations for the N-terminus on the basis of solid state NMR analyses (ssNMR) [112]. They are partially orientated towards the inner cavity of the sHsp oligomer and interact to stabilize the quaternary structure. The remaining N-termini show interactions with their own crystallin domain [44]. In the cryo-electron microscopy (EM) based model of Braun and co-workers the positioning of the N-termini are different compared to the

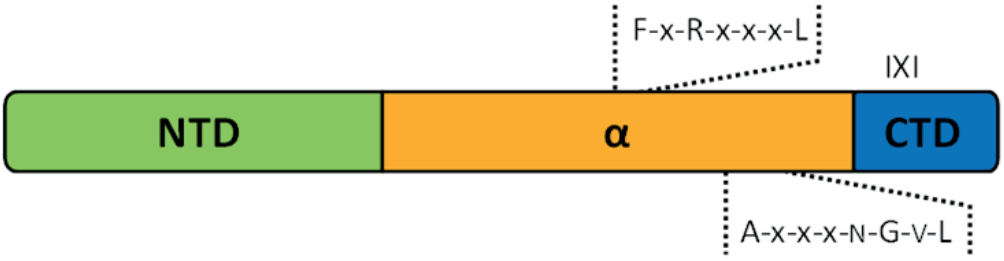

Figure 1.7: The central α-crystallin domain (α) is shown in orange. The flanking N-terminal domain (NTD) and C-terminal domain (CTD) are depicted in green and blue, respectively. The approximate locations of consensus sequences are indicated by dotted lines. Taken from [170].

Jehle-model. Here, they are found to mediate the interaction at the hexameric substructure of the 24-mer and are not located in the inner cavity [25].

The α-crystallin domain is the overall main characteristic for members of the sHsp-family [116]. According to Kriehuber and co-workers the average size of this domain is 90 amino acids, with a variating sequence homology dependent on the phylogenetic tree (20 % to 60 %). Further characteristics of the α-crystallin domain sequence are the high level of charged and the underrepesentation of aromatic amino acids, compared to the distribution in the complete corresponding genome [134]. Through the flexible N- and C-terminal regions, it is severe to analyze the total structure of sHsp in high resolution. In contrast, the α-crystallin domain is highly ordered and several structures of isolated α-crystallin domains are available. All of them form stable dimeric structures, but have not the ability to assemble to higher oligomers [9]. This characterizes the α-crystallin domain as the critical domain for the formation of the basic dimeric building block of sHsps [13, 94]. Regarding this, the α-crystallin domain forms a compact β-sheet structure similar to the immunoglobulin-fold. The dimeric substructure is composed of two layers of three and five strands, respectively, with anti-parallel orientation which are connected by short interdomain loops. A specific feature of sHsps is the dimerization via an intermolecular interaction between two α-crystallin domains. This can occur in two different ways. In bacteria, plants, and archaea one loop (β6) is integrated in the β-sheet layers of the other subunit for the dimerization (fig. 1.8 A and B) [123, 227, 228]. Dimerization via an elongated strand (β6+7) is described for metazoan sHsps (fig. 1.8 C) [9, 111, 137]. In the α-crystallin domain, two conserved sequences are known. The A-x-x-x-x-n-G-v-L motive is the critical marker for and includes three of the few conserved residues in this domain. The second motive consists of F-x-R-x-x-x-L (fig. 1.7).

Compared to the N-terminus, the C-terminus represents a fairly short domain. The structure is very flexible and only partially resolved in the known crystal structures of MjHsp16.5 and TaHsp16.9. The conserved I/L-X-I/L-motive (IXI-motive) is located in the C-terminus (fig. 1.7). In general, this motive is located closer to the end of the α-crystallin domain than to the C-terminal end of the protein, but the exact distance between these two features is not conserved [49]. The IXI-motive binds through hydrophobic interactions into a groove in

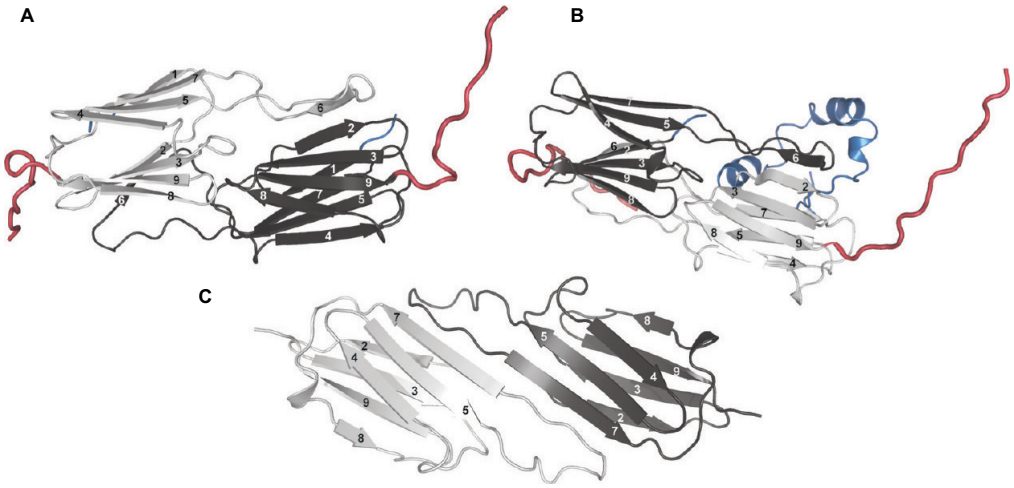

Figure 1.8: sHsp architecture. Hsp dimers with β-strands numbers according to the known crystal structures. (A) depicts the structure of the dimeric MjHsp16.5, (B) the one for the TaHsp16.9 and (C) the dimeric structure of αA-crystallin, which is model from EPR distance analysis [130]. N-terminal regions are colored in blue, the α-crystallin domain in shades of gray, and the C-terminal domain in red. Note the domain-swapped β-strand 6 of MjHsp16.5 and TaHsp16.9 and its absence in αA-crystallin. Modified according to [161].

an adjacent α-crystallin domain [49]. This groove is typically formed by the β4- and β8-sheet of the α-crystallin domain [123, 229, 137]. ssNMR analyses of the αB-crystallin revealed an alternation of the β4/β8-groove and the interaction with the IXI-motive upon changes in the pH value [110]. Still, the interaction of this motive with the α-crystallin domain contributes to the stability and oligomerization of the sHsp [123, 227, 166]. Outside this motive, the C-terminal domain is rather hydrophilic and plays a role in the interaction with substrate proteins [44, 163, 25]. Analyses of the N-terminal regarding its importance for the oligomerization and functionality of sHsps were conducted by Leroux and co-workers on the sHsp of *Caenorhabditis elegans* Hsp16.2 (CeHsp16.2). None of the characterized truncations of the first 44, 32, or 15 N-terminal amino acids revealed chaperone activity, even if they were forming native-like oligomerizations [139]. The same could be shown by Bova et al. and Narberhaus et al. in their studies on Hsp27 and αA-crystallin, or human α-crystallins, respectively [22, 166]. Thus, studies emphasize the importance of the N-terminal domain according to the chaperone function of the sHsps.

Crystal structure analysis and electron microscopy (EM) of sHsps depict a diversity in oligomeric structures and the number of subunits used to build them. Besides the polydisperse αB-crystallin, there are sHsps which form defined quaternary structures. Figure 1.9 A gives an overview of the EM models a crystal structures of five representatives of the sHsp-family. From left to right, Hsp26 of *S. cerevisiae*, an old model of αB-crystallin (*H. sapiens*), MjHsp16.5, Hsp16.3 of *Mycobacterium tubercolosis* (MtHsp16.3), and TaHsp16.9 are depicted. The overall diameter of these oligomeric structures varies from 100 Å to 180 Å. As ScHsp26, αB-crystallin, MjHsp16.5, and MtHsp16.3 reveal hollow spherical oligomers, TaHsp16.9 is arranged in a cylindrical shape. The different described spheres are build up of 24 subunits in the case of ScHsp26 and MjHsp16.5, or

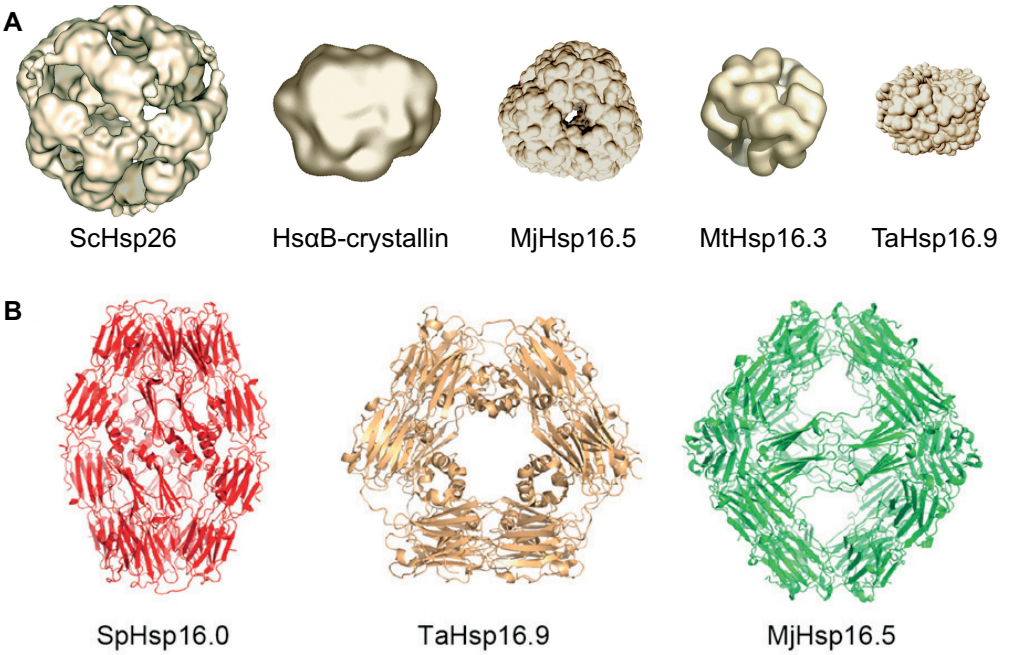

Figure 1.9: Quaternary structure of sHsp oligomers. (A) depicts the quaternary structure of five different sHsps which is to scale. Structures revealed form cryo-EM and crystal structure analyses. ScHsp26 composed of 24 subunits, HsαB-crystallin of 16, MjHsp16.5 of 12, MtHsp16.3 of 12 and TaHsp16.9 of 12 subunits [243, 84, 123, 118, 227]. Figure taken from [240]. (B) shows a comparison of the oligomeric structures of the monodispers sHsp SpHsp16.0, TaHsp16.9 and MjHsp16.5 obtained of crystall structure and SAXS analyses [85]. The three different oligomerizations: elongated sphere for SpHsp16.0, the cylindrical double disc of TaHsp16.9 and the spherical organization if MjHsp16.5 are clearly visible. Figure taken from [85].

of 12 subunits in the case of MtHsp16.3, respectively. The barrel-shaped cylindrical structure of TaHsp16.9 is build up of two double disks each composed of six subunits [123, 230, 84].

Besides the described symmetries of monodispers sHsp mentioned above, a third variant was published by Hanazono and co-workers [85]. They analyzed the sHsp of *Schizosaccharomyces pombe* Hsp16.0 (SpHsp16) via crystal structure and SAXS analyses. SpHsp16.0 forms oligomers in an elongated sphere composed of 16 monomers [85]. The three described oligomerization states are shown in figure 1.9 in a comparable manner.

The direct comparison of the different oligomeric structures of the mentioned sHsps emphasizes the differences between spherical, elongated spherical, and and cylindrical shapes. Later studies showed that MjHsp16.5 also conduct other quaternary structures and is classified as a polydisperse sHsp [91].

Besides the described homo-oligomers above, the formation of hetero-oligomers is reported for some members of the sHsp-family. The sHsp of *E. coli* IbpA and IbpB are forming such hetero-oligomeric structures [157]. The same is true for the human sHsps αA- and αB-crystallin, as well as αB-crystallin and Hsp27 [20, 22].

FUNCTION The function of sHsps is defined by their ability to bind denaturing proteins and prevent them from aggregation. This function is described by

the term "holdase" and was first shown for the bovine α-crystallin and Hsp25 of *Mus musculus* [100, 106]. In the following years, many other sHsp-family member were characterized as holdases. In general, the holdase function is ATP-independent and leads to the formation of stable sHsp:substrate complexes with equimolar masses related to the monomeric concentration of sHsp and substrate [89, 161].

For most sHsps, the function could be analyzed with non-native proteins such as citrate synthase, insulin, lysozyme, and luciferin in so-called aggregation assays. Thereby, the aggregation of a certain model substrate is induced by heat or reduction of the disulfid bonds and monitored by the observation of the light scattering signal [28, 21]. Studies, focusing on the folding state of the bound substrate, showed that sHsp are able to bind their substrate proteins with different degrees of unfolding and ranging from molten globular to unfolded [209, 161]. For example, sHsp bound β- and γ-crystallin revealed significant secondary structures, whereas bound α-lactalbumin is unfolded [17, 40, 209]. As a general rule, the binding of aggregation-prone proteins to sHsps allows them to be kept in a folding-competent state with prospective refolding [40].

The binding of substrate to the sHsps is most likely meditated by the exposure of hydrophobic residues, exposed due to the starting of unfolding of the substrate proteins [160]. Even if the interactions of several substrates with sHsps are reported, the exact binding side is still unknown until now. Nevertheless, several possible binding sites were described after analyzing the sHsp:substrate formation in different truncation mutants and with cross-linking approaches [79, 2, 109]. Predicted binding sites are included in the N- and C-terminal regions [12, 210, 74, 147]. They are all hydrophobic and, in the case of TaHsp16.9, located on the inner side of the oligomeric structure. Mutants of ScHsp26, which carry deletions of the potential binding sites, form inactive dimers [210, 126]. This effect is also observable in other sHsp mutants [225]. Up to now, no general interaction pattern could be described, which leads to the assumption that no specific substrate binding side in sHsp is present; rather, multiple binding sites of the sHsp are required for the interaction with substrate proteins. In this context, especially, the N-terminal domain is necessary for substrate binding [11].

The specificity of the different sHsps is not characterized or known for all described sHsps. More likely, sHsps have a broad range of proteins, which can be bound under certain conditions [89]. For the two sHsps of *S. cerevisiae*, ScHsp26 and ScHsp42, proteomics analysis showed that even if both proteins are present in the same compartment, the profiles of protein substrates are overlapping but are not identical [90, 15].

sHsp/substrate complexes sHsp:substrate complexes are very stable, as describe in the latter paragraph. They show no transferation of bound substrates to other sHsp or spontaneous release of the bound substrates [138, 62].

Since many sHsp-family members assemble to large oligomeric structures, the function is not automatically linked to these superstructures. Hsp25 of *Caenorhabditis elegans* is one contradictable example. It only assembles in a tetrameric structure but is able to suppress the aggregation of citric synthase efficiently [55]. The same is true for the human HspB6. This sHsp is dimeric and

has a holdase function [30]. Hence, the chaperone function of the sHsp-family does not require a specific number of subunits. However, mutations or truncation leading to smaller oligomers as observed in the native form still have an inhibition effect on the chaperone activity of the affected sHsp [140, 225].

For cytosolic sHsps, it was shown that sHsp:substrate complexes trap the substrate in a folding-competent state [208]. Further work elucidated the possibility that sHsps are connected to the Hsp70/Hsp100 pathway (fig. 1.3). After preventing the substrates from aggregation, it is hypothesized that the substrate proteins are transferred to the Hsp70/Hsp100 network, where they are refolded or passed through to the degradation pathways [89]. In contrast, for α-crystallins in the eye lens an irreversible binding of substrate proteins is proposed. This would prevent the formation of light-scattering aggregates, which could lead to cataract formations [44].

REGULATION OF SHSPS Even if sHsps are not ATP-dependent and therefore not linked to nucleotide hydrolysis-controlled cycles, as other member of the molecular chaperones are, they reveal an additional characteristic not listed above. sHsps are presented in two states, a high affinity and a low affinity state. Among others, switching between both states is triggered by certain stress conditions which are able to activate these molecular chaperones [89]. But also posttranslational modifications, such as phosphorylation, can lead to changes of the affinity state. Also, the formation of hetero complexes of sHsp in one compartment can influence the affinity regarding the substrate proteins [22].

1.2.3 HUMAN DISEASES AND SHSPS

In *Homo sapiens* ten different small Heat shock proteins have been found, HspB1 - 10, which are expressed partially tissue specific. HspB1 (Hsp27), HspB5 (αB-crystallin), HspB6 (Hsp20) and HspB8 (Hsp22) are, in contrast to the other members of the sHsp family in humans, ubiquitously expressed [221, 44].

Diseases caused by mutation of the sHsp family in humans are either classified by the location of the mutation of the sHsp (N-, C-, α-crystallin domain), by the type of inheritance (autosomal recessive or autosomal dominant), or by the type of disease correlated with these mutations [44]. Table 1.1 shows a summary modified after Datskevich et al. [44] of known human diseases sorted according to the type of sHsp affected.

Most mutations of sHsps in humans leading to diseases are known for HspB1 (Hsp27). The mutations and deletions cause distal hereditary motor neuropathy diseases with autosomal dominant inheritance, especially the Charcot-Marie-Tooth (CMT) disease of the second type is more often specified [169]. Symptoms of this disease are muscle weakness and the atrophy of several groups of muscles. In the case of CMT, additional damages of the peripheral neurosystem and changes in the neuronal signal transition are observed. In contrast to the Type I variant, the Type II variant mainly damages axons and not the myelin sheaths.

For the muscle-specific HspB3, only one mutation which leads to motor neurophathy is described in the literature [44].

Table 1.1: Mutations of human sHsp and associated diseases clustered according to the different observed diseases. DHMN stands for distal hereditary motor neuropathy, DRM for desmin related myopathy, DCM for dilated cardiomyopathy, DM for distal myopathy, MFM for myofibrillar myopathy, MN for motor neuropathy, PN for peripheral neuropathy and CMT2 for Type II Charcot-Marie-Tooth disease. The abbreviations AR and AD stands for autosomal recessive and autosomal dominant inheritance, respectively.

Protein	Disease	Mutation and type of inheritance	References
HspB1	DHMN	G34R, P39L, E41K (AD),G84K, L99M, R127W, S135F/M, R140G, K141Q (AD), T151I (AD), T180I, P182L/S (AD)	[34, 101, 108, 66, 77, 103, 153, 122]
	CMT2	P39L (AD), G84R (AD), L99M (AR), S135F/M (AD), R136W/L (AD), R140G (AD), T164A (AD), T180I (AD), R188W, pGln175X	[101, 108, 66, 145, 153, 129, 189]
	PN	476_477delCT (AD)	[155]
	Nonpathogenic	S156Y	[4]
HspB3	MN	R7S	[127]
HspB4	Cataract	W9X (AR), R12C (AD), R21L/W (AD), R49C (AD), R54C (AR, AD), G98R (AD), R116C/H (AD), c.350_352delGST or R117/H, Y118del	[177, 86, 51, 82, 154, 194, 149, 83, 215]
	Age-related cataract	F71L	[18]
HspB5	Cataract	R11H (AD), P20S (AD), R56W (AR), R69C (AD), D109H, R120G (AD), D140N, A171T (AD), 450delA or K150fs_184X (AD)	[39, 142, 120, 193, 215, 192, 104, 151, 51, 16]
	MFM	Ser21Alafsx24 (AR), D109H (AD),c.343delT or Ser115Profsx14 (AR), Q151X (AD), 464delCT or L155fs_163X (AD)	[47, 192, 72, 201, 202]
	DRM	R120G	[236]
	DM	G154S	[201, 182, 174]
	DCM	R157H (AD)	[104]
HspB6	Decrease in cardioprotective activity	P20L	[167]
HspB8	DHMN	K141N/E	[105]
	CMT2	K141E (AD)	[220]

Since HspB4 (αA-crystallin) is expressed in the eye lens, mutations of this sHsp lead to different forms of cataract formation, for example lenticular opacity caused by protein aggregation [44, 248]. The homologue αB-crystallin (HspB5), which is ubiquitously expressed, has a variety of syndromes caused by different mutations, ranging from cataracts over myofibrillar myopathy to cardiomyopathy [248].

The mutation described for HspB6 leads to a decrease in the cardioprotective activity of this sHsp. It could be shown that the mutation affects the secondary structure, and the phosphorylation level at Ser16 is decreased. The phosphorylation is necessary for HspB6 to conduct its cardioprotective activity [167].

Also, the mutations indicated for HspB8 lead to distal hereditary motor neuropathies as the mutations in HspB1 do [44, 169].

There are several different hypotheses to explain the diseases caused by mutations in human sHsps. First, as described for HspB1 and HspB8, mutations trap large amounts of wild type sHsps in huge hetero-oligomeric protein complexes. These complexes are are natively formed by both proteins to conduct their activity. Second, the specificity of the sHsps is changed upon mutations (i. e. destabilization of the cytosceleton), and third, the degradation processes of unfolded proteins is accelerated. Fourth, the protective activity of sHsps is lost upon mutation. Generally, one can summarize that mutated sHsps have a reduced chaperone activity when compared to their wild type, which can lead to the accumulation of amyloids and aggregated and denatured proteins in the cell [44].

Besides the already mentioned Charot-Marie-Tooth disease, sHsps are also linked to further neurological diseases such as Alzheimer's disease, Parkinson's disease, amyotrophic lateral sclerosis (ALS) and Huntington's disease. All these diseases share protein aggregation as the significant feature [41]. If the sHsps contribute to the diseases themselves or the ameliorate defects manipulate the sHsps is still unknown [13].

1.3 *C. ELEGANS* - A SCIENTIFIC PET

Caenorhabditis elegans is a free-living nematode in soil. It shares the phylogenetic division eumetazoa with *Homo sapiens* and has 60 - 80 % (dependent on the bioinformatic approach) homologous genes with humans [114]. Therefore, it is a popular model organism, especially in neurosciences, aging, Alzheimer's disease, stress response, protein misfolding [175, 141], and diseases which can be defined on gene level [114]. *C. elegans* researchers also tend to work in close cooperation and share their results from different screens and all other available information on databases such as WormAtlas, Wormbase, PhenoBlast, RNAiDB and many more to promote and facilitate the usage of *C. elegans* as model system [8].

C. elegans is a simple multicellular organism, which gains a body length of about 1 mm and feeds on bacteria. For normal growth and reproduction *C. elegans* needs - besides food - a humid environment, atmospheric oxygen and an ambient temperatures of appr. 20 °C [97].

Adult worms are bilateral symmetrical, not segmented, and exist as two sexes, hermaphrodites and males. The two genera differ in the chromosome composi-

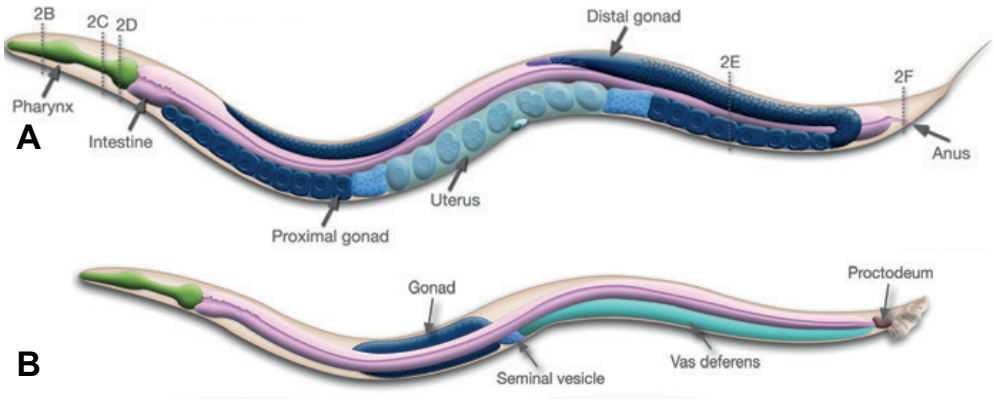

Figure 1.10: Schematic pattern of the two sexes of the nematode *C. elegans* (A: Hermaphrodite and B: Male). The light gray lines indicate pictures of cross-section, which give further inside in the anatomy and can be looked up at http://www.wormatlas.org/hermaphrodite/introduction/Introframeset.html. Modified according to [6].

tion. Hermaphrodites have two X-chromosomes (XX), whereas males only own one (X0). Males occur very rarely, only 0.1 - 0.2 % of the total population and arise from spontaneous non-disjunction on hermaphrodites [26]. Hermaphrodites perform self-fertilization and generate genetically identical progeny. The spermatozoa of them are located at the ends of the gonad arms of the ovary. Every egg is passing this compartment and becomes fertilized during its way to the exit channel. Males differ from hermaphrodites in their morphology, anatomy and behaviour. For example, they are much smaller and slimmer than hermaphrodites, and the shape of the tail is one of the obvious different features. Figure 1.10 depicts a schematic overview of the anatomic features of the two sexes. In the reproductive tissue of males, the second (posterior) gonad is extremely modified to the copulatory apparatus [150, 76].

Hermaphrodites are always composed of 959 cells. 302 of these cells are neurons, 95 are body wall muscle cells [244], 60 cells belong to the intestinal tract, and approximately 30 cells form the pharyngeal muscle cells [97]. Other cells form the hypoderm, the excretory channel and all other organs. The lineage of each cell is known and the generation and decay of each cell is developmentally determined [244]. In contrast, males are build up of 1031 cells including 381 neurons and 136 muscle cells [212, 213]. The increased numbers of neurons and muscle cells is attributed to the differences in the anatomy of the different reproductive organs [6].

LIFE CYCLE The life cycle of each worm is divided in *in uterus* and *ex uterus* development. After fertilization, the first cleavages of the egg cells take place in the uterus. Approximately at the 30-cell stadium, the eggs are laid and further development occurs *ex uterus*. After hatching, four larva stages (L1, L2, L3 and L4) are passed until they reach adulthood, if there are no interfering effects such as crowding, starvation, or dryness. Upon unfavorable conditions, *C. elegans* enters an alternative development cycle at the end of the L2 state, called Dauer pathway. Dauer larvae are able to survive for several months without food

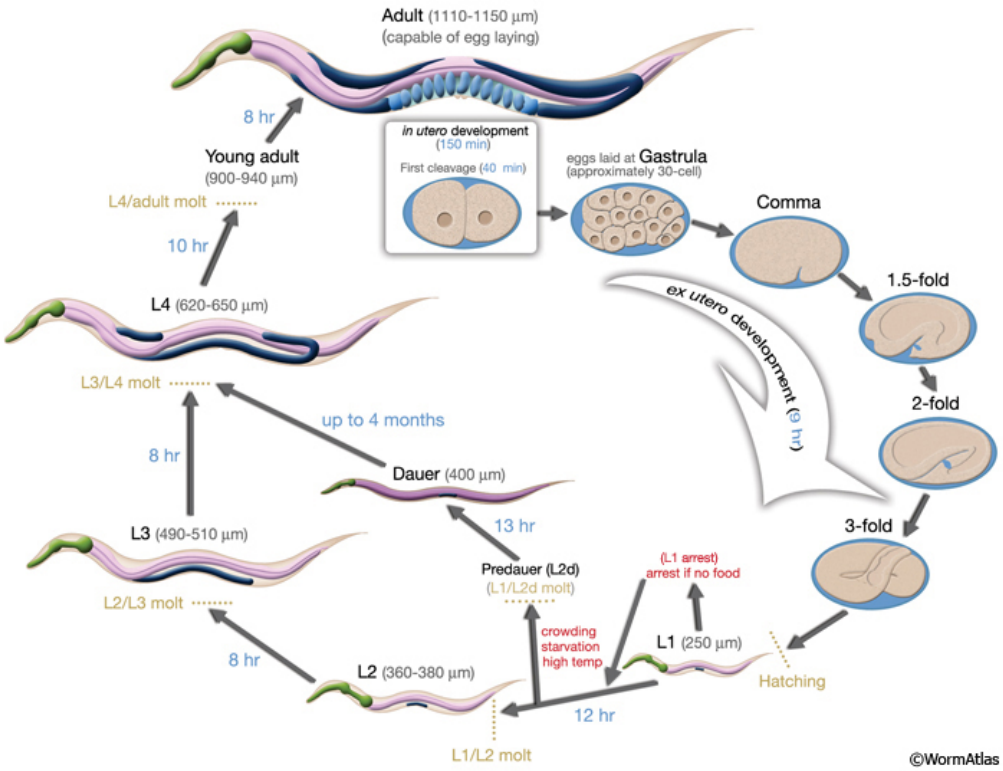

Figure 1.11: Life cycle of *C. elegans*. Depicted times between development stages refer to development at 22°C. [6]

and under poor living conditions. Upon favorable conditions, Dauer larvae exit the Dauer stage within an hour and, after approximately 10 h, mold to L4 stage. Further development is similar to the normal developing cycle, depicted in figure 1.11 [6].

1.4 STRESS RESPONSE IN *C. ELEGANS*

Three different stress responses are characterized in *Caenorhabditis elegans*; activation of the insulin/insulin-like growth factor-1 (IGF-1), the development specific transcription factor SKN-1 (orthologue to the mammalian Nuclear factor-erythroid-related factor), and the heat shock transcription factor Hsf-1 (Heat shock factor-1).

Daf-2 is a close relative receptor to the mammalian IGF-receptor and activates the conserved signal cascade of the phosphoinositide-3-kinase (PI3K). PI3K regulates the FOXO-transcription factor Daf-16 in a negative manner [14]. Inhibition of the Daf-2 gene can lead to the induction of the Dauer state. Upon incomplete inhibition, the worms display a prolonged lifespan and higher resistance against several stress factors [69]. SKN-1 and Hsf-1 are both activated upon stress and mediate stress tolerance and longevity. Hsf-1 is a secondary effector in the insulin signaling and is effected by Daf-2 [102]. It regulates the antioxidant gene expression via the p38 MAPK pathway [23] and is accumu-

lated in the nucleus, if the signal of Daf-2 is increased. Through this interaction, SKN-1 genes are activated independently of Daf-16 [251].

Hsf-1 and Daf-16 regulate a high variety of different genes - among others: genes specific for metabolism, development-specific proteins, antioxidative proteins, and the genes encoding for sHsps in *C. elegans* [14].

Besides the standard analysis of stress response, the characteristics of *C. elegans* to adapt to certain stress conditions were analyzed as well [238, 251]. In some combinations pre-treatment with one stressor can improve the survival under another stressor, e.g. UV irradiation prevents from cadmium toxicity [238]. Up to now, these adaptive responses are biologically not fully understood. The studies so far show that antioxidant defense systems, stress proteins, signal pathways and metabolic regulation are involved in the adaptation step of the worms [251].

1.5 sHSPS IN *C. ELEGANS*

In 1983, Snutch and Baillie analyzed the protein expression patterns in *C. elegans* upon heat shock in S^{32}-labeled nematodes [204]. Besides the identification of major heat shock protein classes and the analysis of the homology between Hsp70 from *C. elegans* and *Drosophila melanogaster*, one prominent S^{32}-labeled protein with the size of 16 kDa was analyzed further and classified as Hsp16.2; the first identified sHsp from *C. elegans* [191]. All other sHsps were found after the genome of *C. elegans* was sequenced and a BLAST (Basic Local Alignment Search Tool, [5]) search was conducted with the α-crystallin as query. Figure 1.12 shows a dendrogram of the sHsp clustered according to the degree of relationship to the α-crystallin domain.

The total number of sHsps in *C. elegans* is proposed to be sixteen, including four copies of Hsp16, whereas there are two copies of Hsp16.11 (T27E4.2, T27E4.3) and Hsp16.48 (T27E4.3, T27E4.9). These two sHsps are clustered with their closest related family members in to two sub-families: Hsp16.11 with Hsp16.2 (Y46H3A.3), and Hsp16.41 (Y46H3A.2) with Hsp16.48, respectively. Further, three very closely related proteins Sip-1 (F43D9.4), F08H9.3 and F08H9.4 belong to that family. Hsp17 (F52E1.7), Hsp43 (C14F11.5), ZK1128.7 are the next related subgroup. The Hsp12-family (Hsp12.1 (T22A3.2), Hsp12.2 (C14B9.1), Hsp12.3 (F38E11.1) and Hsp12.6 (F38E11.2), Hsp25 (C09B8.6) and Y55F3BR.6 are the last representatives of the large family of sHsps in *C. elegans*. The sHsps are encoded on four of the six different chromosomes in *C. elegans*, with most of them located on chromosome IV [33]. Table 1.2 shows a summary of all proposed small Heat shock proteins in *C. elegans*. Up to now, several potential sHsps have been characterized on protein level. Among them the Hsp12-family; for none of them a chaperone activity was reported *in vitro* [125, 140].

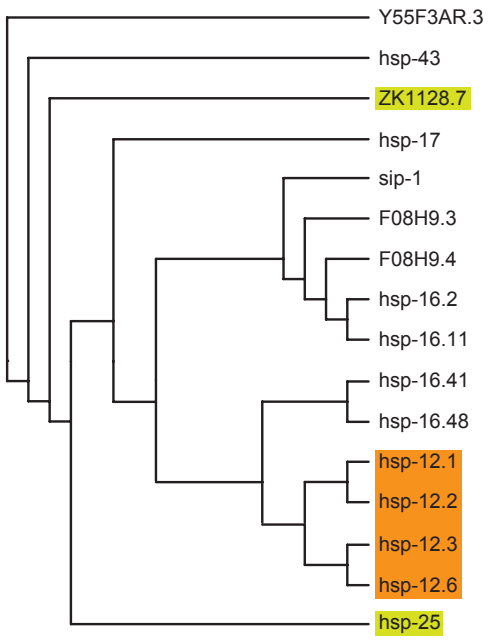

Figure 1.12: Relation between sHsps of *C. elegans* according to the degree of relation to α-crystallin. The Hsp12-family, which is analyzed *in vivo* and *in vitro* in this thesis, is highlighted in orange. Hsp25 and ZK1128.7, which are characterized additionally *in vivo*, are colored in light green. The figure is kindly provided by Dr. Martin Haslbeck.

Table 1.2: Gene loci of sHsps in *C. elegans*. Table according to [159]

	Name	Sequence name	Gene localization	WBGene ID
1	Ce12.1	T22A3.2	I:10582595..10581677	00011906
2	Ce12.2	C14B9.1	III:8138015..8139556	00002011
3	Ce12.3	F38E11.1	IV:9445256..9444875	00002012
4	Ce12.6	F38E11.2	IV:9446861..9446362	00002013
5	Ce16.11	T27E4.2	V:9089919..9090408	00002017
6	Ce16.1A	T27E4.8	V:9087586..9087097	00002015
7	Ce16.2	Y46H3A.3	V:1804799..1804269	00002016
8	Ce16.41	Y46H3A.2	V:1805061..1805703	00002018
9	Ce16.48	T27E4.3	V:9087935..9088421	00002019
10	Ce16.49	T27E4.9	V:9089570..9089084	00002020
11	Ce16A	F08H9.4	V:14464182..14463396	00008592
12	Ce16B	F08H9.3	V:14462576..14461852	00008591
13	Ce17	F52E1.7	V:8385734..8384581	00002021
14	Ce20A	F43D9.4	III:10506686..10505991	00004798
15	Ce20B	ZK1128.7	III:10136966..10138876	00014233
16	Ce21	Y55F3BR.6	IV:838536..835048	00021943
17	Ce25	C09B8.6	X:6039454..6033189	00002023
18	Ce43	C14F11.5	X:6235498..6233115	00002024

1.5.1 HSP16-FAMILY

The Hsp16-family of *C. elegans* can be divided according to their sequence homology. Hsp16.11/Hsp16.2 and Hsp16.41/Hsp16.48 are forming the core of the family and have a high sequence identity. The subfamilies Hsp16.11/Hsp16.2 and Hsp16.41/Hsp16.48 are identical in 70 % of their sequence; within the subfamilies the sequence identity amounts to 93 %. The expression of the Hsp16 core family is induced *in vivo* by different stressors and lasts for approximately two hours [190, 113]. Under normal living conditions, representatives of the core family are not detectable, neither with Northern blot, nor immunostaining [191, 54]. Especially Hsp16.48 seems to play a crucial role in the mediation of heat resistance upon heat stress [131].

A further member of the Hsp16-family is Sip-1 (Stress-induced protein-1), initially named SEC-1 (small embryonic chaperone-like protein-1). It is exclusively expressed in the embryo of *C. elegans*. This corresponds to a development specific regulation and is not inducible by different stressors [146].

The last members of the Hsp16-family are F08H9.3 and F08H9.4. Both proteins share 50 % sequence identity with the Hsp16-core family and are the proteins next related to Hsp16.11/Hsp16.2 and Hsp16.41/Hsp16.48. Both proteins are constitutively expressed in the pharynx (F08H9.3) and the excretoric channel (F08H9.4). Upon heat stress, both proteins are slightly activated and the expression pattern of F08H9.4 extends to intestinal cells [203].

1.5.2 HSP12-FAMILY

The Hsp12-family includes four proteins which are named Hsp12.1, Hsp12.2, Hsp12.3, and Hsp12.6. With a size ranging from approximately 12.2 kDa to 12.6 kDa they belong to the described smallest sHsps [35, 140]. The sequence identity amounts to 67 % at maximum in the case of Hsp12.3 and Hsp12.6 and 42 % at minimum in the case of Hsp12.2 and Hsp12.3. The four corresponding genes are located on chromosome III (Hsp12.1 and Hsp12.2) and chromosome IV (Hsp12.3 and Hsp12.6) in separate loki [33].

In comparison to other sHsps, the Hsp12-family has shortened N-terminal regions (24 - 25 amino acids) and the C-terminal domain is almost entirely missing. Thus, it is proposed that they represent the most reduced size for a stable α-crystallin domain. It is still questionable if members of Hsp12-family can perform chaperone activity. No *in vitro* study was able to show that Hsp12.2, Hsp12.3, or Hsp12.6 function in the standard aggregation assays with insulin or citratic synthase as model substrates [140, 125]. Additionally, all Hsp12-family members, except Hsp12.6, show *in vitro* tetrameric organization, which is quite small and only observed in other small Heat shock proteins upon activation or upon mutation [92, 63]. Hsp12.6 is even smaller and occurs as a monomer in recombinant purified form *in vitro* [140].

In vivo the localization and expression patterns of the Hsp12-family were extensively studied by Ding and Candido [54]. Western blot analysis revealed that Hsp12.6 is mainly expressed in the early larval stages with its peak in the L1 larva. In adult worms the expression is limited to vulval cells and the spermatheca [54]. These results are most likely transferable to the other members

of the family, since immunostaining with a cross-reactive polyclonal antibody for Hsp12.6 showed similar results [54, 140]. Expression analyses upon different stressors (Capton, cadmium chlorid, alcohol and heat shock) showed no change in the expression level of Hsp12.6 [140].

The function of the Hsp12 family proteins in *C. elegans* is quite unclear. Several theories are discussed. First, Hsp12 proteins have a very stringent clientele as substrate proteins. Second, they need to be posttranslational modified, or third they interact with specific co-factors to conduct their function. With the current state of knowledge these three possibilities are not excludable. Since Hsp12.6 could only be detected in small oligomerization states and monomeric form in worm extract, the assumption that the interactions of Hsp12.6, if existing, are more transient, is obvious [240].

1.5.3 HSP25

Hsp25 is a sHsp, 23.5 kDa in size. Using immunostaining, Ding and Candido showed, that Hsp25 is located in the body wall muscle cells and the pharynx of *C. elegans* [56]. It is expressed in all development stages. Experiments with affinity columns revealed that Hsp25 interacts exclusively with Vinculin and α-actinin and not with actin [56]. Consequently, Hsp25 is localized to the M-lines of the sarcomere and the dense bodies [33]. RNAi experiments with double stranded RNA against Hsp25 show no phenotype, which gives rise to the question, whether other sHsps in *C. elegans* can adopt the function of Hsp25 upon knock-down of this member of the sHsp family [56].

1.6 OBJECTIVE

sHsps are a widely spread protein family, with several characteristic features regarding size, structure and function. In higher eukaryotes, typically more sHsp are encoded, compared to smaller eukaryotes, archaea, and prokaryotes, where the number decreases with increasing simplicity of the organisms. Especially in higher organisms with several sHsps the question of specificity of each sHsp is of great interest.

C. elegans has 16 different sHsps, which are not all examined until now. Additionally, the overall sHsp network in this organism is not well understood.

The aim of this thesis is to obtain a better understanding of the Hsp12-family, which is the second largest sHsp-family of *C. elegans*. Besides a comparative *in vitro* analysis of all four Hsp12 proteins, the *in vivo* function of the family should be characterized.

In the *in vitro* studies the focus was laid on the examination of the typical features of sHsp. *In vivo* especially the expression patterns of the Hsp12 proteins with respect to age, RNAi, knock-out, and stress are analyzed.

Additionally, two more sHsps of *C. elegans* were investigated *in vivo*. Hsp25 is one of the sHsps which is expressed development and tissue specifically. ZK1128.7 is predicted as sHsp, but not characterized *in vitro* or *in vivo* until now.

RESULTS AND DISCUSSION 2

2.1 SMALL HEAT SHOCK PROTEINS OF *C. ELEGANS*

2.1.1 ALIGNMENT OF SHSP OF *C. ELEGANS*

The members of the Hsp12-family were identified as small Heat shock proteins of *C. elegans* through BLAST analysis. Since no chaperone activity could be determined for Hsp12.2, Hsp12.3, and Hsp12.6, it is of great interest to analyze the sequences of the family member on characteristic, conserved sequence features of the sHsp-family. Figure 2.1 shows an alignment of the Hsp12-family, Hsp25, ZK1128.7, Hsp16.2 from *C. elegans* and αB-crystallin of *Homo sapiens*. The homology of the protein sequence is highlighted in different shades of blue and the consensus sequence is depicted in black below the alignment. The predicted α-crystallin domains, according to Peschek et al. and Sun et al. are marked with bars of gray and red, respectively. The β-strands of the α-crystallin domain (β2 - β9) are underlined in green.

On its own, the Hsp12-family shows a high sequence identity to each other, as described in 1.5. Compared to the other members of *C. elegans*' sHsp-family, the sequence identity in the N-terminal is very low. With respect to the predicted sizes of the α-crystallin domain of Peschek et al. and Sun et al., the Hsp12-family reveals a N-terminal domain of 19 and 25 amino acids, respectively. The C-terminal domain is completely missing, if the α-crystallin domain of Peschek et al. is considered. For the α-crystallin domain of Sun et al., the C-termini of the Hsp12-family consists of 2 to 3 amino acids. The conserved IXI-motive in the C-terminal of sHsps is missing in the Hsp12-family. This in the C-terminal domain located motive is normally needed to form higher oligomers and to mediate the interaction of the dimeric substructures in sHsp [48]. For Hsp12.2 and Hsp12.3 a tetramer is reported as oligomerization state [140]. With respect to the alignment in figure 2.1, this observation is explainable with the missing C-termini. If these two proteins oligomerize in a comparative pattern to other sHsps, the observed tetramers are dimers of dimers. This leads to the hypothesis that the N-terminal domains are needed to mediate the tetramer formation.

This could further explain the missing chaperone activity of these two proteins [126]. Substrate binding of sHsp can be mediated by the N- and C-termini.

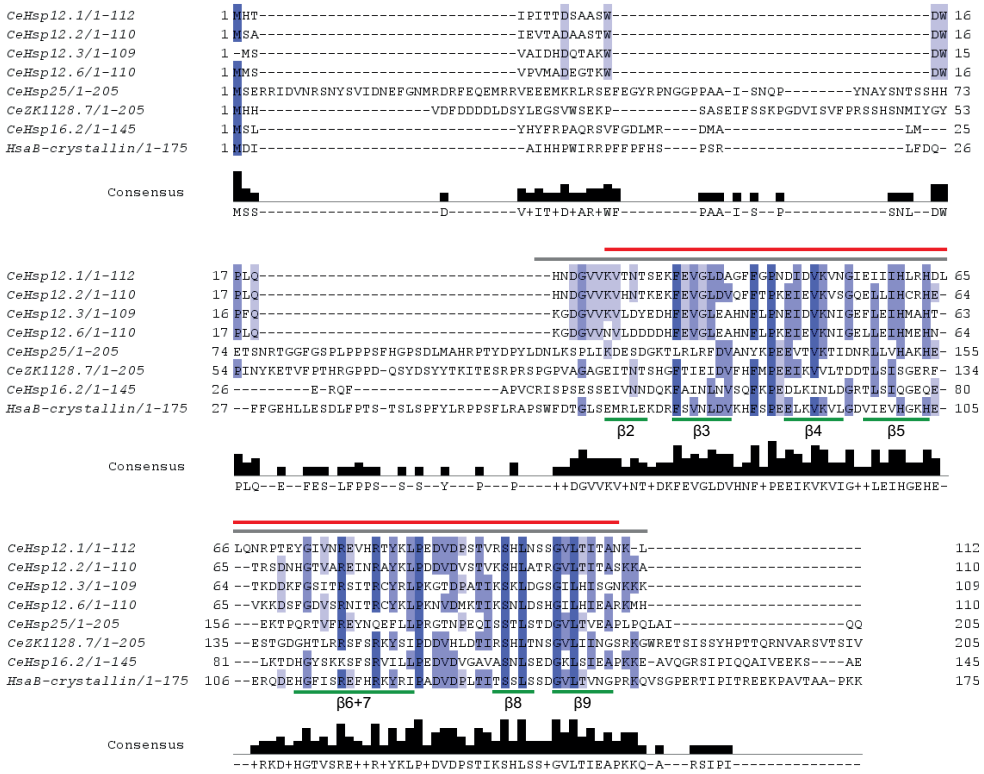

Figure 2.1: Alignment of the Hsp12-family, Hsp25, ZK1128.7, Hsp16.2 form *C. elegans* and the human αB-crystallin. Amino acids are colored according to their degree of homology. Below the alignment, the consensus of the analyzed protein sequences are depicted in black. The gray and red bar indicate the predicted α-crystallin domains according to [171] (gray) and [216] (red). The β-strand of the αB-crystallin structure are underlined in green. The alignment was performed using M-COFFEE.

When the C-terminal domain is missing and the N-terminal domain is included in the tetramer formation, potential substrate binding sites are either not present or blocked.

In the following study, Hsp25 and ZK1128.7 are characterized with several *in vivo* methods. Hsp25 also is a sHsp of *C. elegans* that forms tetramers. On the contrary to the Hsp12-family, Hsp25 revealed chaperone activity in the study of Ding and co-workers [55]. Like the Hsp12-family, Hsp25 has no C-terminal domain with the conserved IXI-motive. It is possible that the tetramer formation is mediated by N-terminal domain. The differences in the activity of Hsp25 to the Hsp12-family could then be explained by the greater length of the N-termini of Hsp25. The N-terminal domain is approximately 4- to 5-times longer than the one of the Hsp12-family.

ZK1128.7 is a predicted sHsp of *C. elegans* and not described any further in the literature. The alignment of this protein reveals a classical organization of the protein domains. N-terminal, α-crystallin, and C-terminal domain are mapped. The sequence homology to αB-crystallin in the predicted α-crystallin domain is comparable to the other analyzed sHsps of *C. elegans*. Still, there is no IXI-motive found in the C-terminal domain as is present in the human HsαB-crystallin and CeHsp16.2. The question whether ZK1128.7 forms higher oligomers as is often observed for sHsps or whether the oligomerization is relatively small as observed for the Hsp12-family and Hsp25 of *C. elegans*, remains unclear and has to be analyzed in continuative analyses.

2.1.2 PURIFICATION OF THE HSP12-FAMILY

For *in vitro* analyses, the members of the Hsp12-family of *C. elegans* were recombinantly expressed and purified. The purification strategy presented in chapter 4.2.5 is an optimization concerning length of washing and elution steps of an already established protocol of Dr. Martin Haslbeck (personally communication).

Each Hsp12 gene was cloned into a pET21a vector that was grown in a *E. coli* BL21 (DE3) p* strain. All expression cultures were prepared as described in 4.2.5 and expression was induced with 1 mM IPTG at an OD_{600} of 0.6 - 1.0.

Overall, the expression of all four proteins - Hsp12.1, Hsp12.2, Hsp12.3 and Hsp12.6 - is very strong, leading to different amounts of insolubly expressed proteins (inclusion bodies). In the case of Hsp12.2 and Hsp12.3 nearly no inclusion bodies were visible after lysis of the bacterial cells. Hsp12.1 and Hsp12.6 formed clearly visible inclusion bodies, which are more prominent amount for Hsp12.1.

All proteins could be purified in a two-step protocol depicted in figure 2.2 A. For Hsp12.1, the elution of the DEAE ff column was performed by a shallow sodium chloride gradient of 0 mM to 250 mM over 10 column volumes, since the protein started eluting during the washing step. Hsp12.2 and Hsp12.3 were eluted with a gradient of 0 mM to 500 mM sodium chloride in 15 column volumes. For these proteins, the elution started at approximately 10 mM of salt. The last member of the Hsp12-family, Hsp12.6, showed the best binding properties on the DEAE ff material. After application of the lysate and washing of the column, a second washing step of five column volumes at a sodium chloride concentra-

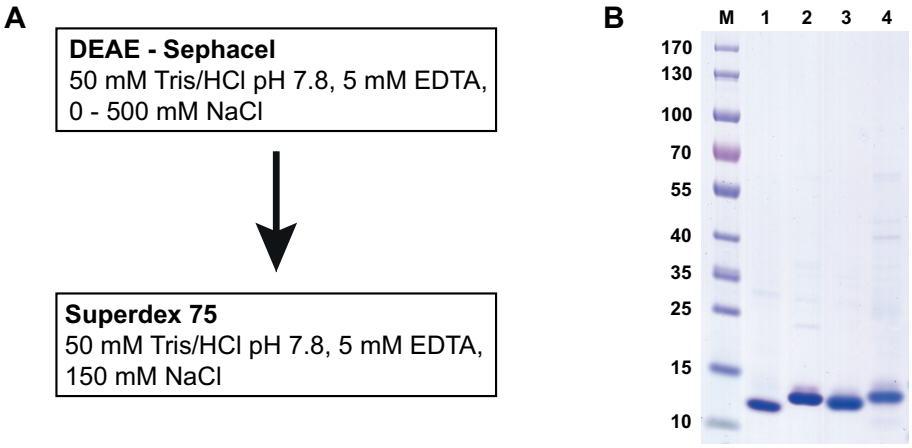

Figure 2.2: Scheme of the purification strategy of the Hsp12-family (panel A). SDS-PAGE of the Hsp12 proteins purified (panel B). Lines labeled with 1 - 4 depict Hsp12.1, Hsp12.2, Hsp12.3, and Hsp12.6, respectively. In line M the loaded marker from Peqlab is shown.

tion of 30 mM was performed. The elution of the protein was conducted with a gradient up to 250 mM salt for 10 column volumes. For the following size exclusion chromatography, the proteins were concentrated and further purified as described in 4.2.5. Representative elution profiles of the DEAE column and the gelfiltration column are depicted in the appendix (fig. 5.1).

The formation of inclusion bodies is reflected by the yield of protein reached from one liter expression culture. Hsp12.2 and Hsp12.3 reached the highest yield with approximately 75 mg protein per liter of cell culture. The amounts for Hsp12.1 and Hsp12.6 were about 15 mg and 30 mg.

All proteins were purified to >95 % purity, as detected by SDS-PAGE (fig. 2.2, panel B). To verify that all proteins were of full length and folded in a correct manner, full length mass and far-UV CD spectra analysis (s. appendix fig. 5.2 and s. below, 2.1.4) were performed, respectively. The proteins were aliquoted and stored according to the protocol in 4.2.5. Prior to every measurement, fresh aliquots of the proteins were thawed and dialyzed in the standard measurement buffer 4.1.15, centrifuged at 4 °C for 45 min, and the concentration was determined as described in 4.2.6.

2.1.3 BUFFER SCREEN FOR SHSPS OF *C. ELEGANS*

A central objective of this thesis is the characterization of the roles and functions of Hsp12-family proteins of *C. elegans in vitro* and *in vivo*. Thomas Kriehuber has shown that solvents of different buffer substances and ionic strength can have an extreme effect on the oligomerization state of sHsps [133]. To eliminate *in vitro* artifacts due to the use of different buffers for different proteins and experiments, a buffer screen with the aim to find one buffer for all members of *C. elegans*' sHsp-family was conducted.

All tested buffers had similar features. Buffers suitable for the investigating sHsps of *C. elegans* should span a buffer area of pH 6.3 to 7.5 and all buffers must have the same ionic strength. Besides simple phosphate buffers, also a combination of MES and MOPS, a three component buffer, and the Theorell-

Table 2.1: Stability of Hsp12.2 and Hsp12.3 in different buffers, analyzed in thermostability assays.

Buffer, ionic strength	Melting temperature of Hsp12.2	Hsp12.3
MES/MPOS, 150 mM	62 °C ± 1 °C	72 °C ± 1 °C
Theorell-Stenhagen, 150 mM	48 °C ± 1 °C	68 °C ± 1 °C
3 component, 150 mM	62 °C ± 1 °C	65 °C ± 1 °C
K-phosphate, 150 mM	55 °C ± 1 °C	60 °C ± 1 °C
Na-phosphate, 150 mM	60 °C ± 1 °C	65 °C ± 1 °C

Stenhagen buffer were analyzed. A complete list of tested buffers can be found in (4.1.15). For the initial buffer screen, three members of the sHsp-family were tested: Hsp12.2 and Hsp12.3, which are members of the Hsp12-family, and Sip" 1, which is a representative of the Hsp16-family. All data obtained for Sip" 1 is part of the ongoing thesis of Tilly Fleckenstein and will not be presented here [71].

A crucial test is the stability of the proteins against denaturation and precipitation during dialysis and prolonged storage in frozen buffer (dialysis storage assays). Proteins were dialyzed against the respective buffers and stored at −20 °C for two weeks. As indicator of stability, the size of the precipitate was used (pellet size in 1.5 mL test tubes). Samples of the tested sHsp were analyzed regarding the precipitate after dialysis, storage at −20 °C, and thawing by centrifugation at 4 °C and 14,000 g for 45 min. MES/MOPS buffer proved to be the best buffer with low or no precipitation for the three proteins tested.

Tilly Fleckenstein performed several chaperone aggregation assays using citric synthase (CS) as model substrate to check the effect of the different buffers in this specific assay (data not shown) [71]. For CS aggregation, the MES/MOPS buffer systems performed best again.

In the CD spectropolarimeter, all buffers performed in their individual measurement very well and showed no signal in the ellipticity and had no effect on the voltage of the lamp in the analyzed range of wavelengths (190 nm to 260 nm). Thus, all buffers seemed to be suitable for CD analyses.

Buffer stability against thermal denaturation was tested in fast screening approaches with thermostability assays (TSA) with SYPRO Orange (Invitrogen) as indicator. SYPRO Orange fluorescence is greatly enhanced by binding to hydrophobic residues. When proteins denature at high temperatures, hydrophobic amino acids side chains, originally buried inside the tertiary structure, are exposed and thus can be bound by the dye leading to a fluorescence increase.

Table 2.1 gives an overview of the melting temperatures of the members of the Hsp12-family tested under different buffer conditions.

According to the described properties of the different tested buffer systems, MES/MOPS buffer seemed to be the best suitable buffer for the *in vitro* characterization of the sHsp of *C. elegans*. However, when testing Hsp12.1 and Hsp12.6 in the dialysis storage assay, Hsp12.1 proved to be completely unstable and precipitated quantitatively, while Hsp12.6 precipitated partially after the dialysis and storage.

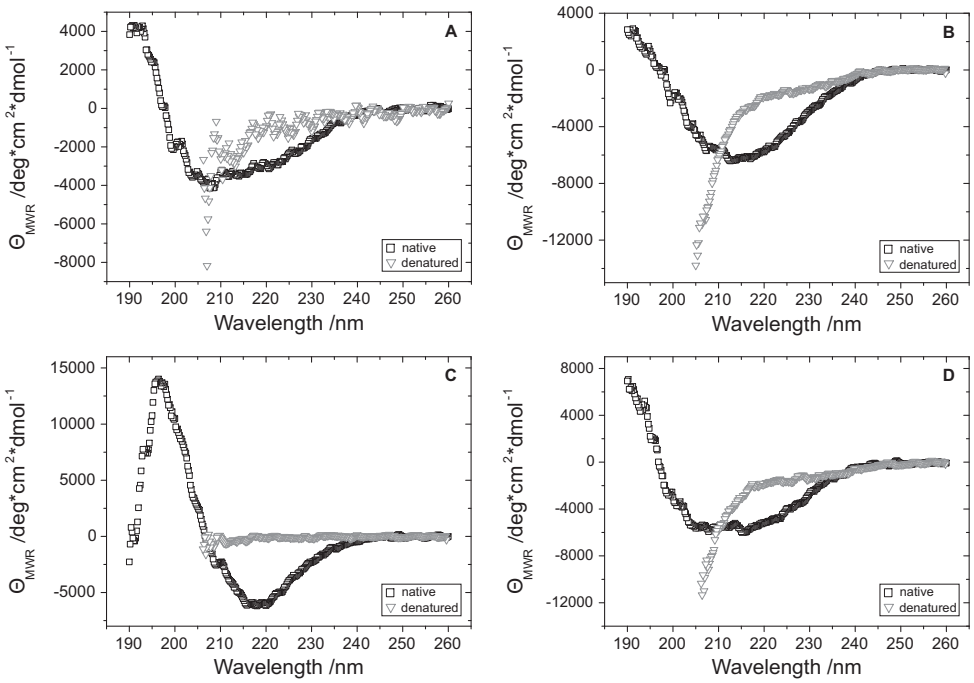

Figure 2.3: Far-UV CD spectra of Hsp12.1 (A), Hsp12.2 (B), Hsp12.3 (C), Hsp12.6 (D). All spectra were detected at 20 °C. Spectra of native protein solutions are colored in black; thermal denatured spectra are depicted in gray. The members of the Hsp12 family show characteristic spectra for β-sheet-rich proteins. For each single spectrum samples of 10 µM protein concentrations were analyzed in a 1 mm quartz cuvette.

Summarizing, it was not possible to find a single buffer suitable for investigation of all sHsp proteins of *C. elegans*. For Sip-1, Hsp12.2, and Hsp12.3, the tested MES/MOPS buffer reveals promising results. Hsp12.1 and Hsp12.6 were not stable in this buffer, consequently a 20 mM sodium phosphate buffer at pH 7.5 with 150 mM sodium chloride was chosen as standard measurement buffer. All Hsp12 proteins were stable in that buffer after dialysis and storage. However, this buffer is not suitable for Sip-1, which is not stable in any phosphate buffer tested [71].

2.1.4 SECONDARY AND TERTIARY STRUCTURE ANALYSES OF THE HSP12-FAMILY

FAR-UV CD SPECTRA Proteins are chiral molecules showing chiroptic effects like optical rotatory dispersion (ORD) or circular dichroism (CD). During folding, protein chains adopt specific backbone structure with α-helices and β-sheets as the main elements. These backbone structures lead to characteristic circular dichroitic effects in the carbonyl absorption band observed at far-UV CD (260 nm to 160 nm). Thus CD spectroscopy is a convenient tool to analyze proteins for their secondary structure features and correct folding after purification.

Table 2.2: Summary of secondary structure fraction according to the Dichroweb analyses depicted in figure 2.4.

	α-helices	β-sheet	unordered
Hsp12.1	4 %	34 %	43 %
Hsp12.2	6 %	30 %	40 %
Hsp12.3	15 %	34 %	27 %
Hsp12.6	7 %	31 %	44 %

Figure 2.3 shows the far-UV spectra of the members of the Hsp12-family. All spectra were measured in standard measurement buffer at 20 °C and corrected for buffer effects. The signals of the native proteins are colored in black and the thermally denatured in gray.

All members show the characteristic features of sHsps. The low signal intensity and the broad minimum around 215 nm are typical for β-sheet rich proteins [117]. α-Helices have their minima typically at 208 nm and 220 nm, but are not clearly observable, leading to the conclusion that the members of the Hsp12-family have a β-sheet enriched structure. Additionally, the minimum values reached in the ellipticity Θ_{MRW} of -4,000 to -6,000 are typical for sHsps and their characteristic β-sheet structure [35, 45]. These small intensities are intercessional for small α-helical structure elements, too [196].

The far-UV CD spectra of Hsp12.2 and Hsp12.3 are in good accordance with the spectra published by Kokke et al. [126]. A comparison of the heated sample of Hsp12.3 published by Kokke and co-workers and the unfolded spectrum presented in figure 2.3 C is only partly possible, since the denatured sample of Kokke et al. is heated up to 65 °C. The denatured sample of Hsp12.3 still shows analogue changes in the signal compared to the published spectra, which are more pronounced in the data of this thesis, since fully denatured proteins were analyzed with CD spectrometry.

For a better understanding of the far-UV CD spectra of proteins, it is possible to assess the amount of secondary structure elements via the comparison of the measured spectra for the different sHsps with a reference set of far-UV CD spectra of proteins of known structure. The quality and quantity of this estimation are very sensitive towards the reference set of spectra used. The CDSSTR algorithm - implemented on the Dichroweb internet page - is one of the most accurate methods to analyze far-UV CD spectra to date [42, 245, 205].

The calculated amounts of secondary structure features of the Hsp12-family are depicted in figure 2.4 and summarized in table 2.2.

For all Hsp12 proteins, a β-sheet content of 30 % - 34 % was calculated. For Hsp12.1, Hsp12.2, and Hsp12.6, most of the structure is classified as unordered, which pleads for highly flexible protein structures. An exception to this scheme is Hsp12.3: it has by far the highest α-helix content (15 %) compared to the other representatives of its family (4 % - 7 %).

The results of the CDSSTR algorithm confirm the interpretations of the far-UV CD spectra above (fig. 2.3). All amounts of secondary structure reflect the known structural features of a sHsp in some parts. For mammalian α-crystallins the β-sheet content is approximately 60 % and 7 % for α-helices [171, 214]. With

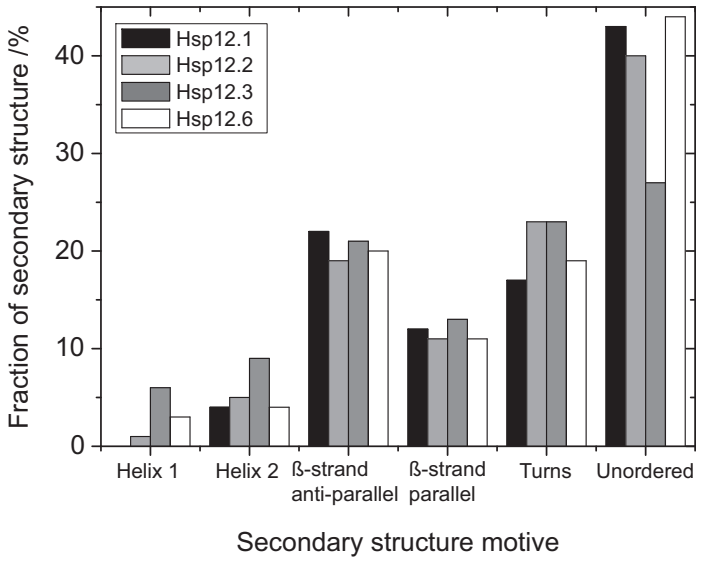

Figure 2.4: Fraction of secondary structures in Hsp12.1 (black), Hsp12.2 (light gray), Hsp12.3 (gray), Hsp12.6 (white). Far-UV CD spectra, recorded with a CD spectropolarimeter were analyzed with the CDSSTR algorithm implemented on the website Dichroweb (4.4).

the same algorithm, Daniel Weinfurtner calculated the β-sheet amount of the Hsp16-family to be 40 % - 50% of the total structure. Additionally, only 10 % of the Hsp16 proteins are folded in α-helices and the rest is categorized as unstructured [240]. With respect to the alignment in 2.1.1, the results of the secondary structure distribution of the Hsp12-family does not reflect the expected secondary structure element. The Hsp12-family is lacking the C-terminal domain and only about 25 amino acids are defined as N-terminus. Hence, the remaining amino acids are aligned to the α-crystallin domain, a higher amount of β-sheets are expected for the Hsp12-family. Thus, the determined amount of secondary structure features reveal the question, whether the Hsp12-family truly forms a α-crystallin domain like structure for example with shortened or missing β-strands within the domain, or whether the tertiary structure of the Hsp12-family is basically different.

NEAR-UV CD SPECTRA CD signals of the aromatic amino acids in the near-UV range (260 nm to 320 nm) allow to detect unique spectra of proteins. The number and nature of aromatic amino acids and the influence of the neighborhood on the aromatic residues are responsible for the magnitude and shape of the near-UV CD spectra [117]. The aromatic side chains themselves are achiral and their chiroptic properties are solely determined by the protein structure they are involved in. However, even if these spectra contain a high level of information regarding the tertiary structure, it is not possible to predict the structure of the protein analyzed based on the information gained form near-UV CD spectra. Therefore these kinds of spectra are classified as fingerprints.

Figure 2.5 shows the near-UV CD spectra of Hsp12.1 (A), Hsp12.2 (B), Hsp12.3 (C), and Hsp12.6 (D). The overall amplitudes of the spectra are very

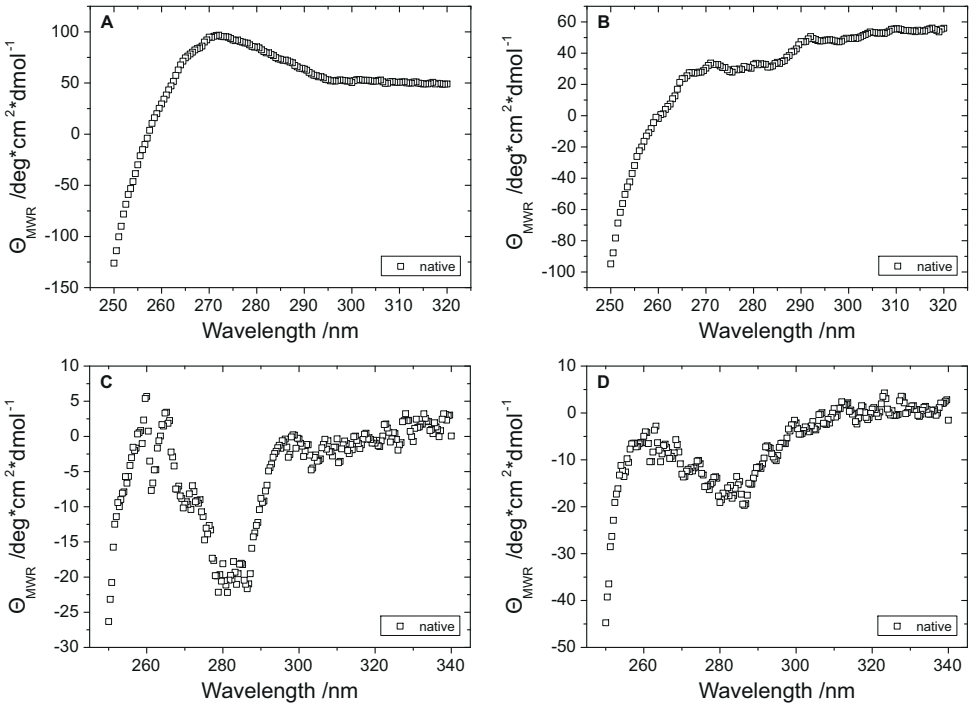

Figure 2.5: Near-UV CD spectra of Hsp12.1 (A), Hsp12.2 (B), Hsp12.3 (C), Hsp12.6 (D). Measurement were conducted in the standard measurement buffer at 20 °C and corrected against a buffer only spectrum. Protein solutions with a concentration of 50 µM were analyzed in a 5 mm quartz cuvette.

low, caused by the small number of aromatic residues in every protein. Signals in the range of 255 nm to 270 nm originate from phenylalanins, 275 nm to 282 nm represent the signals of tyrosins and 290 nm to 305 nm the signals for tryptophans [117].

2.1.5 Quaternary Structure Analysis of the Hsp12-Family

Since sHsps tend to form huge oligomeric structures, the oligomerization of the Hsp12-family was analyzed with analytical ultracentrifugation. Analytical ultracentrifugation provides a method to determine oligomeric states, protein-protein interactions and molecular weights among others (4.2.6).

The oligomerization of the Hsp12-family was characterized by sedimentation velocity experiments as described in 4.2.6. Different concentrations ranging from 0.1 mM to 1.2 mM of each Hsp12 protein were analyzed in the standard measurement buffer, 42,000 rpm and 20 °C in an Xl-A ultracentrifuge equipped with absorption and interference optics from Beckman Coulter (Krefeld, Germany). All measurements were conducted in an 8-hole Ti-50 rotor (Beckman Coulter). Data analyses were performed with a c(s) method in the SEDFIT software of Peter Schuck [200].

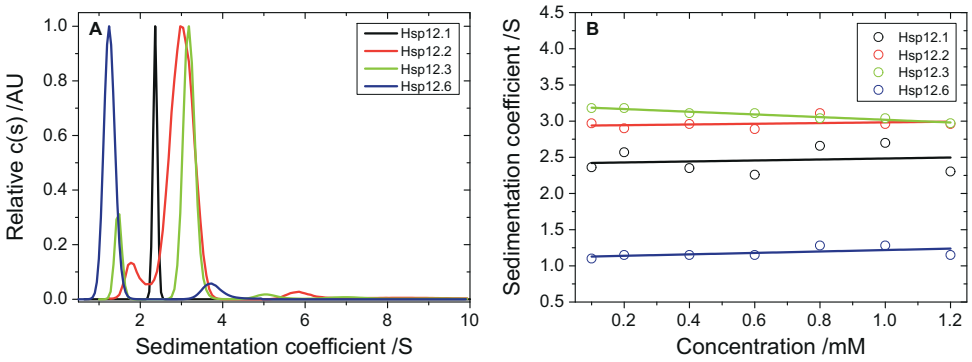

Figure 2.6: Sedimentation velocity experiments of the Hsp12-family. A: Characteristic sedimentation profiles c(s) of the small Heat shock proteins Hsp12.1 (black), Hsp12.2 (red), Hsp12.3 (green), and Hsp12.6 (blue) at a concentration of 100 µM at 42,000 rpm and 20 °C. B: Sedimentation coefficients of each analyzed Hsp12 protein at sample concentrations ranging from 0.1 mM to 1.2 mM. The results for Hsp12.1 are depicted in black, Hsp12.2 in red, Hsp12.3 in green, and Hsp12.6 in blue. The sedimentation coefficients are stable and no formation of higher oligomers occurs at higher concentrations.

In figure 2.6 A, typical diffusion corrected sedimentation coefficient distributions measured for the representatives of the Hsp12-family are depicted. Figure 2.6 B shows that the sedimentation coefficient measured for the major component for each Hsp12 protein is independent of the concentration. The sedimentation coefficient averaged over all analyzed concentrations, is 2.5 S for Hsp12.1, 2.9 S for Hsp12.2, and 3.1 S for Hsp12.3, respectively. Assuming that these proteins sediment as tetramers, this leads to a frictional ratio f/f_0 of 1.25, 1.23, and 1.28, respectively. For compact globular proteins the frictional ratio is expected to fall in the range of 1.1 - 1.3. Thus, these three members of the Hsp12-family exist as compact tetramers in solution. For Hsp12.2 and Hsp12.3 smaller components, which correspond to dimers and monomers, are represented in the c(s) distribution. In contrast, the main component of Hsp12.6 solutions sediments with 1.2 S, indicating that this protein is a compact monomer with a f/f_0 of 1.21. Small amounts of dimers and possibly tetramers are observable in the sedimentation coefficient distribution of Hsp12.6 (fig. 2.6, A).

The oligomerization states obtained with sedimentation velocity experiments are in good accordance to the literature [126, 140]. Kokke et al. characterized Hsp12.2 and Hsp12.3 as a mixture of tetramers, trimers, and/or monomers according to HPLC data and identified the tetrameric species as the main oligomerization state. In the c(s) distribution in figure 2.6 A the main sedimenting species at 2.9 S is asymmetric. This can indicate the presence of trimers or originate from the superposition with the dimer peak at 1.9 S. In contrast to Kokke et al. (1998), the c(s) distribution of Hsp12.3 represents tetramers [126]. The symmetry of the peak at approximately 3 S excludes the presence of trimers. The monomeric form of Hsp12.6 was described by Leroux et al. with a sedimentation coefficient of 1.43 S [140]. Figure 2.6 reveals a smaller sedimentation coefficient for Hsp12.6.

Furthermore, Leroux et al. showed that the oligomerization of Hsp12.6 is stable over a broad concentration range [140]. In this thesis the same could be

shown for the other members of the Hsp12-family (fig. 2.6 B). All Hsp12 proteins were analyzed at different concentrations ranging from 0.1 mM to 1.2 mM via sedimentation velocity experiments as described above. A change in the sedimentation coefficient of the main species is undetectable for any of the members of the Hsp12-family (2.6 B). According to this, the formation of higher oligomers is not induced by increasing concentrations, in the tested range.

Compared to other members of the sHsp family, these small oligomerization states are unusual. The formation of higher oligomeric structures up to 50 subunits is a major characteristic of sHsps [89]. Smaller species of sHsps are usually described as minimum cooperative building blocks and occur in some cases as activated high-affinity states [61]. Reasons for the lack of higher oligomerization of the Hsp12-family are most likely the shortened N- and C-terminal domains. Both are recognized to be important for the oligomerization of sHsps [89, 13].

2.1.6 THERMAL AND CHEMICAL STABILITY OF THE HSP12-FAMILY

Stability analyses of proteins with thermal and chemical approaches, reveal information about the stability of the secondary structure elements, when analyzed with CD spectroscopy. Additionally, changes in the oligomerization can be determined when disassembly of the oligomers leads to changes in the secondary structure level [90]. Circular dichroism spectrometry were used to analyze the thermal and chemical stability of the sHsps. 10 µM samples of each representative of the Hsp12-family were heated up from 10 °C to 90 °C and afterwards cooled down to the starting temperature to detect their thermal stability and refolding capability.

For chemical denaturation guanidinium chloride was added in rising concentrations from 0 M to 4 M to the protein samples with a final protein concentration of 10 µM. Guanidinium chloride is a chaotropic compound and increases the entropy of a protein solution by interfering with non-covalent bonds in proteins, which leads to the denaturation of the protein [73]. All samples for the chemical stability analyses were incubated at least for 12 h to allow the equilibration between unfolded and folded fraction. To analyze the reversibility of the chemical denaturation, proteins were denatured over night in 6 M guanidinium chloride concentration and the samples incubated for another 12 h, after adjustment to low guanidinium chloride concentrations.

Both, thermal and chemical stability, were detected by the change in ellipticity at 220 nm. At this wavelength, all Hsp12 proteins have a minimum in the native far-UV CD spectra (2.1.4) and the difference to the denatured CD spectra is close to its maximum.

THERMAL STABILITY Figure 2.7 depicts the thermal melting curves of the Hsp12-family. All melting curves were almost completely irreversible. To highlight and estimate the melting temperature of each protein, the measurements were fitted against the logistic function provided by Origin8G (4.1.3).

The unfolding reaction of the Hsp12 proteins show comparable temperatures but are different in their cooperativity. All measurements show one transition,

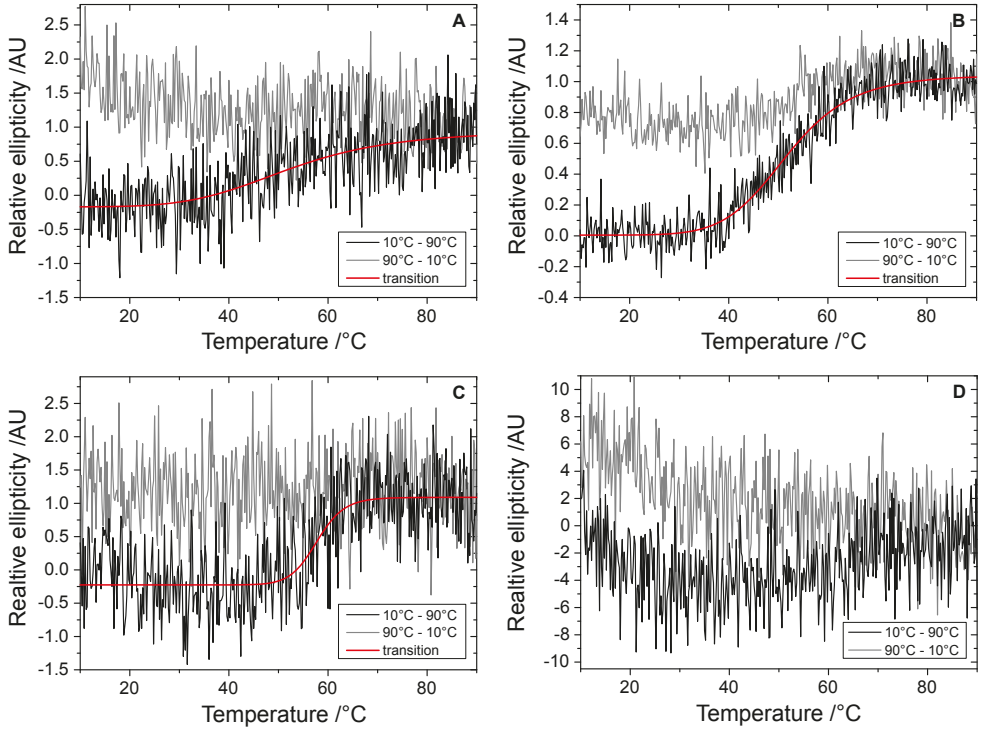

Figure 2.7: Temperature transitions of the Hsp12-family. A: Hsp12.1, B: Hsp12.2, C: Hsp12.3, and D: Hsp12.6. Samples were analyzed in the standard measurement buffer at a concentration of 10 µM for each protein. No Hsp12 protein shows reversibility towards thermal denaturation. For purpose of illustration, all unfolding transitions are fitted with a logistic function to clarify the melting point of the protein. For Hsp12.6 this procedure was not applicable, since the melting curve is highly tilted towards the x-axis.

Table 2.3: Melting temperatures of the Hsp12-family conducted with thermostability assays.

Protein	Melting temperature
Hsp12.1	55 °C ± 1 °C
Hsp12.2	60 °C ± 1 °C
Hsp12.3	65 °C ± 1 °C
Hsp12.6	55 °C ± 1 °C

which originates from the total unfolding of the proteins. This corresponds to the unfolding of the α-crystallin domain and typically occurs between 55 °C to 80 °C [38]. Information of the disassembly of the oligomeric structures of Hsp12.1, Hsp12.2, and Hsp12.3 can not be obtained from the unfolding curves depicted in figure 2.7. For Hsp12.1, Hsp12.3, and Hsp12.6 no refolding is detectable. Hsp12.2 is the only protein of the Hsp12-family that reveals a small amount of refolded protein after the cooling down process. The irreversibility of the unfolding reaction precludes any further quantitative or mechanistic interpretation. To compare the different stabilities of the Hsp12 proteins, melting temperatures were estimated. For Hsp12.1 and Hsp12.2, a melting temperature of approximately 55 °C can be assigned. Hsp12.3 is slightly more stable and melts at a temperature of about 60 °C. An estimation of the melting temperature of Hsp12.6 reveals 55 °C, too. Compared to melting temperatures gained from thermostability assays (table 2.3), the Hsp12-family shows equivalent stabilities and cooperativity in both assays.

Concerning the average temperature range *C. elegans* lives at, all members of the Hsp12-family start to denatured far above this values [95]. Even upon heat stress conditions for *C. elegans* (30 °C to 38 °C), the Hsp12-family members show no change in the far-UV CD signals. That pleads for overall stable structures in the living organism and would allow Hsp12 proteins to conduct their functions even under heat stress conditions.

CHEMICAL STABILITY The chemical transitions of Hsp12.1, Hsp12.2 and Hsp12.3 show a reversible character (fig. 2.8).

In the case of Hsp12.1, Hsp12.2 and Hsp12.3, comparison of the curve shapes of un- and refolding reactions leads to the conclusion that both reactions have the same cooperativity. For Hsp12.6, a proper statement is not possible. Even if the refolding reaction at guanidinium concentrations from approximately 2.5 M to 4 M is integrated well in the unfolding reaction, the curve shape at lower GdmCl concentrations is difficult to interpret according to is irregularities. Hsp12.1 and Hsp12.3 are comparable stable proteins with respect to the chemical denaturant guanidinium chloride. Half of the proteins are unfolded at a concentration of 0.9 M. The analysis for Hsp12.6 revealed a unfolding concentration of $C_{1/2}$ of about 0.8 M, which is slightly lower than the ones calculated for Hsp12.1 and Hsp12.3. Hsp12.2 is the least stable protein of the family in GdmCl denaturation. It unfolds at a concentration of 0.51 M guanidinium chloride. The exact values with error information are outlined in table 2.4.

Like the thermal transitions, the chemical transitions of Hsp12.1, Hsp12.2, and Hsp12.3 show only one midpoint. Consequently, no conclusions of the dis-

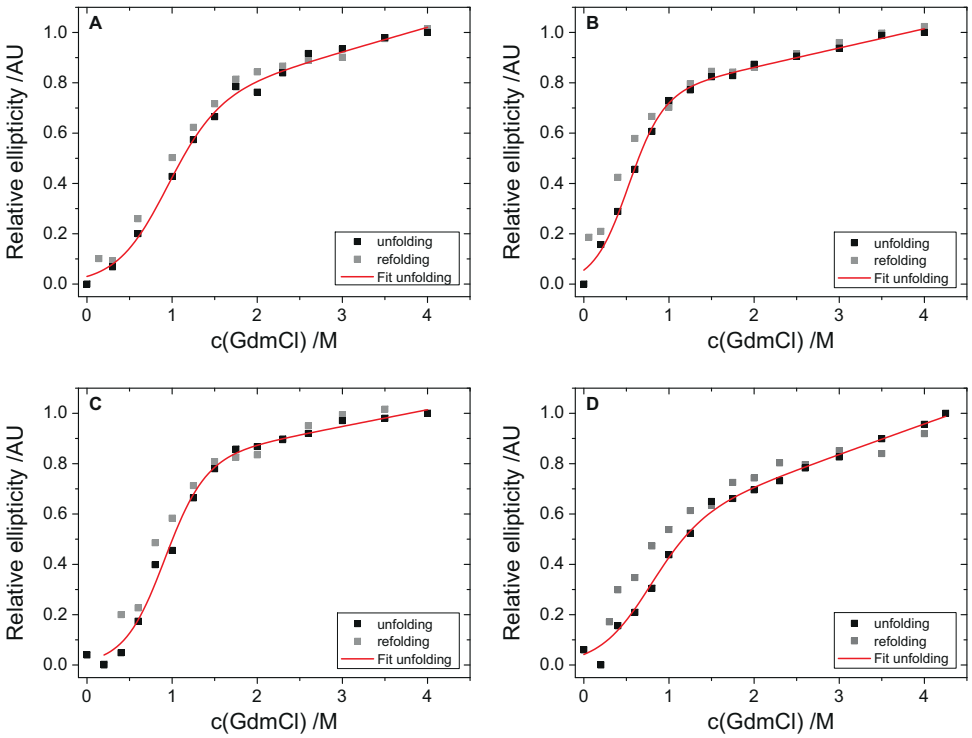

Figure 2.8: Chemical stability analyses of Hsp12.1 (A), Hsp12.2 (B), Hsp12.3 (C) and Hsp12.6 (D). All proteins were denatured with increasing amount of guanidinium chloride (GdmCl). After reaching the equilibrium, the ellipticity of each sample was detected. All chemical transitions are not completely reversible, since the refolding data points are not completely embedded in the unfolding measurements. Hsp12.1 and Hsp12.3 depict a comparable stability concerning GdmCl. Hsp12.6 is only slightly more unstable than Hsp12.1 and Hsp12.3. Hsp12.2 is less stable than the other members of the protein family.

Table 2.4: $C_{1/2}$ values of the Hsp12-family.

	$C_{1/2}$
Hsp12.1	0.90 ± 0.1 M
Hsp12.2	0.51 ± 0.1 M
Hsp12.3	0.89 ± 0.1 M
Hsp12.6	0.79 ± 0.1 M

assembly of oligomers can be made. For Hsp12.1 and Hsp12.2, the unfolding starts at very low GdmCl concentrations and reveal a slightly broadened transition compared to Hsp12.3. This can indicate that the disassembly of the oligomers broadened the unfolding transition of these two proteins. An equal assumption could not be confirmed for Hsp12.3. For this protein the unfolding starts at higher concentrations compared to Hsp12.1 and Hsp12.2. The chemical denaturation of Hsp12.6 showed great differences to the transitions of the other Hsp12-family members. The transition is very broad and follows a linear function at higher GdmCl concentrations. Referred to the Hsp16-family, the chemical transitions of the Hsp12-family are more similar to the transitions of the Hsp16.42/Hsp16.48 subgroup, because they only show a single transition [240]. However, a direct comparison of the chemical stabilities is not possible, due to the different denaturing agents used to conduct them.

2.1.7 Interaction of Hsp12-family with model substrates

One characteristic feature of all sHsps is their ability to bind partially denatured proteins and prevent the formation of aggregates. Several model substrates are used to detect the chaperone activity of sHsps *in vitro*. Here, the citrate synthase and lysozyme were used to analyze the chaperone functions. Citrate synthase (CS) is a homo-dimer composed of two identical subunits (49 kDa in size) and originates from porcine heart. The incubation of CS at 43 °C leads to unfolding, inactivation and aggregation of the protein [28, 206]. Lysozyme from chicken egg white is 14 kDa in size and aggregates under reducing conditions [80].

effect on thermal aggregation To analyze the effect of the sHsps of the Hsp12-family, all members were incubated at different concentrations at 43 °C. After temperature equilibration, 1 µM CS was added and the aggregation process is detected by light scattering measurements as described in 4.2.5. Figure 2.9 shows the CS aggregation assays for the Hsp12-family. Except for Hsp12.1, no member showed chaperone activity with citrate synthase as a model substrate. In fact, the data of Hsp12.3 even revealed a tendency for co-aggregation, because the relative scattering signal increased compared to the CS only sample with higher ratios of sHsp present in the analyzed samples. Hsp12.1 is the only protein which performs chaperone activity in this assay. Compared to other sHsps, the activity is quite small. 50 % suppression of aggregation is reached at a monomeric ratio of approximately 1:32 CS to sHsp. Other sHsps like Hsp26 of *S. cerevisiae* show the same activity at a 2-fold excess [90]. Below a 32-fold access Hsp12.1 shows no influence on the aggregation process at the concentration tested. Since the concentration needed to suppress aggregation is comparatively high, negative controls with bovine serum albumin (BSA, Pierce) were performed. This control allows to determine possible molecular crowding effects on the aggregation (fig. 2.10).

Figure 2.10 exhibits the suppression of CS aggregation by Hsp12.1. Even in a 64-fold excess the aggregation of the CS is not completely prohibited. To exclude that the decrease in CS aggregation is caused by molecular crowding, a negative

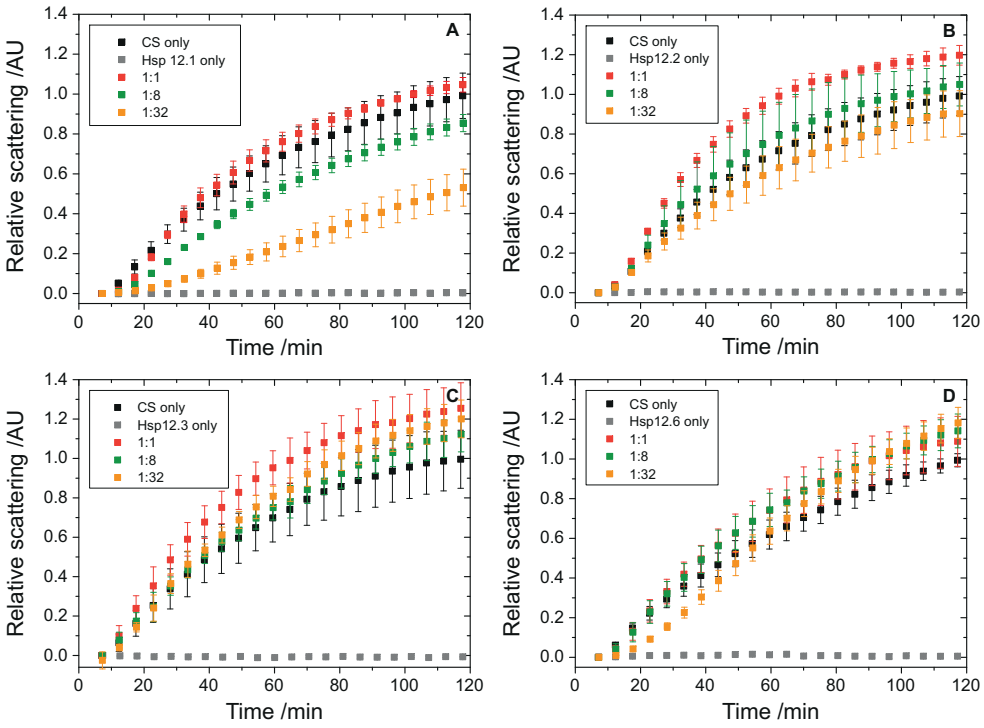

Figure 2.9: Effect on the thermal CS aggregation of Hsp12.1 (A), Hsp12.2 (B), Hsp12.3 (C), and Hsp12.6 (D). Analyzed is the aggregation of 1 µM CS with different ratios of sHsp (1:1 - red, 1:8 - green, 1:32 - orange). The CS only aggregation is depicted in black and the negative control of the sHsp only sample in gray.

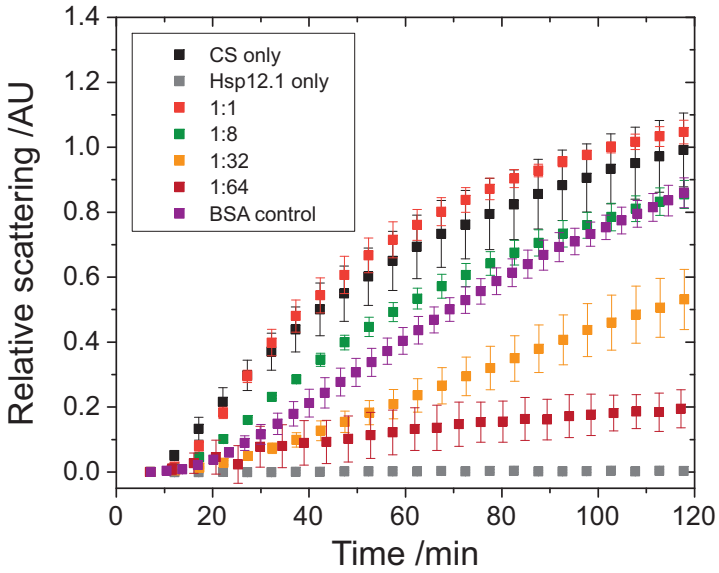

Figure 2.10: Hsp12.1 suppression of thermal induced aggregation of citrate synthase (CS). Different molar ratios of CS to sHsp are depicted in red (1:1), green (1:8), orange (1:32) and dark red (1:64). The BSA control with a molar excess of 64 is colored in violet. The CS only and Hsp12.1 only samples are depicted in black and gray, respectively.

control was measured with 64 µM BSA (violet data, fig. 2.10). BSA on its own shows a very small effect on the aggregation process of CS, which is comparable to an 8-fold excess of Hsp12.1. In the negative control, the aggregation of the model substrate is slightly slowed down, notable by the sigmoidal shape of the aggregation curve. The reduction of the aggregation lies in between the error bars of the CS only sample, consequently no chaperone activity of the BSA control is visible.

EFFECT ON AGGREGATION INDUCED BY REDUCTION To analyze the effects of sHsps on another model substrate, Lysozyme was used. This model substrate has the advantage of being much smaller than citrate synthase. As described in (2.1.5), the Hsp12-family members are forming tetramers (Hsp12.1-Hsp12.3) and monomers (Hsp12.6). The average size of the tetramers is 48 kDa, which is equal to the size of the citrate synthase. Different chaperone activities, dependent on the used model substrate, were described previously by Kokke and co-workers, and de Miguel and co-workers [125, 46].

The results of the lysozyme aggregation assays with Hsp12.1 (A), Hsp12.2 (B), Hsp12.3 (C), and Hsp12.6 (D) are depicted in figure 2.11.

As mentioned above, sHsp differ in their chaperone activity regarding the model substrate. For Hsp12.1, the aggregation assay with lysozyme is not suitable. Despite the inability to inhibit aggregation, the Hsp12.1 samples analyzed aggregated earlier than the lysozyme only sample. Hsp12.2 has no reducing effect on the aggregation of lysozyme. Hsp12.3 and Hsp12.6 revealed co-aggregation behavior in this assay. This is even more pronounced in the

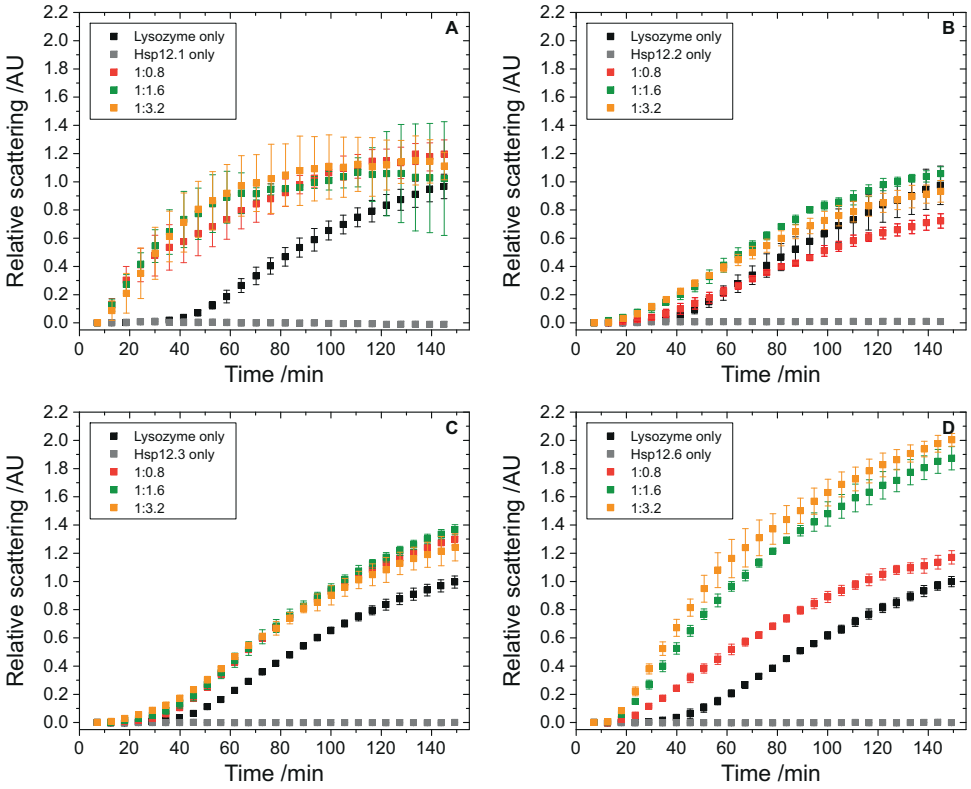

Figure 2.11: Lysozyme aggregation assays of the Hsp12-family. Influences on the aggregation of Hsp12.1 are shown in A, of Hsp12.2 in B, of Hsp12.3 in C, and of Hsp12.6 in D. Molar excesses 0.8-fold are depicted in red, 1.6-fold in green and 3.2-fold in orange. The lysozyme-only sample is colored black and the respective protein only control in gray. None of the Hsp12-family members show an effect on the lysozyme aggregation.

Hsp12.6 samples, where scattering signals for the 1.6- and 3.2-fold samples were twice as high as the lysozyme-only signal. In contrast to the data obtained above, members of the α-crystallin-family exhibit a total suppression of lysozyme aggregation at a 2-fold molar excess [171].

For Hsp12.2, Hsp12.3, and Hsp12.6 the missing chaperone activity was described in [125, 126] and [140]. For all three proteins, CS assays were conducted to describe the chaperone activity. In an additional study, Hsp12.2 was analyzed by creating chimeric proteins with αB-crystallin. Kokke et al. described that the activity of Hsp12.2/αB-crystallin chimeras differ between model substrates with different sizes [125]. The same effect was described for the sHsps of *Toxoplamsa gondii* Hsp28 and Hsp30. Hsp28 can bind CS in stable complexes while Hsp30 interacts more transient with the model substrate [46].

Nevertheless, the chaperone activity of Hsp12.1 is very interesting, because it is a unique characteristic within the Hsp12-family. A reason for the huge amount needed of Hsp12.1 to suppress the aggregation of CS could be the size of the model substrate. As mentioned above the tetramers of Hsp12.1 equal the size of the CS. Thus the effective binding of model substrates and preventing their aggregation needs a higher amount of Hsp12.1.

Summarizing the results of all aggregation assays obtained, lysozyme aggregation is not prevented by any of the Hsp12-family members. Furthermore, lysozyme seems to be a model substrate unsuited for the Hsp12-family, because massive co-aggregation (Hsp12.6) was detected. In contrast, Hsp12.1 acts on high molar ratios as a molecular chaperone in the CS aggregation assay, where none of the other representatives of the Hsp12-family revealed any activity. As discussed in 3.1.1, it is advisable to find native substrates to determine the possible chaperone activity of Hsp12.2, Hsp12.3, and Hsp12.6.

2.2 *IN VIVO* CHARACTERIZATION OF SHSPS IN *C. ELEGANS*

For *in vivo* characterization of the Hsp12-family, several different assays were conducted. Expression patterns under different conditions, such as development, RNAi, and the application of different stressors were analyzed with qRT-PCR experiments in this work. Besides the qRT-PCR experiments, lifespan and thrashing assays were performed. Furthermore, the effects of the gene knock-out of the Hsp12-family were characterized with the same set of methods. Additionally, Hsp25 and ZK1128.7 of *C. elegans* are characterized *in vivo*. Hsp25 is a sHsp, which is especially expressed in body wall muscle cell. ZK1128.7 is a predicted sHsp and not further characterized *in vitro* and *in vivo* up to now.

For the characterization of the different small heat shock proteins of *C. elegans* a color code is introduced: all samples reflecting analysis of Hsp12.1 are depicted in black or white, respectively, Hsp12.2 is depicted in red, Hsp12.3 in green, Hsp12.6 in blue, Hsp25 in cyan, and ZK1128.7 in orange.

2.2.1 QRT-PCR EXPERIMENT SETUP

qRT-PCR experiments are very sensitive approaches for analyzing mRNA levels in many different tissues or model organisms [223]. To verify that the gained results from these analyses are reliable and reproducible, several checkpoints have to be evaluated before the essential experiment can be conducted.

QRT-PCR PRIMER The primer design is a critical point. All primers were designed to span at least one exon and 150 bp (base pairs) or, if possible, span an exon-exon junction. The primer pair for Hsp12.1 is the only one which spans an exon-exon junction; for all other primers a design with respect to this feature was not possible. All primer pairs have a melting temperature of 65 °C ± 1 °C.

To test the specificity of each primer pair – especially for the Hsp12-family – normal PCR reactions on expression plasmids were performed. For the Hsp12-family, each primer pair for qRT-PCR was tested with all four expression plasmids. All primers were specific for their own gene. In a further validation step, the primers were tested against genomic DNA (gDNA) of *C. elegans*. Figure 2.12 shows an agarose gel of the test-PCR with gDNA as template. For all primer pairs, except the one for Hsp12.1, single bands with an average size of 350 bp are visible. The reaction for the Hsp12.1 primer pair should not work, since the binding site for the reverse primer is missing, due to the lack of the exon-exon junction.

Since the sequence identity between the Hsp12-family is quite high, it was very difficult to design specific primers which are not forming primer dimers. Even though primer dimers involve the danger of effecting the efficiency of the qRT-PCR, it was favored to take primer pairs with a higher specificity for their gene and higher trend to form primer dimers than to lose specificity conversely to lesser primer dimer formation. However, it is still possible to reduce the primer dimer amount, when qRT-PCR reactions are optimized concerning their applied primer concentration [223].

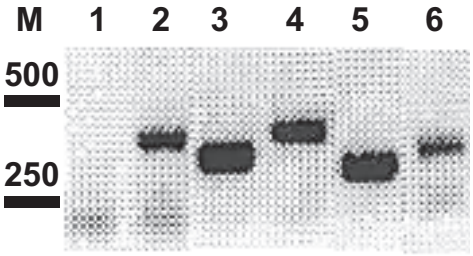

Figure 2.12: Agarose gel of the test-PCR of qRT-PCR primer on genomic DNA of *C. elegans*. Amplified fragments are in the expected range of 250 - 500 bp. Lane 1 - 6 depict the results for the primers in the following order: Hsp12.1, Hsp12.2, Hsp12.3, Hsp12.6, Hsp25, and ZK1128.7.

HOUSEKEEPING GENES For normalization approaches several housekeeping genes were tested. The primers for all analyzed housekeeping genes were designed by Dr. Christoph Kaiser during his thesis and are published in [75]. Besides the two housekeeping genes Actin (Act-1) and phosphoglycerate kinase 1 (PGK-1), also Daf-21 seemed to be a quite promising candidate for the normalization approach. Daf-21 has a very stable expression and is not induced by heat stress [75]. Actin is a widely used housekeeper in the qRT-PCR field and was already employed for *C. elegans* expression pattern analyses by other labs [250, 175].

C. elegans disposes five different isoforms, which belongs to the actin family. The isoform Act-1 was tested during this study. Act-1 is required for the motility of the nematode. Additionally, it is important for proper body wall and pharyngeal muscle structures and is describes as identical to Act-3 [132, 197, 247]. Act-3 was used from Prahlad et al. (2008) for their studies on the "regulation of the cellular heat shock response in *Caenorhabditis elegans* by thermosensory neurons" as housekeeper [175]. Since Act-1 and Act-3 are described as identical a same performance as housekeeper are expected. Pgk-1 is the second housekeeper used from Gaiser et al. (2012) for their expression analysis after different stress conditions. Pgk-1 is the orthologue in *C. elegans* to the human phosphoglycerate kinase 1. Mutations on this gene lead to neurological disturbances and hemolytic anemia. Several other qRT-PCR studies used Pgk-1 as housekeeper, already. Still, latest publications showed that, under certain conditions, Pgk-1 is not suitable for normalization approaches [52]. Daf-21 is a member of the Hsp90 family of *C. elegans*. It is suggested that it belongs to the molecular chaperones needed for life span increment as recognized in *age-1* mutant nematodes, because down-regulation of Daf-21 through RNAi approaches lead to a reduced life span. Additionally, Daf-21 influences the maintenance of muscle structures as diffusible factor [19, 162, 75].

To verify the performance of all possible housekeepers, an exogenous control RNA was used - the AlienRNA provided by Stratagene. For every measurement series an AlienRNA only sample and sample consisting of AlienRNA plus the templates which were to be analyzed were measured.

PRIMER CONCENTRATION QRT-PCRs with several different RNA preparations of mixed nematode populations (4.2.1) and different primer concentrations were conducted to test the performance of all primer pairs. Since SYBR Green

Table 2.5: Ct-values of the primer pair for the Hsp12.2 gene for different primer concentration used.

Primer pair for	Concentration	Average Ct-value of the Reaction	NTC	Difference of Ct-values
Hsp12.2	200 nM	25.40 ± 0.10	28.04 ± 1.04	2.65
	75 nM	24.20 ± 0.04	28.18 ± 0.57	3.99
	50 nM	21.19 ± 0.26	33.41 ± 0.22	12.02

Table 2.6: Averaged Ct-values of the no template controls (NTC) for each primer pair used in the qRT-PCR analyses in this work. All values were measured in triplicates.

Primer pair for	Ct-values of NTC
Hsp12.1	29.41 ± 0.05
Hsp12.2	33.21 ± 0.38
Hsp12.3	33.34 ± 0.22
Hsp12.6	34.36 ± 0.27
Hsp25	35.29 ± 0.41
ZK1128.7	34.29 ± 0.20
Act-1	39.74 ± 0.48
Daf-21	45.88 ± 0.50

was used for the detection of double stranded DNA (dsDNA), it is particularly important to optimize the used primer concentration. Primer concentrations were tested in a range from 50 nM to 200 nM. In table 2.5 an abridgement of the revealed data of the samples analyzed with 200 nM, 75 nM, and 50 nM is shown. The complete list of all primer pairs can be found in the appendix (tab. 5.1). Crucial for the detection of the best primer concentrations are the revealed Ct-values for the normal reaction and the NTC (no template control). The Ct-values were determined with the MxPro-software for the qRT-PCR cycler using the default algorithm (4.2.1). For the Hsp12.2 primer pair the effect of less primers in the reaction is most pronounced. At 200 nM primer concentration, the difference in Ct-values of normal sample and the NTC is 2.65. With the reduction of the primer, the difference increased to 12.02. The rising Ct-value of the reaction can be due to different template qualities or originates from the different primer-template ratios, which could have an effect on the performance of the reverse transcriptase reaction [37]. The increase as observed for the Hsp12.2 primer pair was not determinable for all other primer pairs (tab. 5.1). However, the reduction of the primer concentration leads to an optimization of the qRT-PCR.

Overall, at 50 nM primer concentrations, the measured Ct-values with a total template concentration of 10 ng laid in a range from 16 to 28 cycles. All 'no RT control' samples showed at least a difference in their Ct-values of 2 compared to the corresponding reaction. The measured no template controls (NTCs) for each primer pair yielded Ct-values higher than 29 cycles, which are high enough to permit for reliable data production. Table 2.6 summarizes the results of the NTC measurement. All samples were measured in triplicates.

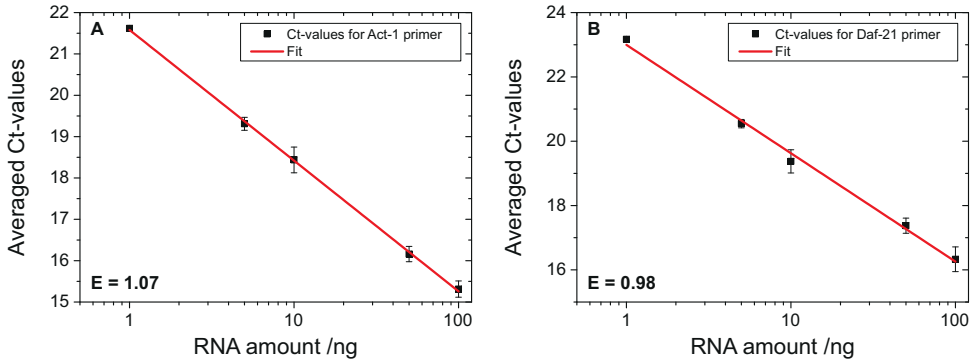

Figure 2.13: Analyses of the efficiency of the qRT-PCR reaction of the housekeeping genes Act-1 (A) and Daf-21 (B). Depicted are the averaged detected Ct-values at the different analyzed primer concentrations, the corresponding fit, and the calculated efficiency E.

During this testing phase, the Pgk-1 primer pair showed no reliable results. Even if it performs in other experiment very well, it showed a high variety and lacked reproducability in all Ct-values detected with different RNA templates of different mixed populations of nematodes. According to this, Pgk-1 was not considered in the following measurement any further.

EFFICIENCIES Differences in the PCR reaction efficiencies of target and housekeeping genes can cause false expression ratios. Hence, it is necessary to analyze the efficiency of every primer pair used and to detect the range of template concentration in which the relation of template concentration and determined Ct-value are linear. Additionally, the detection of the efficiencies allows to calculate fold-changes with an efficiency corrected mathematical model as described below (equation 2.2 and 2.4) [172]. The efficiencies were detected by the analyses of five different template concentrations ranging from 100 ng to 0.01 ng. A total RNA preparation of a mixed population (all developmental stages present) was used to analyze the efficiencies of qRT-PCR. Every template concentration was measured in triplicates. The determined Ct-values are plotted against the logarithm of the template concentration. With the slope of a linear fit of the Ct-values, the efficiency of the reaction can be calculated according to equation 2.1, where E is the efficiency and a the slope of the fit.

$$E = 10^{-a} - 1 \tag{2.1}$$

Figure 2.13 shows the determination of the efficiency for the housekeeping genes Act-1 and Daf-21. In table 2.7 all efficiencies used in the evaluation of the qRT-PCR data are listed, the corresponding fits are depicted in figure 5.3 in the appendix.

For all primer pairs efficiencies of approximately 1 were yielded. This means that all reactions proceed with 100 % efficiency. An exception is the primer pair for Hsp12.6. It's efficiency amounts 1.12, which is slightly enhanced but still in the tolerable range of efficiencies detected for qRT-PCRs [223].

Table 2.7: Overview of the detected efficiencies of all primer pairs used in qRT-PCR analyses in this work.

Primer pair for	Efficiency of the amplification
Hsp12.1	1.04
Hsp12.2	1.02
Hsp12.3	1.03
Hsp12.6	1.12
Hsp25	0.91
ZK1128.7	1.06
Act-1	1.07
Daf-21	0.98

EXOGENOUS CONTROL Besides the endogenous controls (housekeeper or housekeeping genes), AlienRNA from Stratagene was used as exogenous control. This control allows to analyze the quality of the RNA and determine inhibitors or reaction enhancing substances. Additionally, AlienRNA allows to analyze for the variation of housekeepers [43]. AlienRNA itself is a poly-adenylated *in vitro*-transcribed RNA, delivered with highly specific primers. There is no indicative homology of the AlienRNA to any other known mRNA, which ensures that there will be no cross reactions between AlienRNA primer and other mRNAs in the reaction batch. Reaction batches with AlienRNA were prepared as described in the user manual and measured in triplicates [59].

For all qRT-PCR experiments, the total RNA were prepared out of liquid nitrogen-frozen worms as described in 4.2.1. qRT-PC reactions were prepared either with fresh purified RNA or a single frozen aliquot 4.2.1. Test measurements revealed that the freezing step does not influence the RNA quality (data not shown).

2.2.2 EVALUATION OF POTENTIAL HOUSEKEEPING GENES

As mentioned above, two potential housekeeping genes were analyzed in this study more closely. Requirements presented to a housekeeper to analyze developmental stages are extensive. In the nematode, the progress of development is characterized, what simplifies the identification of a proper housekeeper or reference gene. According to the literature, actin is a suitable reference [175, 75]. Act-1 is essential in the early embryonic development and is afterwards needed for the integrity of several muscle cells in the nematode, this indicates that the expression should be stable over the different stages [132, 197, 247].

Daf-21 seems to be of special interest as housekeeper with respect to the also planed analysis of different stressors (s. below 2.2.5, 2.2.10). Gaiser et al. showed that the expression of Daf-21 was stable upon heat stress. To analyze the quality of potential housekeeping genes, the total copy number of each gene was calculated by normalization to the AlienRNA (fig. 2.14). Equation 2.2 was used to calculate the ratio of the potential housekeepers normalized with respect to the AlienRNA in one sample. Since the total copy number of AlienRNA is

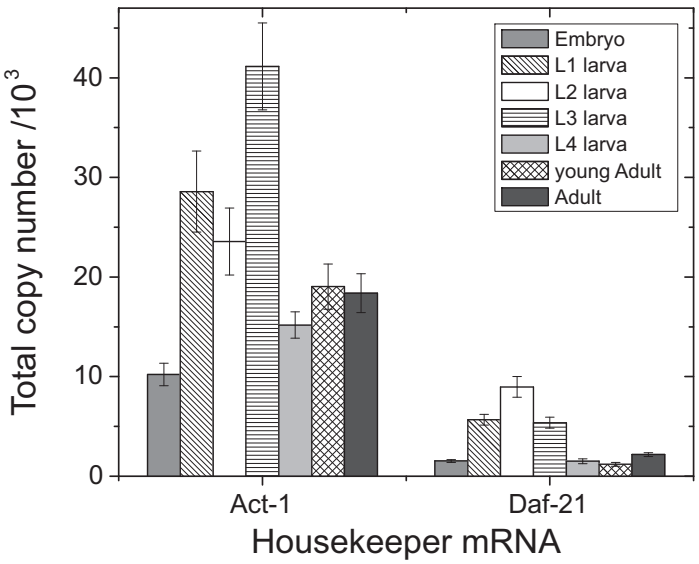

Figure 2.14: Total copy numbers of Act-1 and Daf-21 in 10 ng total RNA preparation of the different development stages of the nematode. Values for the embryo state are colored in gray, L1 larva is patterned with lines of negative slope, L2 larva is white, L3 larva patterned with horizontal lines, L4 larva is depicted in light gray, the young adult samples are filled with rhombus patterns and the adult samples are dark gray.

known, the amount of mRNA of interest can be easily calculated using equation 2.3.

$$amount = (E_{gene} + 1)^{\Delta Ct} \tag{2.2}$$

$$total\ copy\ number = (E_{gene} + 1)^{\Delta Ct} \cdot N_{Alien} \tag{2.3}$$

The ΔCt in equation 2.2 and 2.3 is the difference between the Ct-values of the gene to be analyzed and the gene used for normalization in one sample. N_{Alien} stands for the total copy number of the applied AlienRNA amount.

Comparison of the amounts of the housekeeping genes in the different development stages shows that the expression levels are changing tremendously. For Act-1, the mRNA levels increased from embryo to the L3 larval stage. In the L4 larval stage, the mRNA level of Act-1 was reduced again and stayed stable for the young adult and adult sample. This indicates that the Act-1 only suits as housekeeper for the last three development stages of the nematode. This can be due to the fact that at the end of the L2 larval stage the last 14 body wall muscle cells are generated [211]. The expression patterns of Daf-21 followed a corresponding scheme as seen for Act-1. However, Daf-21 expression reached a value of mRNA copies in the L4 larval stage that is comparable to the embryonic stage.

Based on the differences of Ct-values of different samples, the change of the mRNA level between two different conditions/stages (fold-changes) can be calculated by an efficiency corrected mathematical method according to equation

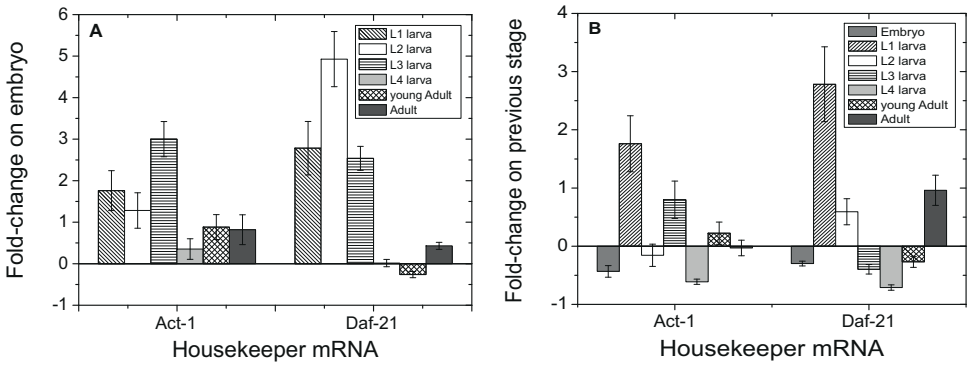

Figure 2.15: Fold-changes of Act-1 and Daf-21 in different development stages of the nematode. A Shows the fold-changes normalized with respect to the embryonic stage and B depicts the normalization with the respective preceding developmental stage. The columns are colored according to the stage that is normalized. For example, all samples of the L2 larva normalized with respect to the embryonic stage or the previous L1 larval stage are colored white. According to this, the embryonic fold-changes are colored in gray (only in B), L1 larva is patterned with lines of negative slope, L2 larva is colored white, L3 shows horizontal lines, L4 larva is depicted in light gray, young adults marked by rhombus patterns, and the adult samples are colored in dark gray.

2.4 [172]. All depicted fold-changes are corrected to zero to illustrate de- and increasing changes. So an increase in mRNA of 100 % is reflected by a fold-change of 1.

For a better interpretation of the determined amounts of the housekeeping genes (s. above), the fold-changes of their expression between the different developmental stages were calculated. Figure 2.15 depicts the fold-changes when normalized with respect to the embryonic stage in A and the normalization to the respective, previous development stage in B, respectively.

$$Fold - change = \frac{(E_{gene} + 1)^{\Delta Ct_{gene}}}{(E_{Alien} + 1)^{\Delta Ct_{Alien}}} \tag{2.4}$$

The ΔCts are the difference in the measured Ct-values of the sample to be analyzed and the reference sample. E_{gene} and E_{Alien} stands for the efficiencies of the reaction of the analyzed genes (gene) and the reference mRNA (Alien).

The fold-changes which are normalized with respect to the embryonic stage clarify the observations described for the total copy numbers of both tested housekeepers. After an increase of the expression in the L1 to L3 larval stage of Act-1, the expression reached an overall constant expression level in the last three development stages. Minor changes in the expression are more pronounced in the normalization with respect to the preceding development stage in figure 2.15 B, as there are only small differences between the L4 larval and the young adult stage (bar with rhombus pattern), and the young adult and adult stage (dark gray bar). In the case of Daf-21, the changes are even more pronounced as for Act-1. For example, the mRNA amount is increased 5-fold in the L2 larva compared to the embryo. In the L1 larva, the amounts rose up to the 4-fold.

The "eleven golden rules of quantitative RT-PCR" demand that housekeeping genes are only allowed to have an averaged range of ± 1 cycles. This would

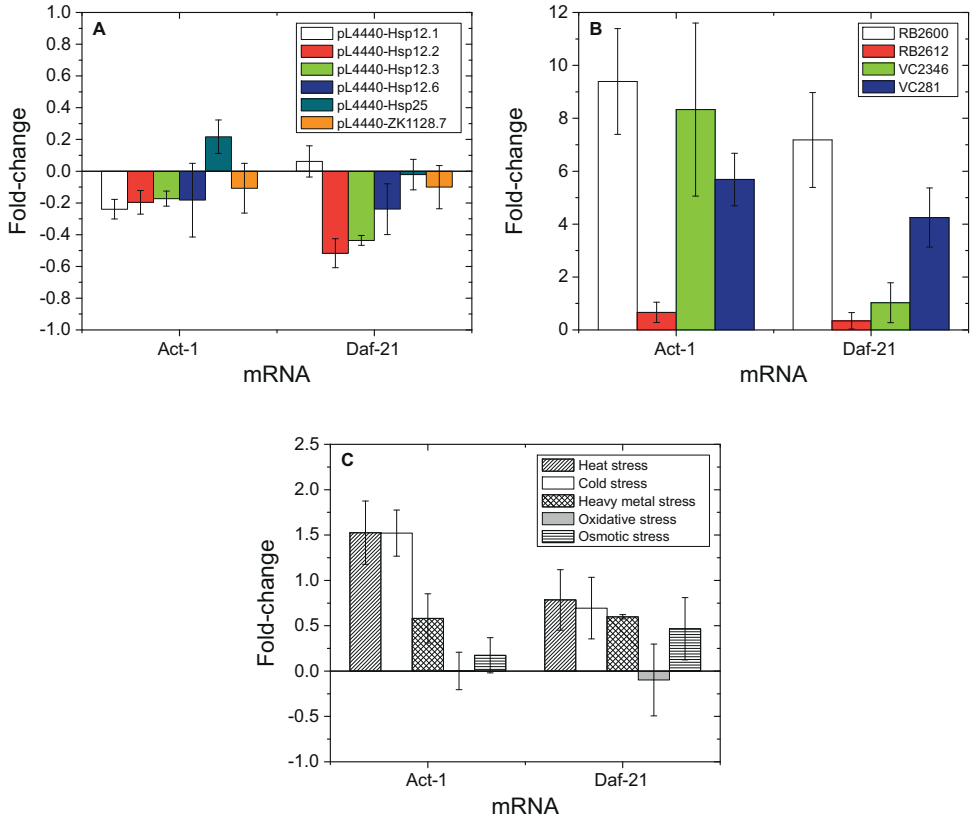

Figure 2.16: Fold-changes of Act-1 and Daf-21 in all further performed qRT-PCR experiments. Results for the RNAi treated worms are depicted in A, analysis of the knock-out strains in B, and the effect of different stressors in C. In A and B, the analyzed templates originating from RNAi treatment and knock-out worms are colored according to the introduced color scheme. Hsp12.1 is white, Hsp12.2 red, Hsp12.3 green, Hsp12.6 blue, Hsp25 cyan, and ZK1128.7 orange. The different stress conditions are patterned with lines of positive slope (heat), white (cold), rhombus (heavy metal), light gray (oxidative), and horizontal lines (osmotic).

mean that fold-changes up to 50 % are allowed in the housekeeping genes [223]. This does not hold true for all developmental stage analyses for both tested housekeepers.

For all other conducted qRT-PCRs, the exogenous controls were also analyzed concerning their potential housekeeper capabilities. Figure 2.16 shows the gained fold-changes for the templates of the RNAi analyses (A), the knock-out analyses, and the characterization of different stressors (C). All depicted fold-changes are normalized with respect to the particular negative control: for RNAi experiments, control worms were fed on pL4440, Ct-values from knock-out strains, and stressed nematodes were corrected with respect to the wild type or unstressed worms, respectively.

For the RNAi-treated nematodes, the changes in both housekeepers are quite low and range from -0.2 to 0.2 in the case of Act-1 and from -0.5 to 0.08 in the case of Daf-21. For this experiment especially Act-1 is suited as housekeeping gene.

Figure 2.16 B depicts the changes for Act-1 and Daf-21 for the Hsp12-family knock-out strains. Since RNAi experiments are often conducted to mimic knock-outs, the observed changes on both housekeeping mRNA levels are unexpected. Only the results for RB2612, the Hsp12.2 deficient worm, are decent in both housekeepers. Small changes below 1 are determined for these to samples. When compared to the wild type sample, a 9- to 8-fold upregulations of Act-1 and Daf-21, respectively, was observable in RB2600 (Hsp12.1 knock-out). Additionally, upregulations in both genes were detectable for the Hsp12.6 knock-out (VC281). Furthermore, Act-1 is notably upregulated in VC2346 (Hsp12.3 knock-out). Daf-21 showed only a minor increase in this strain. For what reasons the expression of the housekeeping genes Act-1 and Daf-21 show these great differences in the Hsp12 protein knock-out strain is unknown and unexpected. The only exception is the knock-out strain of Hsp12.2, where small changes below 1 were detected. However, regarding the properties that housekeeping genes ask for, these changes are too large to be considered as suitable housekeeper in the comparative analysis of the knock-out strains of the Hsp12-family.

The expression pattern of the Hsp12-family, Hsp25 and ZK1128.7 should be analyzed upon different stress conditions. Figure 2.16 C gives the summary of the fold-changes upon different stress conditions. The exact conditions are depicted in table 2.9. The overall changes of Daf-21 are quite low and do not exceed 1, which would correspond to a doubling of the mRNA amount. Still, this amount of change is too high to be used as housekeeper. Act-1 also shows small or even no fold-changes for heavy metal, oxidative and osmotic stress. Upon heat and cold stress, the mRNA levels are increased by the 1.5-fold, which is again not suitable for a housekeeping gene.

Summarizing the results depicted in figures 2.14 to 2.16, none of the tested housekeepers is suitable for all qRT-PCR analyses. To keep the clarity and the comprehensibility of the following results of qRT-PCR experiments, only fold-changes that were calculated using AlienRNA as control will be discussed. Simultaneously, this will only allow a careful interpretation of small changes between no change and 1-fold, because for such an analyses, normalization with respect to at least two robust housekeepers is needed [232].

2.2.3 Characterization of the Expression Patterns of the Hsp12-family

Ding and Candido (2000) analyzed the localization and expression of the sHsps of the Hsp12-family via immunohistochemical approaches [54]. For the Hsp12-family, all members were stained with a poly-clonal Hsp12.6-antibody. They verified that the members of the Hsp12-family were at its maximum in the early larval stages and reaches a minimum in the adult nematode [54, 140].

For a further understanding of the expression patterns during the development cycle, qRT-PCR experiments were performed. The advantages of this approach are the possibility to design primers which are specific for each member of the Hsp12-family. This allows an analysis of each single member of the Hsp12-family, which was not possible with the poly-clonal antibody used by Ding et al. [54]. It is important to clarify that with qRT-PCR measurements only the mRNA

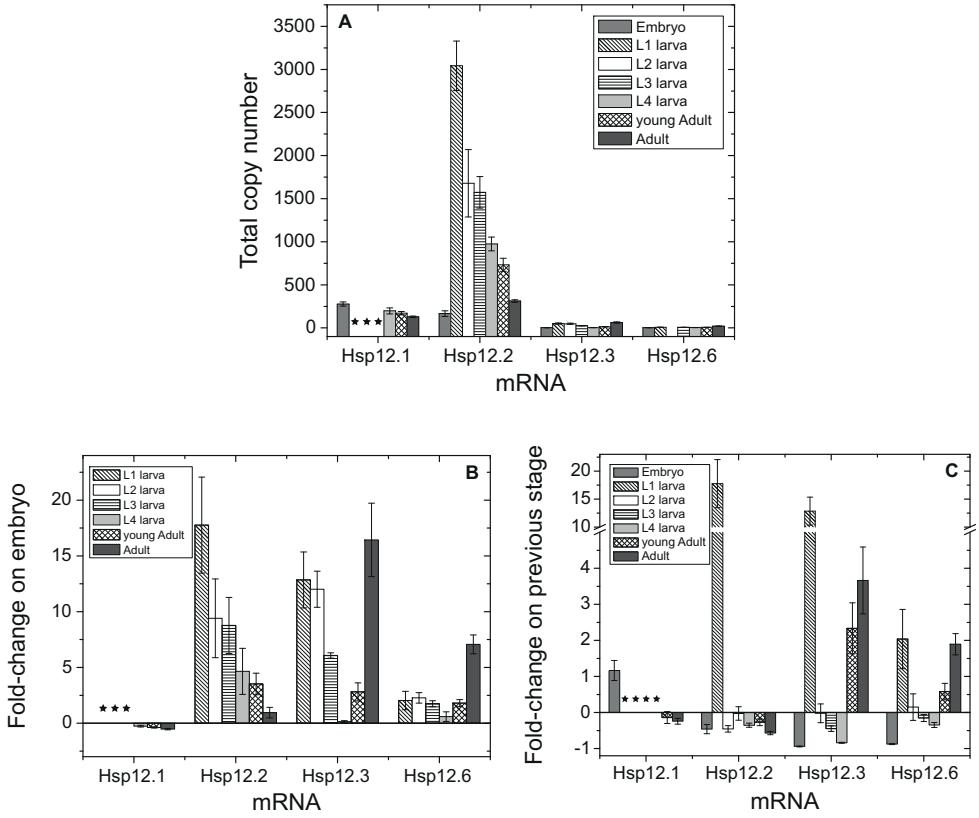

Figure 2.17: Total amount of the mRNA of the different members of the Hsp12-family in different development stages (A) and their fold-changes (B, C). Total copy numbers and fold-changes for the embryo stage are depicted in gray, L1 larva with lines of negative slope, L2 larva in white, L3 larva with horizontal lines, L4 larva in light gray, young adult with rhombus pattern and adult in dark gray. Values that could not be determined are marked with a black star.

levels of a protein are detected. This corresponds to some extent with protein expression but does not necessarily reflect the true amount of protein of each gene analyzed.

To determine the expression pattern in all development stages of *C. elegans* nematode populations were synchronized according to 4.2.4. At least 30,000 worms were used to prepare one total RNA sample for each developmental stage (embryo, L1-4 larvae, young adult, adult). The different developmental stages were distinguished by their growth time at 20 °C and, especially in the case for L4 larva, young adult and adult worms by their anatomic features. All samples, except the embryo sample, were fed on *E. coli* bacteria, before the total RNA preparation. The embryo sample was gained by bleaching of a synchronized nematode population at day four after hatching (fig. 1.11). 10 ng of the total RNA preparations were used as template in the qRT-PCR measurement.

Figure 2.17 shows the total amount of mRNA in the different development stages (A), their fold-changes normalized to the embryo sample (B), and the respective previous development stage (C).

Table 2.8: Total copy numbers of mRNA coding for the Hsp12-family of *C. elegans*. Values which were not determinable are marked with n.d..

	mRNA copies in 10 ng total RNA preparation of			
Stage	Hsp12.1	Hsp12.2	Hsp12.3	Hsp12.6
Embryo	276 ± 24	167 ± 33	4 ± 1	2 ± 1
L1 larva	n.d.	3043 ± 187	50 ± 8	8 ± 2
L2 larva	n.d.	1678 ± 392	48 ± 7	8 ± 1
L3 larva	n.d.	1574 ± 182	26 ± 3	7 ± 1
L4 Larva	198 ± 34	975 ± 34	4 ± 1	4 ± 1
young Adult	172 ± 19	732 ± 76	14 ± 3	7 ± 1
Adult	129 ± 8	312 ± 15	63 ± 8	19 ± 1

Overall, Hsp12.2 showed the highest mRNA expression throughout all developmental stages. For a better comparison, the values of figure 2.17 are summarized in table 2.8. The amount of Hsp12.1 in the first three larval stages is not determinable and marked either with a black star (fig. 2.17 A) or with n.d. (tab. 2.8), respectively.

The fact that expression values for Hsp12.1 mRNA could not be determined in the first three larval stages indicated that this protein is only expressed in small amounts or absent in these stages. However, mRNA for Hsp12.1 is present in the other development stages, with its highest value during the embryonic stage. Hsp12.2 has a different pattern of expression. While the amount is similar to the value obtained of Hsp12.1 in the embryonic stage, its expression increases in the following larval stages with the highest level in L1 larvae. The expression rate decreases 10-fold from the L1 larval to the adult stage. Hsp12.3 as well as Hsp12.2 showed the highest amount of mRNA in the L1 larva. After a decrease in the L2, L3 and L4 larval stage, the expression rose again in the young adult and adult stages. Hsp12.6 was the Hsp12 protein with the lowest expression. The mRNA level of Hsp12.6 increased in the L1 and L2 stage and reached its highest level in the adult worm. Since the expression levels were very different within the Hsp12-family, their comparison by calculated fold-changes draw a more lucid picture. The calculated fold-changes normalized to the embryo (B) and the respective previous development stage (C) are depicted in figure 2.17.

Hsp12.2's expression was highly increased in the L1 larva and decreases with increasing age of the nematode. This corresponds to the immunohistological data of Ding and Candido (2000) [54]. The expression patterns of Hsp12.3 and Hsp12.6 showed some similarities. Both proteins had high expression in the L1 larva stage, which decreased until the forth larval stage. Afterwards the expression was increasing again. Compared to Hsp12.6, Hsp12.3 showed more pronounced changing within this pattern.

Ding and Candido, and Leroux and co-workers determined that the Hsp12-family is mainly expressed in the early larval stages throughout the whole worm [54, 140]. With increasing age, the expression patterns changed from an ubiquitously expressed protein family to more specific localizations within the reproductive tissues. There, members of the Hsp12-family were localized in specific vulva cells, vulval muscle cells, and in the sperm in hermaphrodites. In male

worms, especially the male germ cells were labeled extensively, which led to the assumption that the Hsp12 proteins are located in the spermatids and possibly in the spermatocytes [54].

With respect to the data obtained in this thesis, these results suggest that Hsp12.3 and Hsp12.6 are important in the reproduction process of *C. elegans*. The uniform change in the expression pattern of these two proteins and the close sequence relationship give rise to the assumption that both proteins perform comparable functions and may even have compensatory effects on each other. However, Hsp12.2 seems to be more involved in the development process of the nematode. It is however not possible to draw a conclusion for Hsp12.1 from the presented data.

These results show that the question of expression and specificity of the members of the Hsp12-family is not easily answered to determine. The expression patterns need a more detailed analyses to verify these assumptions. One possible way to further address this question is to generate transgenic nematodes with Hsp12 proteins fused to a fluorescent protein. The expression patterns are analyzable in nematodes that are modified in this way if a specific Hsp12 promoter is used. Furthermore, the effect of different influences like aging and stressors can be determined easily.

2.2.4 Characterization of the Gene Knock-Downs of the Hsp12-Family

Specific gene knock-down can be achieved by injection of specific RNA into living organisms. This effect is called RNA interference (RNAi) and was developed by Andrew Z. Fire and Craig C. Mello [222]. In principle, the administration of double stranded RNA (dsRNA) via injection, soaking or feeding of bacteria containing the DNA sequence of gene of interest on a plasmid, respectively, leads to gene inactivation. This inactivation is achieved by the specific degradation of the target mRNA. The effect of RNAi is spread throughout the different tissues of the worm and even in its progeny. Exceptions of this rule are a few neuronal cells, which are resistant to this kind of gene silencing [32]. In this work the feeding approach was used (s. 4.2.4). The RNAi constructs pL4440-Hsp12.1, pL4440-Hsp12.2, pL4440-Hsp12.3, pL4440-Hsp12.6, pL4440-Hsp25, and pL4440-ZK1128.7 were purchased from Fisher Scientific. All RNAi constructs were tested for their correct sequence and stored as glycerol stocks at −80 °C. Every RNAi bacterial culture used were freshly inoculated from the glycerol stocks. To test the effect of dsRNA feeding, twenty adult nematodes were analyzed by western blot analysis. The detection of Hsp12.1/Hsp12.2 and Hsp12.3/Hsp12.6 was conducted with poly-clonal Hsp12.1 and Hsp12.6 antibodies, respectively. With both antibodies, a reduction in the protein levels was detectable after RNAi treatment verifying the principle of RNA interference.

qRT-PCR To analyze the effect of knock-down of one member of the Hsp12-family on the expression of the three remaining Hsp12 proteins, qRT-PCR were conducted according to the protocol described in 4.2.1. The analyses were performed with the normalization procedure using the exogenous control AlienRNA.

The effect of RNAi was analyzed in late L3 larvae. In this development stage the worms fed for one day on dsRNA containing bacteria and the RNAi effect should be completely evolved. Supplemental, the amount of all members of the Hsp12-family - especially with respect to Hsp12.1, which mRNA level was not detectable in the L3 larval but in the L4 larval stage - should be in a detectable ranges. Figure 2.18 depicts the results of the qRT-PCR analyses.

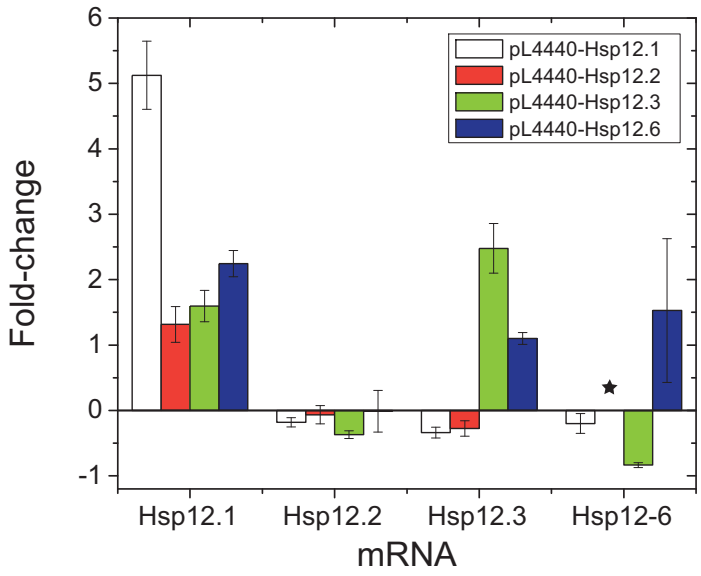

Figure 2.18: Fold-changes of Hsp12-family in dsRNA fed nematodes. All results for the pL4440-Hsp12.1 fed worms are colored in white, pL4440-Hsp12.2 in red, pL4440-Hsp12.3 in green and pL4440-Hsp12.6 in blue. The black star labels not calculable changes due to Ct-values out of the reliable data range.

The mRNA level of Hsp12.1 increased 5-fold upon RNAi treatment against Hsp12.1. When the other members of the Hsp12-family were down-regulated, the expression of Hsp12.1 also rose slightly. Hsp12.2 shows no changes in the mRNA-levels. RNAi treatment against Hsp12.1 and Hsp12.2 led to a slight decrease in the mRNA levels of Hsp12.3. Knock-down of Hsp12.3 and Hsp12.6 however increased the mRNA levels of the same gene. The transcription of Hsp12.6 was impaired slightly upon feeding of pL4440-Hsp12.1 and strongly upon feeding of pL4440-Hsp12.2 and pL4440-Hsp12.3. In the Hsp12.2 down-regulated population the detected Ct-value for Hsp12.6 was very low and not in the reliable range of the data, so no fold-change was calculable (fig. 2.18 black star). In general, small fold-changes below 1-fold upregulation as observed here, are difficult to interpret and may not be reliable when compared between several biological replicates. Thus the changes of mRNA-levels in between that range are regarded as 'no changes' and will not be discussed further.

The fact that RNAi treatment against Hsp12.1 led to an increase in the mRNA amount of the target gene was very unexpected. In the western blot analysis a decrease of the protein level was detectable. Since, under RNAi treatment the mRNA of the specific gene analyzed should be degraded, the revealed increase

is unexpected. Several reasons could be responsible for these observation. After feeding of dsRNA containing bacteria, the worms are washed of the remaining bacteria in the solution. To exclude false positive detection of dsRNA remaining in the harvested worm culture, all nematodes were incubated for 1.5 h at 20 °C to allow a final digestion of the bacteria eaten by the worms. If the RNAi effect is not that strong, this incubation time could be enough that the RNAi effect is less observable. Additionally, a development independent negative feedback regulation of gene expression of Hsp12.1 could be a reason for the increases observed. Thus, the degradation of Hsp12.1 would lead to an increased transcription rate of the corresponding mRNA. A constant expression of the gene within the developmental stage would be possible, with such a regulation mechanism. The same could be true for the expression of Hsp12.3, as the mRNA level is also increased upon RNAi treatment against this gene. Furthermore, during the preparation of the mRNA the worms are incubated for one hour at 20 °C to digest remaining bacteria after the harvesting procedure. Maybe the expression of the Hsp12-family is highly upregulated in this time span to compensate the previous down-regulation.

Since no information about the expression regulation of the Hsp12-family is available, this could be a first clue for a regulation processes.

LIFESPAN Further characterization of the RNAi effect was performed with the detection of the lifespan of RNAi treated worms. Since the function of none of the Hsp12 proteins is known, differences in the lifespan compared to RNAi untreated worms can give a clue for potentially affected systems in the nematode. The livespan assay was conducted twice with 20 individuals as described in 4.2.4. Only worms which could be examined as alive or dead were accounted in this assay. Figure 2.19 shows the average survival rates of both experiments. The empty RNAi vector pL4440 was used as negative control.

The average lifespan for all analyzed nematodes was approximately 13 days. This value is at the lower end of the reported range of averaged lifespans for N2 hermaphrodites, which encompasses 11.8 to 20 days [231, 119]. The averaged lifespan detected of the dsRNA against members of the Hsp12-family only differed slightly from the value determined for the pL4440 fed nematodes. The control and Hsp12.2 down-regulated nematodes revealed the same average lifespan of 13.5 days. pL4440-Hsp12.1 and pL4440-Hsp12.3 fed nematodes lived for about 12.5 days, which is, in average, one day shorter than the control worms. pL4440-Hsp12.6 worms had the shortest average life time with 11.2 days. All these values are within the standard deviation of the control sample, thus it can be assumed that the RNAi treatment against the Hsp12-family has no effect on the nematode's lifespan.

THRASHING BEHAVIOR During the lifespan assays it was recognized that the worms, treated with dsRNA against the members of the Hsp12 proteins, show a decrease in their motility. To verify this observation, thrashing assays were performed as described in 4.2.4. Six individual worms of every RNAi treatment were transferred in a drop of M9 buffer. If the worms were swimming freely in the liquid, the thrashings were counted for one minute. Only a complete sinusoidal movement of the body was counted as thrashing. During these

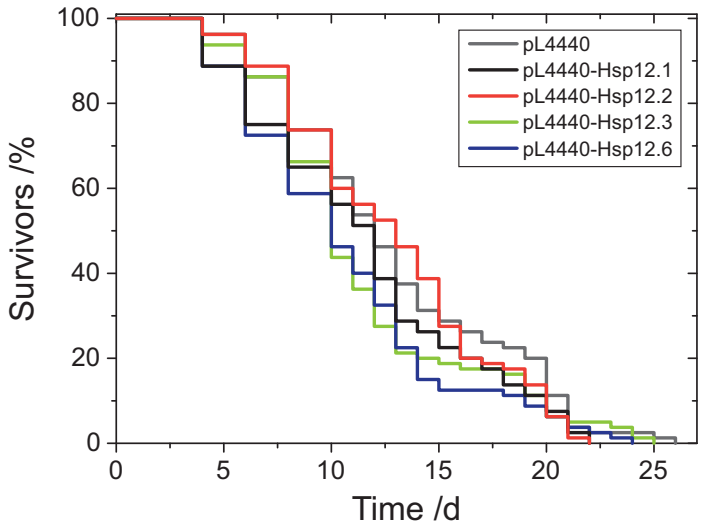

Figure 2.19: Reduced Hsp12.1, Hsp12.2, Hsp12.3, or Hsp12.6 expression levels have no effect on the lifespan of hermaphrodites. A Kaplan-Meier plot comparing the effect of different RNAi constructs. The lifespan of 40 individuals in total was analyzed after hatching at 20 °C. RNAi effect was gained by feeding different RNAi constructs in *E. coli* HT115. The average lifespan was determined to be 13.5 ± 1.6 days for pL4440 fed hermaphrodites (gray), 12.3 ± 0.1 days for pL4440:Hsp12.1 fed (black), 13.5 ± 0 days for pL4440:Hsp12.2 fed (red), 12.2 ± 1.3 days pL4440:Hsp12.3 fed (green), and 11.2 ± 0.7 days for pL4440:Hsp12.6 fed hermaphrodites (blue).

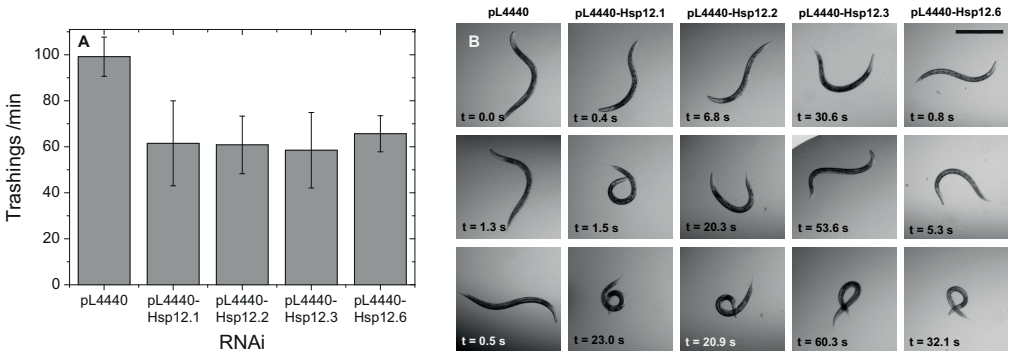

Figure 2.20: Thrashing assay of RNAi against Hsp12.1, Hsp12.2, Hsp12.3 and Hsp12.6 treated wild type worms. A depicts the total thrashings in one minute and B shows characteristic movements during the elicitation of the thrashing data.

experiments, the constrained movement of the Hsp12 knock-down worms was even more pronounced. Figure 2.20 A depicts the average of total thrashings in one minute of six individual worms. The negative feeding control (pL4440) showed approximately 100 thrashings, which are comparable to the numbers determined for wild type nematodes [29, 1].

The thrashing of the nematodes, which were fed with dsRNA against one of the Hsp12 proteins, were significantly reduced in the thrashing numbers. It was recognized that the Hsp12 dsRNA-treated worms tend to overbend their bodies during the analyses. This overbending leads to a complete curling of the nematodes' body. Additionally, this curling is often foregone by spastic-like trembling of the whole body. This movement can reflect the uncoordinated movement of head and tail described by Ackley and co-workers (2003) [1]. The nematodes behave like wild type worms and thrash with smooth swimming movements in between the curling and trembling movements. Figure 2.20 B shows three representative pictures of a photo series taken of each dsRNA-treated hermaphrodites.

In 2003, Ackley et al. described the observed overbending and body curling phenotype during the characterization of nidogen and type XVIII collagen deficient nematodes (*nid-1* and *cle-1* worms). Both proteins are components of the basement membrane in *C. elegans* and are required for the correct formation of neuromuscular junctions [1]. Thrashing of *nid-1* and *cle-1* worms were characterized by the same impairment as described in the experiment above (2.20). This allows to conclude that the neuronal system is somehow impaired in the RNAi treated worms. A direct effect on the muscular structures is unlikely because no localization of the Hsp12-family within the muscle cells were described until now. To verify this conjecture, it is necessary to characterize the observed mild phenotype more closely.

2.2.5 Effect of different stressors

In vitro studies of the Hsp12-family revealed a classical chaperone activity for Hsp12.1 only (2.1.7). However, the question about the functions of the Hsp12-family members remains. To address the question whether the activity of the Hsp12 proteins are triggered by different stressors, L3 larva were treated with heat, cold, heavy metal, oxidative, and osmotic stress, respectively. The different stress conditions are described by Gaiser et al. (2011) [75, 246, 135, 31, 168]. Comparable analyses were conducted by Leroux et al. for the characterization of Hsp12.6. In this study, they treated L1 larvae with different stress conditions for osmotic, oxidative, heavy metal, heat, and cold stress for 1.5 h. In western blot analyses, no change in the protein amount of Hsp12.6 was observed [140].

Table 2.9 gives an overview of the different stress conditions applied to the nematodes. All worms were harvested and treated as described above after the stressing procedure (4.2.1).

The results of expression analyses for the different stress conditions applied are depicted in figure 2.21. Hsp12.1 shows a significant decrease of expression compared to the unstressed worms. In contrast to the strongly down-regulated expression of Hsp12.1, Hsp12.2 shows an almost stable expression independent

Table 2.9: Overview of the different stress conditions applied on wild type nematodes [75, 246, 135, 31, 168].

Stress	Condition	Timespan
Heat	water bath, 35 °C	120 min
Cold	cold room, 4 °C	300 min
Heavy metal	10 mM $CdCl_2$, 20 °C	120 min
Oxidative	2 mM H_2O_2, 20 °C	180 min
Osmotic	NGM plates with 0.5 M, 20 °C	360 min

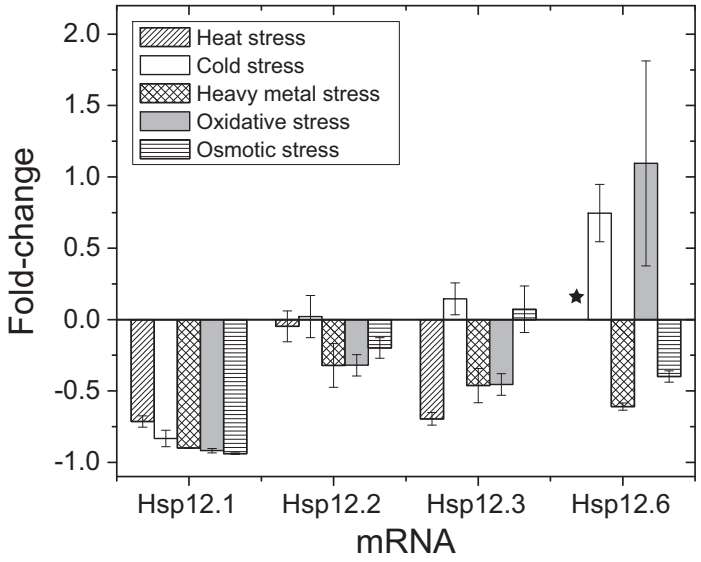

Figure 2.21: Effect of different stressors on the expression on the Hsp12-family. Fold-changes normalized to an unstressed N2 nematode sample. Results of the heat-stressed samples are patterned with lines of positive slope, cold stress in white, heavy metal stress with rhombus pattern, oxidative stress in light gray and the osmotic stress with horizontal lines.

of the stress conditions applied. The results for Hsp12.3 show a mixed picture of stress-induced changes. Upon cold and osmotic stress, the expression is not changed as compared to the unstressed sample. However, the expression of Hsp12.3 in heat, heavy metal, and oxidative stressed samples is decreased. Astonishingly, the expression of Hsp12.6 was not as stable as expected. For heat stress, no value in the range of confident data was detectable (black star). This is giving rise to the assumption that Hsp12.6 is massively down-regulated. Downregulation was also detectable for heavy metal and osmotic stress conditions. In contrast to this, the expression is slightly increased upon cold and oxidative stress.

In general, all observed changes are very small and have to be further verified. As for Hsp12.6, no change in protein levels was detected upon treatment with different stress condition [140]. It is most likely that the Hsp12-family is not influenced in their expression by different stress conditions. This leads to the hypothesis that the Hsp12-family is specific for different developmental stages. And only Hsp12.6 is slightly up-regulated by cold and oxidative stress.

2.2.6 Characterization of *C. elegans* knock-out strains

Further characterization of the *in vivo* function of the Hsp12-family was conducted with the analysis of the knock-out worms received from the Caenorhabditis Genetics Center (CGC). In the following chapter all knock-out worms will be described with their strain names, consisting of two letters and three to four numbers. The letters refer to the laboratory the strain originates from and the number is the allele prefix [98]. The knock-out strain analyzed of Hsp12.1 (RB2600) originates from Barstead's laboratory in the Oklahoma Med Research Foundation (Oklahoma City). It is homozygous and carries an approximate 400 bp deletion on chromosome I, which corresponds to a complete deletion of the Hsp12.1 coding sequence. The Hsp12.2 knock-out RB2612 comes from the same lab and has a deletion of about 400 bp located on chromosome III. In this deletion not the total coding sequence of the protein is deleted. The deletion spans approximately two thirds of the gene locus and cuts off the sequence after the first intron. The knock-out strains for Hsp12.3 (VC2346) and Hsp12.6 (VC281) were generated in Gilchrist's laboratory at the *C. elegans* Reverse Genetics Core Facility (Vancouver). VC2346 carries a deletion of 533 bp on chromosome IV and VC281 is described as superficial wild type. The CGC website does not provide further information on this strain. In both strains, the complete gene loci of the respective Hsp12 protein are missing.

qRT-PCR A complex picture of down- and up-regulation within the Hsp12-family was shown by the characterization of the knock-out strains with qRT-PCR (fig. 2.22). The expression of Hsp12.1 seemed to be reduced in all knock-out strains, except VC281. In this strain, a slight increase in the mRNA level of Hsp12.1 was detected. Hsp12.2 showed the largest differences in between the knock-out strains. In RB2612 the expression was notably reduced, as it was expected. In addition in VC2346, the expression was lower than in the wild

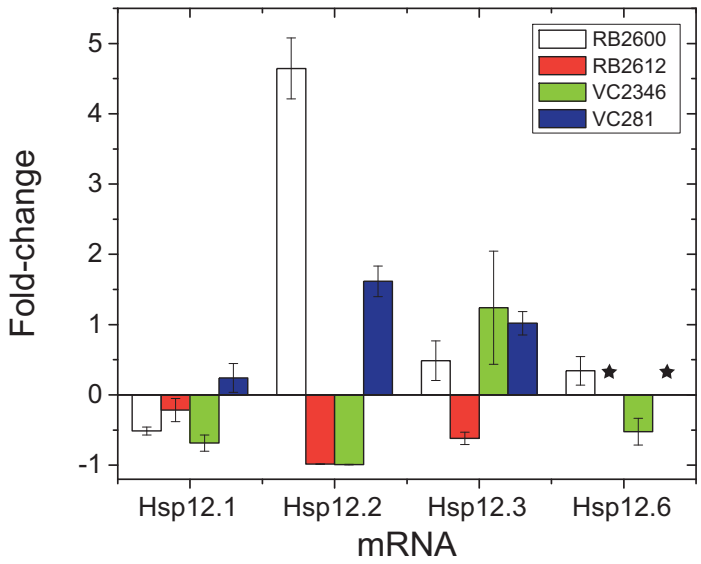

Figure 2.22: Results of the qRT-PCR analysis of the knock-out strains. Depicted are the fold-changes normalized to N2 wild type nematodes. Template of RB2600 is colored white, RB2612 red, VC2346 green, and VC281 in blue.

type strain. In the knock-out strains of Hsp12.1 and Hsp12.6, an increase in the expression of Hsp12.2 was detected. The increase corresponded to an approximately 5.5 and 2.5 fold-change. These pronounced changes may be due to compensation effects. In the case of Hsp12.1 this can be well explainable, hence Hsp12.2 and Hsp12.1 are closely related (2.1.1). Hsp12.3 exhibited no decrease of expression in the corresponding knock-out strain, rather an increase was observed. For RB2600 and VC281 the expression of Hsp12.3 increased as well. Interestingly, the expression decreased in the Hsp12.2 knock-out strain. The increased expression in its corresponding knock-out strain is unexpected, but is possible, since it is not known if VC2346 is homozygot. Similar to Hsp12.1 and Hsp12.2, Hsp12.6 showed very low or no expression (black star, fig. 2.22). This was also the case for the VC2346 template. In the RB2600 strain, the expression was slightly increased, mirroring the changes of Hsp12.1 in the Hsp12.6 knock-out strain VC281.

LIFESPAN ANALYSIS Likewise as for the dsRNA-treated worms, the lifespan of the knock-out strains was investigated. Figure 2.23 depicts the Kaplan-Meier plot of the lifespan analysis. The wild type hermaphrodites had an average lifespan of nearly 15 days, which is in good accordance with the literature and the detected value for the pL4440-fed worms in the RNAi lifespan experiment. The lifespans of RB2600 and VC2346 were decreased in comparison to the wild type (11.2 days and 10.9 days vs. 14.7 days). However, RB2612 and VC281 showed only slight decreases in the average lifespans.

The averaged lifespans of the knock-out strains compared to the results obtained from RNAi fed nematodes (2.2.4) are comparable for the negative con-

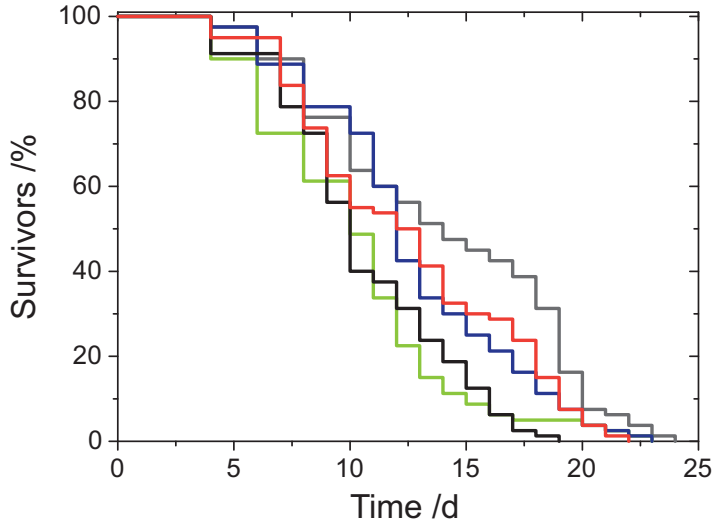

Figure 2.23: In knock-out worms for the Hsp12.1 and Hsp12.3 the lifespan is reduced compared to the wild type N2 hermaphrodites. Kaplan-Meier plot of *E. coli* OP50 fed knock-out and wild type worms. In total 40 individuals were analyzed after hatching at 20 °C for their lifespan. The mean lifespan is 14.7 ± 0.6 days for N2 hermaphrodites (gray), 11.2 ± 1.1 days for RB2600 (black), 13.1 ± 1.2 for RB2612 (red), 10.9 ± 0.2 days for VC2346 (green) and 13.2 ± 1.7 for VC281 worms (blue).

trols and Hsp12.2. For Hsp12.1 and Hsp12.3 the lifespan is more reduced in the knock-out strain compared to the RNAi fed nematodes. For Hsp12.6 opposing properties were determined. The RNAi-treated sample showed a more reduced lifespan than the knock-out.

Since the exact function of the Hsp12-family is not clear, the reducing effects on the lifespans in the knock-out strains can be explained by the mild phenotype of the RNAi-treatment (2.2.4). The neuromuscular junctions seem to be impaired by RNAi-treatment. The same effects could be true for the knock-out strain and reduces the averaged lifespans.

2.2.7 Phenotype Characterization of VC281

The knock-out strain of Hsp12.6 showed a specificity in expression in the analysis above (2.2.6). Immunohistological analyses showed that in the adult nematodes the expression is localized in the reproductive tissues. The location was determined to be in a few vulval cells and in the sperm of the nematode [140, 54].

The male rate increased significantly in VC281 populations after incubation and growth at 24 °C. Figure 2.24 shows a representative picture after the first appearance of this phenotype. In this population, the numbers of males can be estimated to be 50 - 60 %. Compared to the wild type worms, the increase is tremendous, since, only 0.1 - 0.2% of the total population are males in N2 populations.

Further analysis of the VC281 strain, which was grown at 24 °C, revealed that the amount of males decreased only very slowly during the following gener-

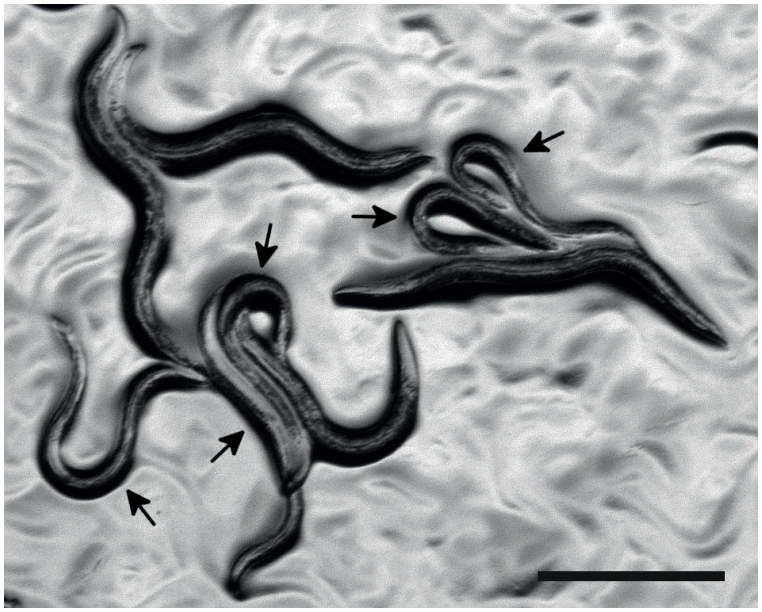

Figure 2.24: Representative picture of a VC281 population after growth at 24 °C. All male nematodes are labeled with black arrows. The scale bar correspond to 500 µm.

ations. All following generations were incubated at 20 °C to analyze if the rate of male nematodes decreases to normal levels again. After approximately six generations, the amount of males was still increased (fig. 2.25) and accounts for 20 % of all counted worms. This generation was also analyzed for their ability to reproduce the behavior of its ancestor population. After bleaching and growth at 24 °C, the ratio of males increased to 40 % of the total population again (fig. 2.25). This is not as high as observed in the ancestor population, but still remarkable.

It is generally accepted that males originate from the fusion of X-lacking (nullo-X) and X-bearing gametes [239, 96]. In 2003, Prahlad and coworkers described that the sexes can be changed post-embryonically. Cross-progeny of a hermaphrodite and a male were analyzed concerning their sexes on feeding on *E. coli* OP50 in log- or stationary phase. A progeny from self-fertilization was used as control. In the cross-progeny, an equal distribution of male and hermaphrodites were expected, but, surprisingly, were not observed under different feeding conditions [176]. Log-phase bacteria led to a 59 % male frequency compared to 49 % not effected cross-progeny. The authors assumed that the cross-progeny most likely looses one of their two X-chromosomes. For the direct evidence for that the paternal X-chromosome was GFP-labeled, which lead to fluorecent progeny, when both X-chromosomes are present in the nematode. With this approach it could be shown that *C. elegans* is able to change its sex and loose the paternal X-chromosome under certain feeding conditions [176]. It is not reported if other factors besides the different diets could cause this change until now.

Theoretically, the male and hermaphrodite larvae only differ in a few cells after hatching [148]. Additionally, the development of the sex specific reproductive tissue is different. Bread at 20 °C, VC281 populations have normal frequencies of

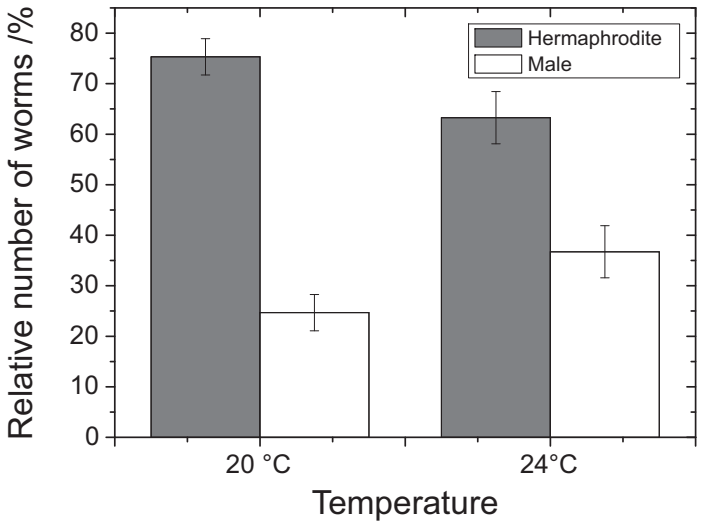

Figure 2.25: Amount of males in VC281 progeny populations grown at 20 °C and 24 °C for four days after bleaching, respectively.

males in their population. Subsequently it is likely that all nematodes analyzed are carrying double X-chromosomes.

In the experiments presented, only fertilized eggs with a defined sexual chromosome pairing were analyzed. Upon incubation at 24 °C the numbers of male increased massively to a ratio of 50 - 60 %. Thus, the increase in the male frequency seems to involve an impaired or changed cell fate by the deletion of Hsp12.6. In the following generation, a decrease to regular male frequencies was not observable. After six generations, the male nematodes still account for about 20 % of the total population. This is explainable by studies of Ward and Carrel (1979), which described that the male frequency is increased in populations with a high amount of males [239]. Their argumentation is based on the equal distribution of nullo-X and X-bearing gametes. If the observed increment of males in the progeny generations truly originates from the observation of Ward and Carrel, the meiosis in VC281 males has to be somehow influenced by the deletion of Hsp12.6, or, as suggested by Prahlad et al. (2003), one of the X-chromosomes is lost in the first two larval stages upon heat-treatment of the VC281 nematodes [239, 176].

The exact reason that led to the increased male frequency upon Hsp12.6 knockout, needs to be further analyzed. It is necessary to determine if VC281 worms loose one of their X-chromosomes upon incubation at 24 °C. For example, the same approach as performed by Prahlad et al. would be a suitable experiment. Furthermore, the genetic predisposition in the L1 larvae of the male features should be characterized.

2.2.8 EXPRESSION OF HSP25 AND ZK1128.7

As shown in 2.1.1, Hsp25 and ZK1128.7 belong to the sHsp-family of *C. elegans*. Hsp25 is a sHsp of *C. elegans* mainly expressed in the muscle cells, where it is associated with the dense bodies. Expression studies of Ding and Candido (2000) showed that this specific sHsp is located in the pharynx and the body wall muscle cells [55]. They could show that Hsp25 is localized with the dense-bodies and M-lines in the body wall muscle cells and assumed that Hsp25 interacts with focal adhesion structures. ZK1128.7 is a predicted sHsp of *C. elegans* that is not investigated in detail yet. Since the *in vitro* analysis of this member of the sHsp family was not possible – due to an insufficient recombinant expression (insoluble) and unstable refolded protein (data not shown) – the focus of characterizing this sHsp is laid on the *in vivo* characterization.

For Hsp25 and ZK1128.7, the same experiments as for the Hsp12-family were conducted. Figure 2.26 A depicts the total copy numbers of Hsp25 and ZK1128.7 mRNA in 10 ng total RNA preparation of nematodes in their different development stages and the corresponding fold-changes normalized to the embryonic stage (B) and to the preceding development stages (C).

The total copy numbers of Hsp25 are in average 5- to 10- times higher than the ones calculated for ZK1128.7, suggesting that Hsp25 is more abundantly expressed than ZK1128.7. Hsp25 had a very low expression in the embryonic state. Until the third larval stage the expression of Hsp25 increased massively, reflected by approximately 8-fold more mRNA as in the embryo. The mRNA levels of Hsp25 were quite stable in the three remaining developmental stages. Ding and Candido (1999) reported that Hsp25 is most likely involved in the maintenance, turnover, or assembly of focal adhesion structures. More specifically, an interaction with vinuclin and α-actinin could be determined. These two proteins are components of the dense bodies in the muscles of *C. elegans* [55].

The mRNA-levels detected of Hsp25 can be brought into good accordance with this hypothesis. Until the end of the L4 larval stage, the nematode undergoes large physiological changes. Post-embryonical 14 of the 95 body wall muscle cells are generated shortly before the molt from L2 to L3 larval stage [211]. Integration of these cells would need new adhesion structures and the increase in Hsp25 expression hints to this coherence. After the development of the musculature is finished, the expression of Hsp25 decreases to a constant level, which can be linked to the maintenance of the focal adhesion structures in the body wall muscle cells.

ZK1128.7 showed an overall increasing expression pattern. The lowest value is detected for the embryo stage and the highest for the adult stage. In the L1 stage the mRNA levels of ZK1128.7 seem to rise to a constant level, which showed a small increase in the L4 stage. Afterwards, the mRNA level increasdd again and peaks in the adult development stage of *C. elegans*. Since no information about the localization of ZK1128.7 is known, no linkage as in the case for Hsp25, can be assumed. Still, one can hypothesize that the importance of ZK1128.7 is increased with higher age of the nematode, because the total copy numbers were highest in the adult worm.

In the detected total copy numbers, Hsp25 is the second highest expressed sHsp of *C. elegans* in this work. ZK1128.7 revealed total amount in the range

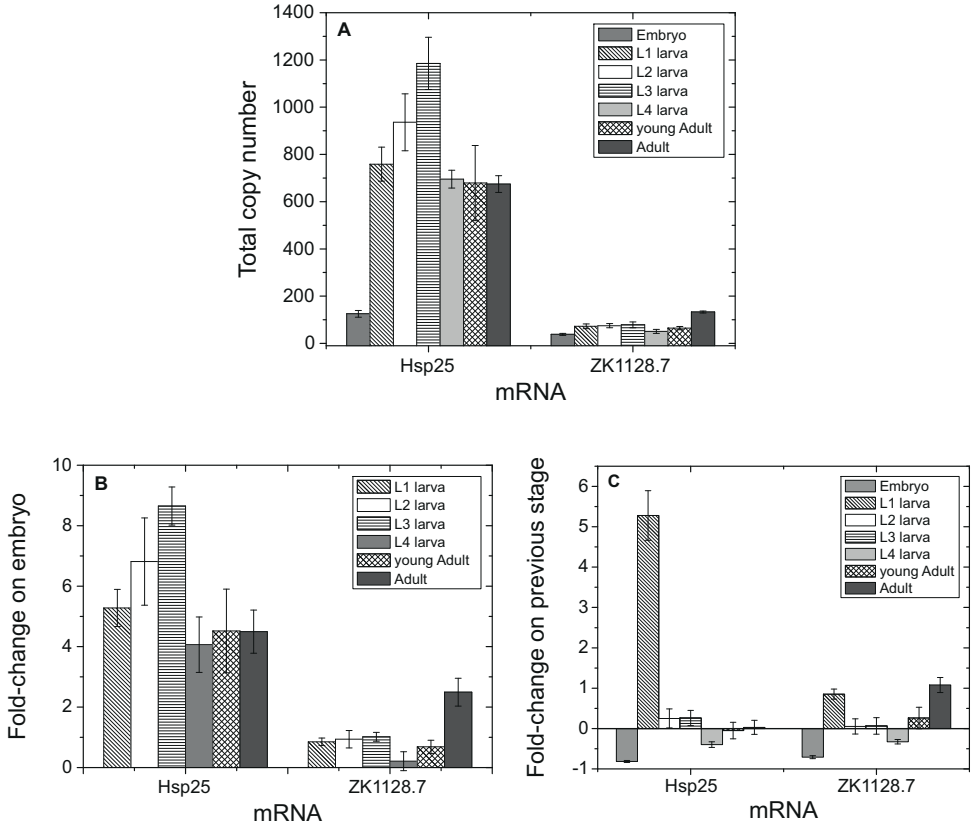

Figure 2.26: Total copy numbers of Hsp25 and ZK1128.7 mRNA in 10 ng total RNA preparation of embryo, L1, L2, L3, L4, young adult and adult nematodes. Values on the basis of the embryo sample are patterned in gray, L1 larva with lines of negative slope, L2 larva in white, L3 larva with horizontal lines, L4 larva in light gray, young adult with rhombus lines, and adult in dark gray.

of Hsp12.3 and Hsp12.6. The expression patterns of Hsp25 and ZK1128.7 are different from the ones detected for the Hsp12-family. Hsp25 expression peaks in the third larval stage, whereas for Hsp12.2, Hsp12.3, and Hsp12.6 the expression is highest in the first larval stage. After the larval stages, the expression of Hsp25 stayed constant, which is not observed for the Hsp12-family. In contrast, ZK1128.7 showed a constant expression in the first developmental stages and peaks in its mRNA level in the adult worm. Such a pattern was not observed for the other sHsps analyzed in this work. These results suggest that Hsp25, ZK1128.7 and Hsp12-family have different importances during the development of the nematode.

2.2.9 RNAI AFFECT AGAINST HSP25 AND ZK1128.7

RNAi experiments against Hsp25, performed by Ding and Candido (2000), showed that the viability and the development are not altered upon down-regulation. Consequently it is still of interest whether other sHsps in *C. elegans* are able to supplement the missing Hsp25 [55]. To analyze the RNAi effect more closely, qRT-PCR, lifespan and thrashing assays were performed. N2 nematodes were treated with dsRNA against Hsp25 by the feeding approach and analyzed in the same way as for the Hsp12-family (2.2.4). To characterize whether the down-regulation of ZK1128.7 reveals an observable phenotype, nematodes were fed with pL4440-ZK1128.7 containing *E. coli* HT115 and analyzed with regard to their expression levels, thrashing performance, and lifespan.

QRT-PCR Besides the detection of the expression levels upon RNAi treatment, Hsp25 and ZK1128.7 were analyzed with regard to their influence on each other in the qRT-PCR experiment. Figure 2.27 shows the changes in expression upon RNAi treatment.

In case of Hsp25, in both RNAi-treated samples a reduction of about 50 % in mRNA levels was detectable. On the one hand, these results verify that the fed dsRNA had an effect on the Hsp25 expression and on the other hand the decrease in the ZK1128.7 down-regulated sample is unexpected. Still, these small changes have to be treated carefully according to the small changes in fold-changes as described in 2.2.1 and may not hold true.

In contrast to this, the mRNA levels for ZK1128.7 showed increased values. The fold-change in the pL4440-Hsp25 fed worms corresponds to an increase of about 80 %. This change is quite small and has to be carefully interpreted. For RNAi against ZK1128.7 template, the expression was increased about 2.5-fold. Again, as already discussed for the analysis of for data revealed from knock-downs of the Hsp12-family, this is unexpected. As discussed for the Hsp12-family this could be a consequence from the incubation between dsRNA treatment and RNA preparation. However, this would suggest that the dsRNA does not have a strong effect on the expression, since the levels should be down-regulated. Additional similar conclusions for the regulation of the ZK1128.7 expression as for the Hsp12-family made are conceivable.

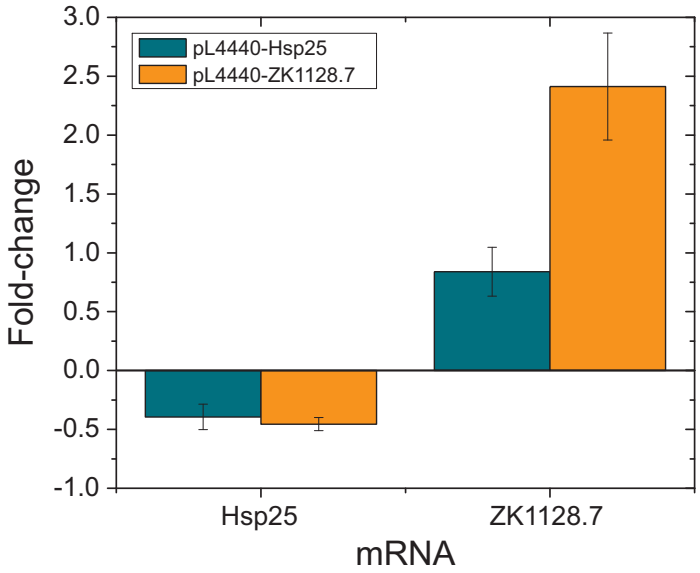

Figure 2.27: Fold-changes of Hsp25 and ZK1128.7 in total RNA preparations of pL4440-Hsp25 (cyan) and pL4440-ZK1128.7 (orange) fed nematodes.

LIFESPAN For a more detailed analysis, the lifespan of nematodes treated with RNAi against Hsp25 and ZK1128.7 were analyzed (fig. 2.28).

With 11.3 days, the average lifespan of worms treated with dsRNA directed against Hsp25 showed a slight decrease compared to the average lifespan detected for the control worms. RNAi against ZK1128.7 revealed a one day shorter lifespan than the control worms. Taking into account the large uncertainty of the value (13.5 $\pm$ 1.6 days and 12.5 $\pm$ 2.6 days) a change cannot be detected.

The slight reduction of Hsp25 mRNA led to a small reduction in the average lifespan, which can be explained by an impairing effect on the muscles. Since Hsp25 is localized in the focal adhesion structures of the body wall muscle cells and seems to have a function in the maintenance of them, down-regulation of Hsp25 can lead to an impaired function of the muscular ultrastructure. Corresponding effects were described by Gaiser et al. (2011) for the down regulation of the Hsp90 system in *C. elegans* [75].

THRASHING ASSAY Hsp25 is localized on the M-lines of the dense bodies in the body wall muscle cells of *C. elegans*. Thus, to analyze if the down-regulation of Hsp25 has an effect on the mobility of the nematodes, thrashing assays were performed. Figure 2.29 A depicts the total number of thrashing movements averaged over 6 individual worms. In figure 2.29 B representative pictures of the swimming movements of dsRNA against Hsp25 and ZK1128.7 are shown.

Down-regulation of Hsp25 resulted in a reduction of thrashing movements of about 35 thrashings per minutes. This reduction of movements was not accompanied by rolling movements as found for knock-downs of the member of the Hsp12-family. In principle, the movements were comparable with the ones from the wild type but slowed down and appeared to be ponderous. This leads to the

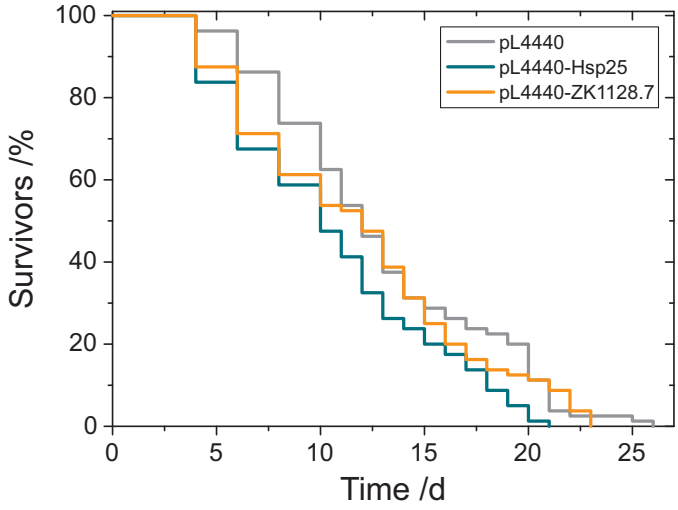

Figure 2.28: Lifespan analyses of nematodes treated with RNAi against Hsp25 (cyan) and ZK1128.7 (orange). The average lifespans are 13.5 ± 1.6 days for the control, 11.3 ± 0.2 days for pL4440-Hsp25 and 12.5 ± 2.6 days for pL4440-ZK1128.7 fed nematodes.

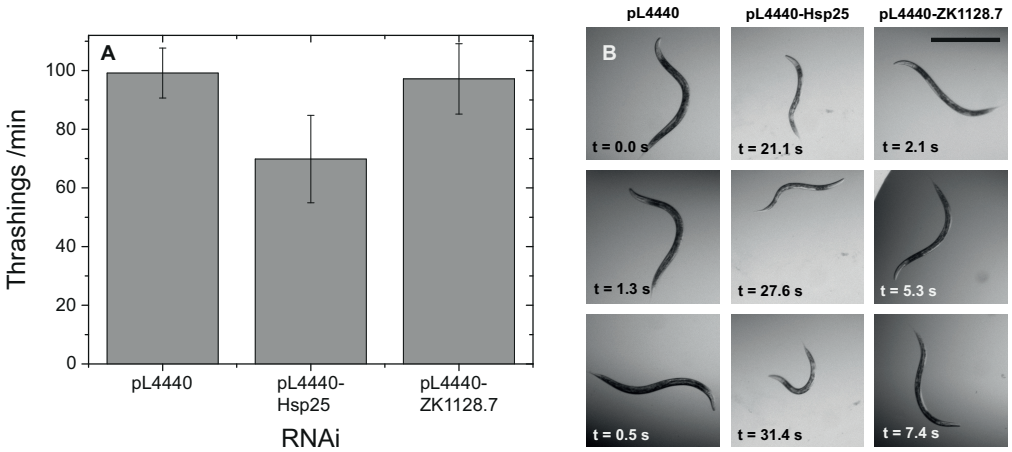

Figure 2.29: A: Thrashing assays of pL4440:Hsp25 and pL4440:ZK1128.7 fed nematodes. As negative control, pL4440 fed worms were conducted. B: Pictures of typical thrashing movements of the analyzed nematodes in (A).

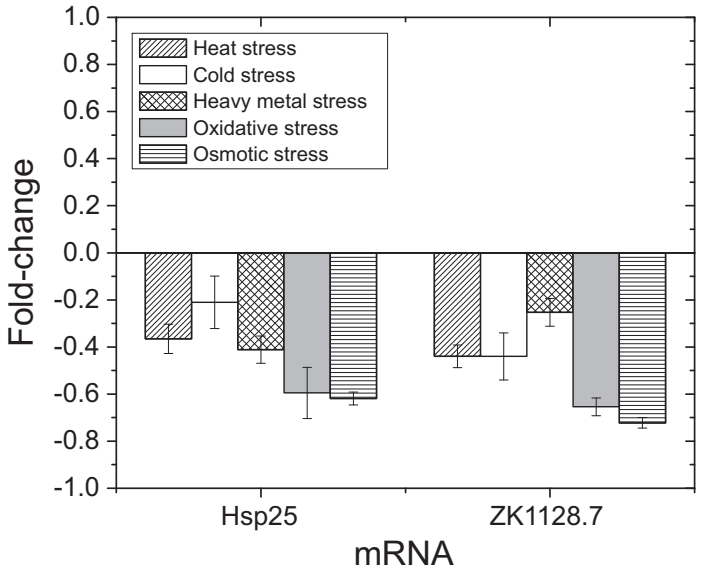

Figure 2.30: Changes in mRNA levels of Hsp25 and ZK1128.7 upon different stress conditions. Template of heat stress are depicted with lines of positive slope, cold stress in white, heavy metal stress with rhombus, oxidative stress in light gray and osmotic stress with horizontal lines.

assumption that the functionality of the body wall muscles are truly impaired by the down-regulation of Hsp25. This effect is not as pronounced as expected and led to the conjecture that there are some compensatory mechanisms. Ding and Candido assumed that Hsp43, the largest sHsp of *C. elegans* could somehow complement the function of Hsp25 because both proteins are localized to desmosomes and adhesion structures [56].

The number of thrashing movements in the ZK1128.7 down-regulated nematodes are comparable to the number of the negative control – wild type mimicking – individuals. Swim thrashings are smooth and fast in their performance. This result indicates that ZK1128.7 has no influence on the formation and maintenance of the muscles in *C. elegans*. Also, no effect on the neuromuscular junctions as supposed for the Hsp12-family, is indicated by the swimming abilities of the analyzed worms.

2.2.10 Expression of Hsp25 and ZK1128.7 under different stressors

Even if Hsp25 is a quite well characterized sHsp of *C. elegans*, no analyses concerning the expression patterns upon different stressors were conducted. As for the Hsp12-family heat, cold, heavy metal, oxidative, and osmotic stress were applied on synchronized L3 larvae. The exact stress conditions are summarized in table 2.9. The fold-changes of the mRNA levels of Hsp25 and ZK1128.7 are depicted in figure 2.30.

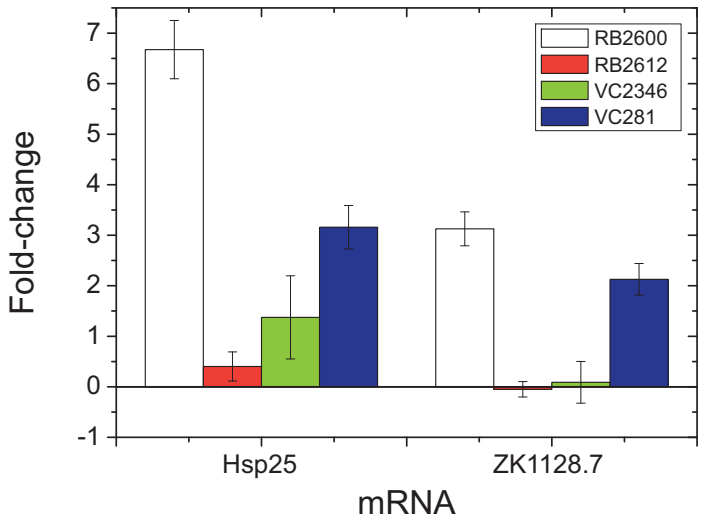

Figure 2.31: Fold-changes of the expression patterns of Hsp25 and ZK1128.7 in the knock-out strains of the Hsp12-family (RB2600 - white, RB2612 - red, VC2346 - green and VC281 - blue). Hsp25 is upregulated in all knock-out strains, while ZK1128.7 only reflects changes in the Hsp12.1 and Hsp12.6 knock-out.

Both, Hsp25 and ZK1128.7, showed down-regulation of the respective mRNA levels upon different stressors. Upon oxidative and osmotic stress conditions, these effects were the strongest with a 60-70 % decrease. For Hsp25, after heat and heavy metal stress, the reduction is about 40 %. Under cold stress conditions, only a slight reduction was observable. 40 % down-regulation of mRNA levels for ZK1128.7 was detected in the temperature-stressed samples (heat and cold). Compared to the unstressed wild type sample, the expression fell of about 80 % upon heavy metal stress.

As described for the Hsp12-family, Hsp25 and ZK1128.7 are not inducible by different stressors. Consequently, the assumption is that Hsp25 and ZK1128.7 have development and/or tissue specific functions. Especially the high amount of down-regulation of Hsp25 and ZK1128.7 upon oxidative and osmotic stress supports this assumption.

2.2.11 HSP25 AND ZK1128.7 IN HSP12-FAMILY KNOCK-OUT WORMS

To analyze whether the deletion of one member of the Hsp12-family influences the expression of Hsp25 and ZK1128.7, qRT-PCR experiments were conducted (4.2.1). Figure 2.31 summarizes the changes in mRNA levels of Hsp25 and ZK1128.7.

Hsp25 showed an increase in the mRNA-levels in all four knock-out strains. Especially in RB2600 the mRNA is increased 6.5-fold. The knock-out of Hsp12.2 and Hsp12.3 had only mildly increased Hsp25 levels and VC281 reflected a 4-

fold rise. Changes in the ZK1128.7 levels were only detectable in the RB2600 and VC281 strains and, in total, are less pronounced as for Hsp25.

Since the Hsp12-family seems to be important during the development of the nematodes, these results suggest that the sHsp network in *C. elegans* is very complex. Changes in the expression levels of Hsp25 were not expected, because for the Hsp12-family no expression in the same structures as Hsp25 have been reported. According to the RNAi analysis of the Hsp12-members, maybe the formation of neuromuscular junctions is impaired upon down-regulation of the Hsp12 proteins. Since Hsp25 is needed for the focal adhesion structures in the nematode, the interaction with neuromuscular junctions is conceivable. Thus, the upregulation of Hsp25 corresponds to a compensating effect.

The exact function and location of ZK1128.7 is not known yet. Hence, the possibility of a rise in expression to compensate the deletion of Hsp12.1 and Hsp12.6 is conceivable.

2.3 ANALYTICAL ULTRACENTRIFUGATION

Diverse and manifold analytical ultracentrifugation analyses were performed during this thesis as part of internal and external cooperations. The following two subsections will give an overview of the experiments conducted and the variety of the applications of analytical ultracentrifugation. All presented data will be published elsewhere (ongoing thesis Lorenz, unpublished; ongoing thesis Fleckenstein, unpublished) and is provided by courtesy of Tilly Fleckenstein and Oliver Lorenz. In this chapter, the focus will be laid on the methods employed with the aim to present examples for the experiments carried out. Integration in the respective research area and further interpretation can be found in [152, 71]. Experiments were setup by the cooperating partner, measurement and further analyses were conducted in the work within this thesis.

2.3.1 CHARACTERIZATION OF OLIGOMERIZATION STATES

In analytical ultracentrifugation oligomerization states can be analyzed with sedimentation velocity or sedimentation equilibrium experiments. In the following example, Sip-1, which is one of *C. elegans*' sHsps, was analyzed with sedimentation velocity experiments to determine its oligomerization state.

Sip-1 is exclusively expressed in the embryo of the nematode and shows different activity in the aggregation assay dependent on different pH values [240]. As the oligomerization state has an effect on the activity of Sip-1, 79 µM protein was analyzed at different pH values with sedimentation velocity experiments at 20 °C and 42,000 rpm. MES/MOPS buffers (10 mM MES, 10 mM MOPS, 141 mM sodium chloride and 1 mM calcium chloride) with constant ionic strength and pH values ranging from 5.8 to 8.2 were used as measurement buffers. All measurements were conducted in a Beckman Coulter XL-A equipped with absorption and interference optics, using a four-hole Ti-60 or eight-hole Ti-50 rotor from Beckman Coulter, respectively.

Figure 2.32 shows the c(s) distribution of Sip-1 at different pH values in the MES/MOPS buffer system. At the highest analyzed pH value, Sip-1 sedimented in a narrow peak with an s-value of apparently 17 S, indicating that only one oligomerization state is adopted. This species is representing a oligomeric structure build up by 32 subunits [71, 240]. With decreasing pH value, the oligomerization of Sip-1 changed to smaller oligomerization states. A change in pH of 1.9 towards more acidic conditions resulted in the disassembly of the 32-mer to a 28-mer - with an s-value of 15 S - as main species and several smaller species. The smaller species at approximately 12 S, 9 S, 6 S, and 4 S are not well defined in the c(s) distribution, indicating that they are not clearly characterizable as one certain oligomerization state. More likely, these different oligomers have highly variable structures and tend to interact with each other, forming different oligomers during the sedimentation process. This would lead to an extreme superposition of different sedimentation peaks calculated by SEDFIT and explains the undefined c(s) distribution. The species at 2 S corresponds most likely to dimers, which are released from the large oligomers. The disintegration

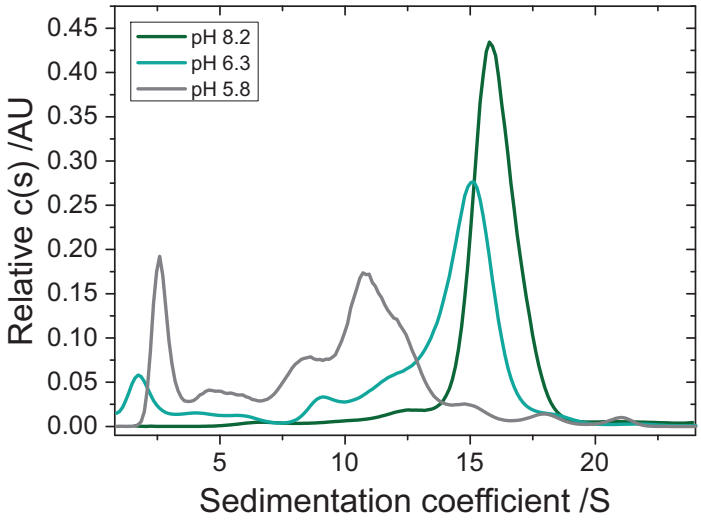

Figure 2.32: c(s) distributions of Sip-1 analyzed at different pH values. The distribution at pH 8.2 is depicted in green, pH 6.3 in cyan, and pH 5.8 in gray. Sip-1 formed smaller oligomers with decreasing pH values.

of the 32-mer was even more pronounced at pH 5.8. Here, the main sedimentation peak was at 11 S with a small right-handed shoulder, which is supposed to correspond to a 18-mer. Smaller species are found with 8 S (12-mer) and 3 S (dimer). At 5 S a very broad not separated peaks of different smaller oligomers are located.

The oligomerization analyses of Sip-1 at different pH values show that for proteins with a large number of possible oligomerization states, sedimentation velocity experiments are more suitable for characterization. The evaluation of sedimentation equilibrium datasets would be nearly impossible with clear conscience. For better understanding of the different oligomeric structures assumed by Sip-1 and better interpretation of the analytical ultracentrifugation data, Tilly Fleckenstein performed further analyses with electron microscopy studies (ongoing thesis, unpublished).

2.3.2 Characterization of protein-protein interactions

Binding studies in the analytical ultracentrifuge can be performed by sedimentation velocity experiments. Upon the interaction of two proteins, the formed complex sediments with different properties compared to the complex forming proteins on their own [224]. Hsp90 of *S. cerevisiae* (yHsp90) is a very interesting protein to analyze with analytical ultracentrifugation due to the following reasons. It is a homo-dimer itself and undergoes tremendous conformational changes under different nucleotide conditions [186, 93]. Trapping yHsp90 in specific conformations with the help of - for example - non-hydrolyzable ATP (AMP-PNP), influences the binding of co-chaperones [144].

Besides the analysis of the effect on members of the chaperone cycle of Hsp90, the binding properties of clients can be analyzed by this system [152].

Figure 2.33 shows binding studies of the ligand binding domain of the glucocorticoid receptor (GR-LBDm), a Hsp90 client [152]. Depicted are the relative c(s) distributions gained from SEDFIT analysis of the sedimentation boundaries and normalization on the total signal of the distribution curves.

The experiment was conducted with an Atto-488 randomly cysteine labeled GR-LBDm at 20 °C and 42,000 rpm in a Beckman Coulter XL-A equipped with a fluorescence detection system by Aviv. A 20 mM HEPES buffer pH 7.5 with 20 mM potassium chloride, 5 mM magnesium chloride, 5 mM DTT, and 50 µM Dexamethasone was used as standard measurement buffer. To achieve the different nucleotide conditions, 2 mM ADP or ATP were added prior to each analysis.

The labeled GR-LBDm sedimented with an apparent S-value of 3 S. Upon addition of yHsp90 (orange distribution), the nucleotides ATP (green distribution) and ADP (red distribution), a decrease in the GR-LBDm only (gray distribution) peak with a synergistic appearance of an interaction peak at apparently 6.3 S was observable. The shifted positions of the interaction peaks is due to the different conformations yHsp90 adopts upon the influence of different nucleotides (1.2.1). Comparing the three analyzed conditions - no nucleotide, ATP and ADP - the largest interaction peak in the c(s) distributions was observable in the ATP sample. This indicates that the binding of the ligand binding domain of the GR to yHsp90 is preferred in a closed conformation of yHsp90. The exact nature of this conformation was further analyzed by SAXS, NMR and FRET assays by Oliver Lorenz [152].

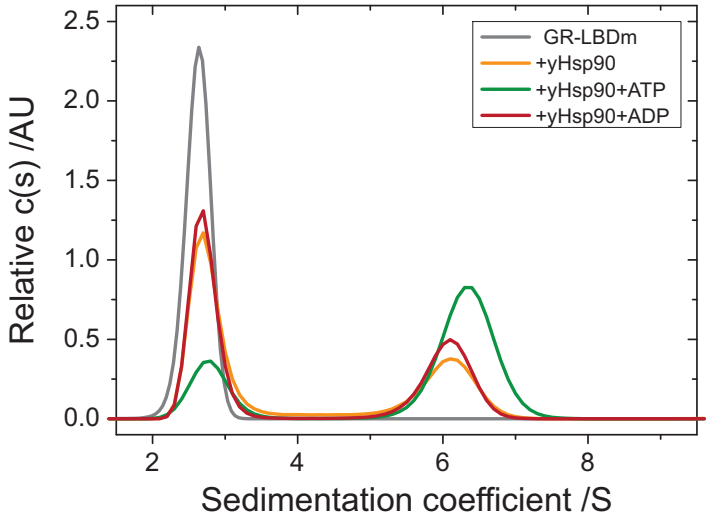

Figure 2.33: GR-LBDm binding to yHsp90 upon different nucleotide conditions. Presented are the c(s) distribution of each sample calculated with SEDFIT from Peter Schuck [198]. * indicates the Atto-488 label of GR-LBDm. Sedimentation of GR-LBDm is depicted in gray, GR-LBDm:yHsp90 complex in orange and the effect on the sedimentation of different nucleotides in green (ATP) and red (ADP).

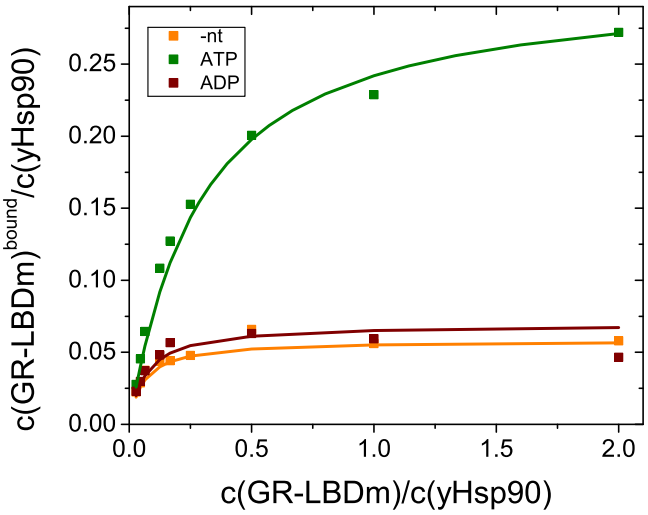

Figure 2.34: Co-sedimentation of GR-LBDm and varying concentrations of yHsp90 upon different nucleotide conditions. The measurement conducted with no nucleotide is depicted in orange, with ATP in green, and with ADP in red. The binding isotherms were calculated from the slow and fast sedimenting species in the titration experiments. The affinity constants could be detected as $4.5 \cdot 10^{-4}\,\mathrm{M}^{-1}$ for the ATP, $9 \cdot 10^{-5}\,\mathrm{M}^{-1}$ for ADP and $7.5 \cdot 10^{-5}\,\mathrm{M}^{-1}$ for no nucleotide conditions.

Besides this analysis, analytical ultracentrifugation allows for more specific analyses of protein interactions. For example, the affinity constant of the binding can be determined when the interaction peak of the complex is well separated from the protein only peaks [224]. In the presented system, only one interaction partner is visible because of the fluorescence label. The separation of GR-LBDm and GR-LBDm:yHsp90 with a difference in the s-values from about 3 S to 6.3 S is sufficient for further study of the binding.

Figure 2.34 shows the co-sedimentation of 400 nM GR-LBDm with different concentrations of yHsp90 dimer under three nucleotide conditions (no nucleotide - orange, ATP - green and ADP - red).

The single measurements were performed and analyzed as before. The amount of GR-LBDm in the free and interacting species (bound) were calculated by integration of the concentration distribution represented in the c(s) distributions. The yielded areas were proportioned to the total concentration of used GR-LBDm to calculate the concentration of GR-LBDm in the slow and fast sedimentation boundaries (equations 2.5 and 2.6). Note that this calculation of the GR-LBDm concentration in both species is only possible, because there are no quenching or magnifying effects on the fluorescence observable in this interaction system. The overall signal is quite stable and does not change upon the addition of different yHsp90 amounts.

$$c_{GR}^{free} = \frac{c_{GR}^{total}}{A^{total}} \cdot A^{slow} \tag{2.5}$$

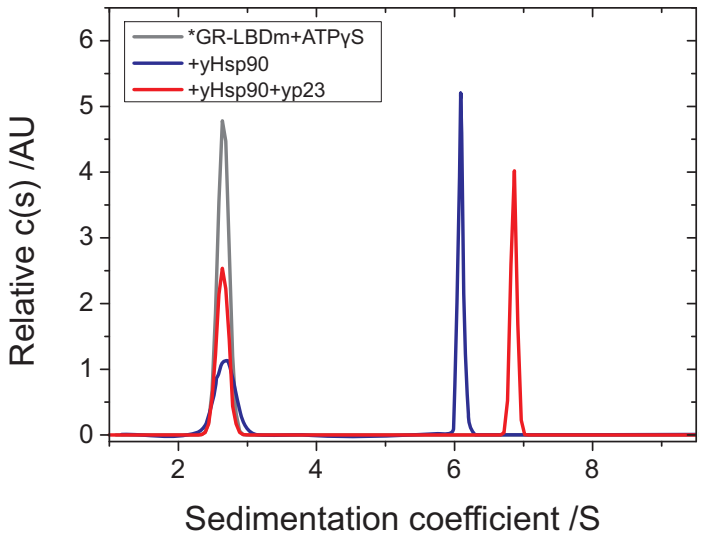

Figure 2.35: Effect of yp23 on the GR-LBDm:yHsp90 complex under ATPγS conditions. Depicted are the c(s) distributions of Atto-488 random labeled (*) GR-LBDm only (gray), the *GR-LBDm:yHsp90 complex (blue), and the *GR-LBDm:yHsp90:yp23 complex (red).

$$c_{GR}^{bound} = \frac{c_{GR}^{total}}{A^{total}} \cdot A^{fast} \tag{2.6}$$

c_{GR} describes the concentration of GR-LBDm in the free (exponent $free$) and bound (exponent $bound$) fraction. A^{fast} and A^{slow} are the calculated areas below the c(s) distribution of the interaction species (fast boundary) and the free GR-LBDm amount (slow boundary), respectively.

$$K_a = \frac{c_{GR}^{bound}}{c_{GR}^{free} \cdot (n \cdot c_{yHsp90}^{total} - c_{GR}^{bound})} \tag{2.7}$$

The affinity constants were calculated according to equation 2.7, based on the law of mass action. Since yHsp90 is a dimer with two potential binding sites, it was assumed that n equals 2. c_{yHsp90}^{total} describes the yHsp90 concentration [224].

With the assumption for yHsp90 mentioned above and ATP, GR-LBDm has an affinity constant K_a of $4.5 \cdot 10^{-4}\,\mathrm{M}^{-1}$. Compared to the affinities in the presence of ADP ($9 \cdot 10^{-5}\,\mathrm{M}^{-1}$) and no nucleotide ($7.5 \cdot 10^{-5}\,\mathrm{M}^{-1}$) conditions, this is the highest affinity to bind to yHsp90 and confirmed the result as described above (fig. 2.33, [152]). The small differences between the affinity constants for ADP and no nucleotide condition are negligible and plead for the same binding behavior under these conditions [152].

After characterizing the basic interactions of yHsp90 with co-chaperones [144] and client proteins [152] *in vitro*, it is possible to combine both systems to analyze the effect of the client protein on the yHsp90 system *in vitro* [152]. In figure 2.35 a combination of the characterization strategies described in [144] and [152] is shown. It is possible to detect the already described ternary complexes

of GR-LBDm, yHsp90, and yp23 [57]. This gives rise to investigate the Hsp90 cycle with respect to the effect of co-chaperones and clients in general [152].

The presented data reflect the multiple applications of analytical ultracentrifugation. Besides the characterization of single protein systems, and the analysis of their oligomerization, more complex analyses with several proteins can be conducted as well. For the characterization of these multi protein systems the fluorescence optic opened a new dimension concerning scanning time and the required amounts of protein. Latest developments in the AUC field show that this method is still of high potential. Especially the development in theoretical and computational methods keeps analytical ultracentrifugation a state of the art method to characterize proteins on their own as well as their interaction behavior [199].

SUMMARY AND CONCLUSIONS 3

3.1 THE HSP12-FAMILY

The *in vitro* characterization revealed that the Hsp12-family of *C. elegans* have only a few sHsp-characteristic features. This family is typically described by five characteristics: the small monomeric size, the α-crystallin domain, the dynamic quaternary structure, a high oligomeric size, and the inducability upon different stress conditions [89, 134].

In vivo the expression patterns of the Hsp12-family were analyzed in development, RNAi-treated worms, knock-out strains, and after the application of different stressors. For the Hsp12-family, the total expression patterns were analyzed with immunohistochemical approaches by Ding et al. (2000) and Leroux et al. (1997) [54, 140]. In this work, the expression patterns were closely studied under several different conditions on mRNA levels with qRT-PCR. The overall results of these experiments, clustered according the different conditions, are depicted in table 3.1. Red color-coded values reflect all decreases in expression, green marks the increased expression values, and light green the values which show a increasing tendency.

HSP12.1 The monomeric size of Hsp12.1 of 12.5 kDa fits perfectly to the typical size range of sHsps. The alignment of the amino acid sequence to the well studied αB-crystallin, showed that Hsp12.1 lacks the C-terminal domain with an IXI-motive. Besides 25 amino acids, which are forming the N-terminus, the rest of the protein is aligned to the α-crystallin domain. Analysis of the secondary structure elements showed that approximately 34 % of the protein is folded into β-sheet structures, the amount of α-helices is small (about 4 %), and the rest of the protein is classified as unordered.

Regarding the distribution of the typical domains in sHsp, this result is unexpected and questions whether the structure of Hsp12.1 corresponds to typical sHsp features. Besides this, Hsp12.1 forms concentration independent tetramers. Classical aggregation assays using heat denatured CS and reductively denatured lysozyme as model substrate were conducted to determine possible chaperone/holdase functions. Hsp12.1 showed a weak chaperone activity in the aggregation assay with CS. Even at a 64-fold excess of Hsp12.1 the aggregation is not completely depressed. Hsp12.1 has no effects on the aggregation of lysozyme and does not reveal any chaperone activity.

Table 3.1: Summary of fold-changes determined in qRT-PCR analyses in this thesis. Clustered according to experiments and proteins. Reliable fold-changes are colored in green, carefully interpreted positive fold-changes in light green, no changes are uncolored, and negative fold-changes are colored in red.

	Template	Hsp12.1	Hsp12.2	Hsp12.3	Hsp12.6	Hsp25	ZK1128.7
development on previous stage	embryo	1.17 ± 0.28	-0.46 ± 0.13	-0.94 ± 0.01	-0.87 ± 0.01	-0.82 ± 0.03	-0.71 ± 0.04
	L1 larva	–	17.76 ± 3.30	2.85 ± 1.51	2.03 ± 0.82	5.28 ± 0.61	0.85 ± 0.13
	L2 larva	–	-0.45 ± 0.09	-0.02 ± 0.26	0.15 ± 0.37	0.25 ± 0.23	0.05 ± 0.19
	L3 larva	–	-0.03 ± 0.19	-0.45 ± 0.08	-0.15 ± 0.10	0.26 ± 0.19	0.07 ± 0.20
	L4 larva	–	-0.35 ± 0.06	-0.84 ± 0.01	-0.35 ± 0.07	-0.40 ± 0.07	-0.33 ± 0.06
	young adult	-0.14 ± 0.16	-0.27 ± 0.09	2.33 ± 0.70	0.58 ± 0.23	-0.05 ± 0.20	0.26 ± 0.27
	adult	-0.24 ± 0.08	-0.57 ± 0.05	3.66 ± 0.93	1.89 ± 0.29	0.03 ± 0.17	1.08 ± 0.19
RNAi on negative control	pL4440-Hsp12.1	5.12 ± 0.52	-0.18 ± 0.07	-0.34 ± 0.08	-0.20 ± 0.15	–	–
	pL4440-Hsp12.2	1.32 ± 0.27	-0.07 ± 0.14	-0.28 ± 0.12	–	–	–
	pL4440-Hsp12.3	1.60 ± 0.24	-0.37 ± 0.06	2.46 ± 0.38	-0.84 ± 0.04	–	–
	pL4440-Hsp12.6	2.24 ± 0.20	-0.01 ± 0.23	1.10 ± 0.09	1.53 ± 1.10	–	–
	pL4440-Hsp25	–	–	–	–	-0.39 ± 0.11	0.84 ± 0.21
	pL4440-ZK1128.7	–	–	–	–	-0.46 ± 0.06	2.41 ± 0.45
Knock-out strains on wild type	RB2600	-0.51 ± 0.06	4.64 ± 0.43	0.49 ± 0.28	0.34 ± 0.20	6.67 ± 0.58	3.13 ± 0.34
	RB2612	-0.22 ± 0.16	-0.98 ± 0.00	-0.62 ± 0.09	–	0.40 ± 0.29	-0.05 ± 0.15
	VC2346	-0.69 ± 0.12	-0.99 ± 0.00	1.24 ± 0.81	-0.52 ± 0.19	1.37 ± 0.82	0.09 ± 0.41
	VC281	0.24 ± 0.21	1.62 ± 0.22	1.02 ± 0.17	–	3.16 ± 0.43	2.13 ± 0.31
stressors on unstressed sample	heat stressed	-0.71 ± 0.04	-0.05 ± 0.11	-0.70 ± 0.04	–	-0.37 ± 0.06	-0.44 ± 0.05
	cold stressed	-0.83 ± 0.06	0.02 ± 0.15	0.15 ± 0.11	0.75 ± 0.20	-0.21 ± 0.11	-0.44 ± 0.10
	heavy metal stressed	-0.90 ± 0.00	-0.32 ± 0.15	-0.46 ± 0.12	-0.61 ± 0.03	-0.41 ± 0.06	-0.25 ± 0.06
	oxidative stressed	-0.92 ± 0.01	-0.32 ± 0.07	-0.45 ± 0.08	1.10 ± 0.72	-0.60 ± 0.11	-0.65 ± 0.04
	osmotic stressed	-0.94 ± 0.01	-0.20 ± 0.07	0.07 ± 0.16	-0.40 ± 0.04	-0.62 ± 0.03	-0.72 ± 0.02

In the *in vivo* analysis, Hsp12.1 showed an increase in the embryonic stage. In L1 to L3 larval stages, no Ct-values were detectable in the reliable range of data, which leads to the assumption that the expression is low. This corresponds to a decrease in the expression compared to the embryonic stage. For the L4 larval stage the expression of Hsp12.1 is detectable again. The expression in the young adult sample showed no changes compared to the L4 larval stage. The same is true for the expression in the adult nematode. Connecting these results to the localization studies of Ding et al. (2000), the detected signal for the Hsp12-family in the early larval stages is not caused be the presence of Hsp12.1 [54]. Upon RNAi treatment against all members of the Hsp12-family, the expression of Hsp12.1 is increased in all analyzed samples. Especially in the pL4440-Hsp12.1 fed worms the expression increased 5-fold. This suggests that the expression of Hsp12.1 is regulated via a negative feedback loop. Since the sequences of all Hsp12 proteins are closely related, it could be possible that the RNAi against Hsp12.2, Hsp12.3, and Hsp12.6 also effects the expression levels of Hsp12.1. If the negative feedback regulation holds true, the upregulation of the mRNA levels is explainable by the cross reaction of the fed dsRNAs. If the different dsRNA constructs do not effect the expression of the not corresponding mRNAs of the Hsp12-family, the upregulation indicates further compensatory effects in between the Hsp12-family. Possible compensatory effects are easily analyzable in the different knock-out strains of the Hsp12-family. For Hsp12.1, the qRT-PCR analyses revealed no compensatory effects for the other members of the Hsp12-family, because no up-regulation was detectable. Upon different stress conditions the expression of Hsp12.1 was strongly impaired (tab. 3.1). This reflects that Hsp12.1 is no stress inducible sHsp in *C. elegans*, which leads to the assumption that Hsp12.1 is expressed development specifically.

Lifespan assays revealed that the down-regulation of Hsp12.1 has only minor effects on the average life of the nematode. In thrashing assays the swim movements are impaired compared to the negative control. Furthermore, the pL4440-Hsp12.1 fed worms tend to overbending movements and uncoordinated movements of head and tail. This mild phenotype was described by Ackley et al. (2003) and was attributed to defects on the neuromuscular junctions. The same can be assumed for the Hsp12.1 knock-down.

HSP12.2 As described for Hsp12.1, Hsp12.2 has a monomeric size that is characteristic for sHsps (12.2 kDa) and lacks the C-terminal domain. The ratios of the different secondary structures were determined to be 6 % for α-helical structures, 30 % β-sheet, and 40 % unordered structure parts. Again the low β-sheet amount is untypical for sHsp. Hsp12.2 oligomers are unusually small, compared to other sHsps. Again, a tetrameric oligomerization was detected, which is independent of the concentration. A holdase function was indeterminable for Hsp12.2 in the chaperone assays.

The expression pattern of Hsp12.2 peaked in the L2 larval stage and decreases in the following development stages in the *in vivo* analyses. Compared to the known expression patterns, this reflects the results of Ding et al. (2000) quite well. They detected an expression of the Hsp12-family throughout the whole worm in the first larval stages. This expression decreased until the adult stage and changed its localization specific to the reproductive tissue of the nemat-

ode [54]. In the RNAi treated worms no effect on the expression levels of Hsp12.2 were detectable. Either the dsRNA did not work properly or the effect of down-regulation is compensated by an increased mRNA production during the cleaning procedure for the total RNA preparation as discussed above (2.2.4). The expression in the knock-out strains for the Hsp12-family showed interesting changes when compared to the wild type nematode. As expected, the expression of Hsp12.2 was almost completely reduced in the Hsp12.2 knock-out strain (RB2612). Surprisingly, also the expression was down-regulated in VC2346, the Hsp12.3 knock-out. In the remaining two knock-out strains, RB2600 (Hsp12.1 knock-out) and VC281 (Hsp12.6 knock-out), the expression of Hsp12.2 was increased about 5- and 2-fold, respectively. This enlarged amount of Hsp12.2 pleads for compensatory effects within the Hsp12-family. However, the decrease of expression in VC2346 worms indicated a regulatory connection between the expression of Hsp12.1 and Hsp12.2. The treatment with different stress conditions did not have an effect on the expression of Hsp12.2. This confirm development specific expression for the Hsp12-family again.

Lifespan analysis of Hsp12.2 knock-down nematodes revealed no differences compared to the control sample. In the thrashing assays a reduction in the swimming movement was determined, which is comparable to the findings for the Hsp12.1 knock-down. Additionally, the same mild phenotype as described for Hsp12.1 above is observable. Again, this speaks for the possibility that the RNAi constructs target more than one member of the Hsp12-family and that the reduction in the expression of this family leads to dysfunctions in the neuromuscular junctions.

HSP12.3 *In vitro* characterization of the 12.3 kDa sHsp Hsp12.3 showed comparable results as determined for Hsp12.2. Both proteins form tetramers, which are stable over a broad concentration range and lack their C-terminal. Hsp12.3, like Hsp12.2, has no chaperone activity and even shows co-aggregation with the model substrate lysozyme.

In the L2 larva, young adult, and adult development stage, Hsp12.3 showed the highest expression *in vivo*. The mRNA-level was reduced in the other larval stages and the embryonic stage. In the localization studies of Ding et al. (2000), these changes in mRNA-levels reflected the described expression pattern and led to the assumption that the function of Hsp12.3 is more important in the adult stage than the function of Hsp12.1 and Hsp12.2, because these both proteins showed a decrease in their expression pattern. Upon RNAi down-regulation, the expression seemed to be unaffected by knock-down of Hsp12.1 and Hsp12.2. An increment of expression in the corresponding RNAi treated samples were detectable for Hsp12.3, as found for Hsp12.1 and Hsp12.6. Again the possibility of a negative feedback regulation of the expression can be assumed. Supplementary, the Hsp12.3 mRNA-level is increased in the Hsp12.6 down-regulated template. According to these findings, compensatory effects of Hsp12.3 for Hsp12.6 are assumable. Corresponding positive changes of the Hsp12.3 expression are observed in the knock-out strains VC2346 and VC281. The result for the Hsp12.3 knock-out (VC2346) itself is surprising. No up-regulation of the mRNA was expected. Thus, it is not known, if the knock-out strain is homozygous, the remaining second allele could still be present and responsible for the detected

expression. The increase in the VC281 template underlined the assumption of a compensatory effect of Hsp12.3 towards Hsp12.6. Moreover, the expression of Hsp12.3 was decreased in the Hsp12.2 knock-out strain. This reflects the vice versa effect as described for Hsp12.2 and pleads for a connection between the expression levels of Hsp12.2 and Hsp12.3. The analyses of different stressors only revealed an effect of heat treatment, which led to a decrease in the expression. In all other tested stress conditions, the expression is not altered.

Again, the thrashing assay showed an impaired ability of movement, which is accompanied with the mild phenotype described by Ackley et al. (2003). The lifespan of the Hsp12.3 down-regulated nematodes is slightly decreased compared to the control. This could be an effect of the somehow impaired neuromuscular junctions as discussed in 2.2.4.

hsp12.6 Hsp12.6 has a unique characteristic in the Hsp12-family. It is a monomer over a brought range of concentrations. As for the other members of the Hsp12-family, the monomeric size of 12.6 kDa fits perfectly in the range predicted for sHsps. The missing oligomerization and function in classical aggregation assays led to special questions of the functionality of this protein. Typically, sHsps form large oligomeric structures which allow them to bind aggregation-prone proteins [161, 185]. The expression analyses of Hsp12.6 gave a picture comparable to the Hsp12.3 distribution throughout the different development stages. The expression was reduced in the embryo, peaked in the first larval stage, and, after a reduced expression in the L2 to L4 larval stages, increased again in the young adult and adult stage. Upon RNAi treatment against Hsp 12.2 and Hsp12.3, the amount of Hsp12.6 mRNA was decreased. In the Hsp12.6 dsRNA fed template, the mRNA level of Hsp12.6 itself showed a total increase of 1.5-fold. Comparing the result for the RNAi experiment with the analyses of the knock-out strains, comparable values were revealed for the influence of Hsp12.1, Hsp12.2, and Hsp12.3 on the Hsp12.6 mRNA-level. The results for the Hsp12.6 knock-out confirmed the deletion of the gene loci for Hsp12.6. The effect of different stressors is most pronounced for Hsp12.6. In heat shocked samples the expression is not detectable, which reflects a strong decrease in expression. Additionally, decreasing effects on the expression are shown by heavy metal stress. Upon cold and oxidative stress the expression is slightly increased. This speaks for a mild response to different stress conditions. Overall the expression may be development specific, but can be altered upon different stress conditions.

Results of the lifespan and thrashing assay reflect comparable results to the observation made for Hsp12.3. The average lifetime is slightly impaired and the mild thrashing phenotype was observed. Both led to the same assumption as reported above for the other members of the Hsp12-family.

Growth of a synchronized VC281 (Hsp12.6 knock-out) population at 24 °C led to massive increase (50 - 60 %) of the male frequency within this population. Since the male fraction was only decreasing to approximately 20 % upon incubation at 20 °C, it is most likely that XX-hermaphrodites lose one of their X-chromosomes induced by the higher growth temperature. Furthermore, the repeated treatment of a later generation of the phenotype-revealing VC281 population showed an increase in the male frequency. This time, the male rate

rose to approximately 40 %. According to this, the knock-out of Hsp12.6 had a remarkable effect on the sex determination of *C. elegans*. If this effect is caused exclusively by the loss of one X-chromosome or if the deletion of Hsp12.6 has an effect on the development of sex specific reproductive tissue has to be examined in further experiments.

3.1.1 CONCLUSIONS FOR HSP12-FAMILY

Summarizing the obtained *in vitro* data, it could be shown that the Hsp12-family may belong to the sHsp-family but shows characteristic differences to the classical features of that large protein family. The secondary structure of this family reflects the typically β-sheet rich structure. But the overall amount of β-sheet structure is smaller than excepted with respect to the presented alignment. This raises the question if the members of the Hsp12-family truly fold to an α-crystallin domain like structure, or if they have a completely different structure. However, the lack of higher oligomerization and undetectable chaperone function for most of the members of the Hsp12-family are unusual. Hsp12.1 to Hsp12.3 predominantly exist as tetramers with small amounts of dimers and monomers present in the Hsp12.2 and Hsp12.3 samples. However, Hsp12.6 sediments as a monomer. Such a small oligomerization is quite rare and is also described for Hsp25 of *C. elegans* [55]. For the tetramers of the Hsp12-family no subunit exchange by FRET assays as described in [171] were determinable (data not shown). These results do not correspond to the typical features of the sHsp-family. Hsp12.1 is the only representative of the Hsp12-family that revealed chaperone function with a standard substrate in the aggregation assay. For the Hsp12.2, Hsp12.3, and Hsp12.6 a chaperone function is not excluded, but was not detected with the used standard substrates. As discussed above 2.1.1, it is possible that the oligomerization of the sHsps is mediated by the short N-termini. Such oligomerization would block hypothesized substrate binding motives in the N-terminal domain and could be one reason for the missing chaperone function. Additionally, the N-terminus on its own is quite short in all members of the Hsp12-family. Besides the possible oligomerization through the N-terminus, the length itself and possible association of missing substrate binding sites could be responsible for the missing chaperone activity. Furthermore, the slight chaperone activity of Hsp12.1 could be a hint for holdase function of the Hsp12-family, which are not ascertainable by the known standard substrates for aggregation assays.

With respect to the obtained *in vitro* data, the question whether the Hsp12 proteins are molecular chaperones is left unanswered. Since structure, oligomerization, and function show obvious differences to the classical picture of sHsps, a final classification of Hsp12.1, Hsp12.2, Hsp12.3, and Hsp12.6 as sHsp is not possible.

With the help of the conducted *in vivo* experiments, this work confirmed that the expression of the Hsp12-family has a peak in the L1 larvae. All members are highly expressed in this stage, but the total amount of Hsp12.2 is the highest and seems to be the main protein that contributed to the results of Ding et al. (2000) [54]. In the different developmental stages, the expression pattern of

Hsp12.1/Hsp12.2 and Hsp12.3/Hsp12.6 show similar changes, which indicates similar functions. Additionally, it was shown that the Hsp12-family is not inducible by stress in their expression, except for Hsp12.6, which revealed a mild increase in expression upon cold and oxidative stress. It is unclear which exact mechanism is responsible for these changes. The analyses of the Hsp12-family members' knock-out strains suggest compensating effects in this family. Especially Hsp12.2 and Hsp12.3 seem to be linked to each other. Furthermore, the expression of Hsp 12.3 and Hsp12.6 show comparable patterns.

3.2 OTHER SHSPS OF *C. ELEGANS*

3.2.1 HSP25

In 1999, Ding and co-workers showed that Hsp25 has *in vitro* chaperone activity and is localized to focal adhesion structures, like M-lines in muscle and desmosomes in spermateca *in vivo*. The function of Hsp25 is assumed to be linked to the maintenance, formation and turnover of adhesion structures. In this work, the expression of Hsp25 was further analyzed with qRT-PCR regarding the development stages, RNAi, knock-out strains of the Hsp12-family, and different stress conditions.

The overall expression of Hsp25 peaked in the third larval stage and was afterward decreased to a constant level in the later development stages. The maximum in expression corresponds to the formation of the last body wall muscle cells and is in accordance with the assumed function of Hsp25. Upon different stress conditions, the expression of Hsp25 decreased and reflected the missing inducability of that protein. As shown for the Hsp12-family, this reflects that the function of Hsp25 is more development- and tissue-specific than linked to any condition. The analyses of the expression levels in Hsp12 protein knock-out strains revealed changes in the amount of Hsp25. Dependent on the knocked-out Hsp12 member, the increase in the expression is more or less pronounced. Especially in the case of Hsp12.1 the mRNA-level of Hsp25 rised 6.5-fold. In the Hsp12.6 knock-out the increment was not as much pronounced and corresponded to a 3-fold increase. This change leads to the assumption that the expression of Hsp25 is somehow connected to both, Hsp12.1 and Hsp12.6. Upon RNAi treatment, the mRNA-levels of Hsp25 were only slightly altered. This observation should be verified by further biological replicates and normalization to several housekeeping genes. Still, a RNAi effect was detectable in the lifespan and thrashing assays. A reduction of Hsp25 led to a reduced thrashing behavior. This effect was accompanied by a slight reduction in the average lifespan. Both observations can be related to impaired body wall or pharyngal muscles, respectively.

3.2.2 ZK1128.7

ZK1128.7 was not described in the literature until now. Basic *in vivo* characterization showed that the expression in the different development stages was at

a maximum in the adult nematode. After the embryonic developmental stage, the mRNA level rose first in the L1 larva and stayed stable until it increased again in the adult stage. This indicates that ZK1128.7 seems to be most important in the adult worm. RNAi treatment against Hsp25 led to a slight increase of the expression, which could reflect a connection between these two sHsps. Down-regulation of ZK1127.8 also revealed an increment in the corresponding mRNA. This was not expected and could be explained by an inhibitory feedback regulation. A connection between Hsp12.1 and Hsp12.6 to ZK1128.7 seems to be likely, concerning the expression analyses of ZK1128.7 in the knock-out strain of Hsp12.1 and Hsp12.6. It can not be stated whether there is a direct connection between these three sHsps or whether the deletion of Hsp12.1 and Hsp12.6 leads to a general increase in expression of the sHsp network. As the other examined sHsps in this thesis, ZK1128.7 showed no increase upon different stress conditions. In the oxidative and osmotic stress nematodes, the expression actually decrease. No alteration of expression can be detected for the other tested stressors.

In the lifespan and thrashing assays, no change toward the negative controls was detected. This allows the assumption that ZK1128.7 has no influence on the maintenance of the muscles or the neuronal system as described for Hsp25 and the Hsp12-family.

3.3 ANALYTICAL ULTRACENTRIFUGATION

Manifold analytical ultracentrifugation experiments were performed during this thesis. In section 2.3 two main analysis strategies are depicted to give an overview of the performed analysis variants.

The example of Sip-1 revealed that, in certain cases, it is better to analyze oligomerization by sedimentation velocity than by sedimentation equilibrium experiments. Since Sip-1 is a highly polydisperse protein under different buffer conditions, the analyses in sedimentation equilibrium experiments is remarkably aggravated. In the presented data the distribution of the polydisperse oligomerization is well reflected. Still, the exact calculation of protein masses and correct oligomerization is an estimation and has to be further analyzed. In her thesis, Tilly Fleckenstein characterizes the different oligomerization states with electron microscopy in cooperation with the group of Prof. Weinkauf to reveal the correct number of subunits represented in the different species [71].

Interaction studies with a high number of possible interaction partners were facilitated since a fluorescence detection system is available for analytical ultracentrifuges. Advantages of this optical system is the detection of exclusively labeled interaction partners and the low amount of proteins needed for each analysis. This allows for the testing of many different conditions, concentration ranges, etc. in less time.

In the presented examples, the interaction studies were exclusively performed with Atto488-labeled proteins. Besides the basic characterization of the GR-LBDm binding to yHsp90 under different nucleotide conditions, also the effect of p23 on the *GR-LBDm:yHsp90 complex could be analyzed. This allows the *in vitro* characterization of the effect of other co-chaperones on the *GR-

LBDm:yHsp90 complex in more detail. Oliver Lorenz investigates this issue with several different methods and works on the elucidation of the influence of the GR-LBDm on yHsp90 cycle [152].

3.4 OUTLOOK

Summarizing this thesis, it was possible to show *in vitro* that the Hsp12-family of *C. elegans* is a closely related protein family, with comparable secondary structure. Concerning the oligomeric state and function, the family reveals different results. To verify the chaperone activity of all members, the identification of native substrates and the characterization of their interaction with the respective sHsp is of great interest. Furthermore, the identification of the structure of this Hsp-family would resolve the question, whether Hsp12 proteins are molecular chaperones or not.

In vivo analyses of the expression revealed that Hsp12.2 is the most prominent member of the Hsp12-family concerning mRNA-levels. Further, the changes in expression levels of the Hsp12-family partially show comparable and compensating changes. For more detailed analyses of the expression, the effects of RNAi, and different stressors, the *in vivo* characterization should be accomplished through reporter constructs in transgenic worms. Such experiments would allow an easy visualization of the specific protein under many different experimental conditions. Furthermore, the identification of the exact localization of each member of the Hsp12-family would be possible.

The observed phenotype of the Hsp12.6 knock-out strain (VC281) upon mild heat treatment is not explainable with current knowledge of the Hsp12.6 expression. To reveal a better understanding of the observed effect, it is necessary to verify whether really one of the X-chromosomes is lost at a higher growth temperature. Furthermore, the development of reproductive tissue-specific cells has to be analyzed, concerning their presents and development. These further analyses would reveal a deeper understanding of the phenotype itself and the specific function of Hsp12.6 in the nematode. Since the correct functions of all Hsp12-family members within the nematode is unclear, the question arises if the other knock-out strain RB2600 (Hsp12.1) , RB2612 (Hsp12.2), and VC2346 (Hsp12.3) show a comparable phenotype to the one observed for VC281, concerning the increase in male frequency and potential genetic alteration.

ZK1128.7 is a predicted sHsp of *C. elegans*, which has its highest expression in the adult worm and is most likely development specific expressed. The same strategy as used for the Hsp12-family is recommended for further characterization *in vivo* and *in vitro*. Especially with respect to the overall comparison of sHsps of *C. elegans* it is necessary to conduct *in vitro* analyses of ZK1128.7.

MATERIALS AND METHODS 4

4.1 MATERIALS

4.1.1 CHEMICALS

Table 4.1: Chemicals.

Chemical	Producer
2-mercaptoethanol	Sigma (St. Louis, USA)
Acetic acid	Roth (Karlsruhe, Germany)
Acrylamid/Bis Solution 19:1 (40 % w:v)	Serva (Heidelberg, Germany)
Agar Agar	Serva (Heidelberg, Germany)
Agarose	Serva (Heidelberg, Germany)
Ammonium persulfate (APS)	Roth (Karlsruhe, Germany)
Ampicillin sodium salt	Roth (Karlsruhe, Germany)
BactoPeptone	BD Biosciences (San Jose, USA)
BactoTryptone	BD Biosciences (San Jose, USA)
Coomassie Brilliant Blue R-250	Serva (Heidelberg, Germany)
Cholesterol	Roth (Karlsruhe, Germany)
Desoxynucleoside triphosphates (dNTPs)	Roth (Karlsruhe, Germany)
Dimethyl sulfoxid (DMSO)	Sigma (St. Louis, USA)
Dithiothreitol (DTT)	Roth (Karlsruhe, Germany)
EDTA (Triplex III)	Merck (Darmstadt, Germany)
Ethanol	Merck (Darmstadt, Germany)
Ethidium bromide	Roth (Karlsruhe, Germany)
Formaldehyd 37 %	Roth (Karlsruhe, Germany)
Glucose	Merck (Darmstadt, Germany)
Glutathione (oxidized)	Sigma (St. Louis, USA)
Glutathione (reduced)	Sigma (St. Louis, USA)
Glycerol 99 %	Roth (Karlsruhe, Germany)
Guanidinium chloride (GdmCl)	Sigma (St. Louis, USA)
Hydroxy chloride 32 %	Roth (Karlsruhe, Germany)

Table 4.1: Chemicals.

Chemical	Producer
Isopropanol	Merck (Darmstadt, Germany)
Isopropyl fi-d-1-thiogalactopyranoside (IPTG)	Serva (Heidelberg, Germany)
Kanamycin sulfate	Roth (Karlsruhe, Germany)
LB_0 medium	Serva (Heidelberg, Germany)
Magnesium chloride	Merck (Darmstadt, Germany)
MES	Roth (Karlsruhe, Germany)
Milk powder	Roth (Karlsruhe, Germany)
MOPS	Roth (Karlsruhe, Germany)
Phenylmethanesulfonyl fluoride (PMSF)	Sigma (St. Louis, USA)
Protease inhibitor Mix FY, G, HP, M	Serva (Heidelberg, Germany)
Potassium chloride	Roth (Karlsruhe, Germany)
Potassium phosphate (mono-, di-hydrate)	Merck (Darmstadt, Germany)
Potassium sulfate	Merck (Darmstadt, Germany)
Sodium dodecylsulfate (SDS)	Serva (Heidelberg, Germany)
Sodium phosphate (mono-,di-hydrate)	Merck (Darmstadt, Germany)
Stain G	Serva (Heidelberg, Germany)
Tris(2-carboxyethyl)phosphine hydrochloride solution pH 7.0 (TCEP)	Sigma (St. Louis, USA)
N,N,N',N'-Tetramethylethylendiamin (TEMED)	Roth (Karlsruhe, Germany)
Triton-X	Merck (Darmstadt, Germany)
Tris(hydroxymethyl)aminomethane (Tris)	Roth (Karlsruhe, Germany)
Tween-20	Merck (Darmstadt, Germany)
Urea	Merck (Darmstadt, Germany)

All other reagents were p.a. quality and purchased from Merck (Darmstadt, Germany), except fluorescence labels, which were provided by Atto-Tech (Siegen, Germany). For the preparation of buffers, only deionized water(TKA GenPure, Thermo Scientific, Niederelbert, Germany) was used.

4.1.2 DEVICES

Table 4.2: Devices.

Device	Producer
Autoclave Varioclav EP-Z	H+P (Oberschleißheim, Germany)
Cell Disruptor Apparatus Basic Z	Constant Systems (Daventry, UK)
Centrifuges	
Avanti J25 and J26 XP	Beckman Coulter (Krefeld, Germany)
ProteomeLab XL-A (equipped with FDS)	Beckman Coulter/Aviv (Krefeld, Germany/Lakewood, USA)
Optima XL-A	Beckman Coulter (Krefeld, Germany)
Rotina 46R	Hettich (Tuttlingen, Germany)
Universal 32R	Hettich (Tuttlingen, Germany)
Tabletop centrifuge 5415 C	Eppendorf (Hamburg, Germany)
Chromatography systems	
ÄKTA FLPC	GE Healthcare (Munich, Germany)
ÄKTA Prime	GE Healthcare (Munich, Germany)
GradiFrac	GE Healthcare (Munich, Germany)
Circular dichroism spectropolarimeters	
J710 (with PTC 343 Peltier device)	Jasco (Groß-Umstadt, Germany)
J715 (with PTC 343 Peltier device)	Jasco (Groß-Umstadt, Germany)
Fluorescence spectrophotometers	
Spex FluoroMax-2	Jobin Yvon (Unterhaching, Germany)
Spex FluoroMax-3	Jobin Yvon (Unterhaching, Germany)
Gel documentation system Biodoc II	Biometra (Göttingen, Germany)
Gel electrophoresis and blotting devices	Hoefer (Holliston, USA)
Homogenizer Ultra Turrax DIAX900	Heidolph (Schwabach, Germany)
HPLC systems	Jasco (Groß-Umstadt, Germany)
Ice maker	Ziegra (Isernhagen, Germany)
Incubator	New Brunswick Scientific (Connecticut, USA)
Magnetic stirrer Heidolph MR2000	Heidolph (Schwabach, Germany)
Mass spectrometers	
Ultraflex II MALDI ToF/ToF	Bruker Daltonics (Bremen, Germany)
Microscopes	

Table 4.2: Devices.

Device	Producer
Leica MZ16FA	Leica Microsysteme (Wetzlar, Germany)
Stemi SV11 (with KL1500LCD)	Zeiss/Schott (Oberkochen, Germany/Mainz, Germany)
Stemi 2000 (with CL1500ECO)	Zeiss/Schott (Oberkochen, Germany/Mainz, Germany)
Axiovert 200 with HAL100 and HBO100	Zeiss/Schott (Oberkochen, Germany/Mainz, Germany)
MM400 beatmill	Retsch (Haan, Germany)
Mx3000P QPCR System	Agilent (Böblingen, Germany)
pH meter	WTW (Weilheim, Germany)
Power amplifiers EPS 3500, 3501 and 1001	GE Healthcare (Munich, Germany)
Scales	
BP 121 S	Sartorius (Göttingen, Germany)
BL 310	Sartorius (Göttingen, Germany)
Thermal cycler Primus 25	MWG (Ebersberg, Germany)
Thermomixer	Eppendorf (Hamburg, Germany)
Thermoblock TB 1	Biometra (Göttingen, Germany)
Typhoon 9200	GE Healthcare (Munich, Germany)
Ultra filtration cell 8050	Millipore (Billerica, USA)
UV/VIS spectrophotometers	
Varian Cary 50 Bio	Agilent (Böblingen, Germany)
Varian Cary 100 Bio	Agilent (Böblingen, Germany)
Nanodrop	Peqlab (Erlangen, Germany)
Novaspec II	GE Healthcare (Munich, Germany)
Vortex MS2	IKA (Staufen, Germany)
X-ray film processor Optimax TR	MS Laborgeräte (Dielheim, Germany)

4.1.3 Software, Databases and Web-based Tools

Software

Table 4.3: Software.

Program	Company/Developer
Adobe Illustrator CS2	Adobe Inc.
Adobe Photoshop CS2	Adobe Inc.
Ape Plasmid	M. Wayne Davis
DCDT+	John Philo
EndNote Web	Thomson Reuters
ImageQuant	GE Healthcare
MikTex	Open Source
MMass	Open Source
Origin 8.0G	OriginLab Corp.
Pymol	Schrödinger
Sedanal	Walter Stafford
SedFit	Peter Schuck
Sednterp	John Philo
Sedphat	Peter Schuck
SedView	Hayes, Stafford
UltraScan	Borries Demeler

Databases

Table 4.4: Databases.

Database	Internet address
PDB	www.rcsb.org/pdb
PDBe	www.ebi.ac.uk/pdbe
PubMed	www.ncbi.nlm.nih.gov/pubmed
ISI Knowledge	portal.isiknowledge.com
UniProt	www.uniprot.org
Wormbase	www.wormbase.org

Web-based Tools

Table 4.5: Web-based Tools.

Web-based Tools	Internet address
ClusterW2	http://www.ebi.ac.uk/Tools/msa/clustalw2
FindPept	http://web.expasy.org/findpept
NCBI Blast	http://blast.ncbi.nlm.nih.gov
PeptideCutter	http://web.expasy.org/peptide_cutter
ProtParam	http://web.expasy.org/protparam
ProtScale	http://web.expasy.org/protscale
Primer-BLAST	http://www.ncbi.nlm.nhi.gov/tools/primer-blast

4.1.4 CONSUMABLES

Table 4.6: Consumables.

Consumables	Producer
Amicon Ultra-15 Centrifugal Filter Units	Millipore (Billerica, USA)
Amicon Ultra-4 Centrifugal Filter Units	Millipore (Billerica, USA)
Blotting paper	Whatman (Maidstone, UK)
Cuvettes, plastic, 1 mL	Brand (Wertheim, Germany)
Cuvettes, plastic, half-micro	Brand (Wertheim, Germany)
Dialysis membranes Spectra/Por (various MWCOs)	Spectrum Laboratories (Rancho Dominguez, USA)
Immobilon-P membrane (PVDF)	Roth (Karlsruhe, Germany)
Fluorescent antibody membranes	Millipore (Billerica, USA)
Membrane discs	Sartorius (Göttingen, Germany)
PCR tubes	Nerbe plus (Winsen/Luhe, Germany)
PE tubes, 15 mL and 50 mL	Greiner & Söhne (Nürtingen, Germany)
Petri dishes, PS, 94 mm	Greiner & Söhne (Nürtingen, Germany)
pH indicator	Merck (Darmstadt, Germany)
Reaction tubes, various volumes	Nerbe plus/Eppendorf (Winsen/Luhe, Germany/Hamburg, Germany)
disposable acryl UV cuvettes	Brand (Wertheim, Germany)
X-ray film X-OMAT AR	Kodak (Rochester, USA)

4.1.5 CHROMATOGRAPHY MATERIAL

Table 4.7: Chromatography material.

Material	Producer
DEAE Sephacel ff	GE Healthcare (Freiburg, Germany)
Sephacryl S-300 HR	GE Healthcare (Freiburg, Germany)
Superdex 75 Prep Grade (16/60)	GE Healthcare (Freiburg, Germany)
Superdex 200 Prep Grade (16/60)	GE Healthcare (Freiburg, Germany)

4.1.6 *E. COLI* STRAINS

Table 4.8: *E. coli* strains.

Strain	Genotype	Origin/Reference
Cloning		
XL1 Blue	recA1 endA1 gyrA96 thi-1 hsdR17 supE44 relA1 lac [FproAB lacIqZDM15 Tn10 (TetR)]	Stratagene (La Jolla, USA)
Mach 1	ΔrecA1398 endA1 tonA Θ80ΔlacM15 ΔlacX74 hsdR(r_K^- $m4_K^+$)	Stratagene (La Jolla, USA)
Expression		
BL21 (DE3)	F^- dcm ompT $hsdS_B(r_B^-m_B^-)$ gal λ(DE3)	Stratagene (La Jolla, USA)
BL21 (DE3) p*	F^- dcm ompT $hsdS_B(r_B^-m_B^-)$ gal λ(DE3)	[123]
feeding bacteria		
HT115 (DE3)	F^-, mcrA, mcrB, IN(rrnD-rrnE)1, rnc14::Tn10(DE3 lysogen: lavUV5 promoter -T7 polymerase) (IPTG-inducible T7 polymerase) (RNase III minus)	Caenorhabditis Genetics Center (Minneapolis, USA)
OP50	-	Caenorhabditis Genetics Center (Minneapolis, USA)

4.1.7 *C. ELEGANS* STRAINS

Table 4.9: *C. elegans* strains.

Strain	Genotype	Origin/Reference
N2	*C. elegans*wild isolate	Caenorhabditis Genetics Center (Minneapolis, USA)
RB2600	hsp-12.1 (ok3622)I.	Caenorhabditis Genetics Center (Minneapolis, USA)
RB2612	hsp-12.2 (ok3638) III.	Caenorhabditis Genetics Center (Minneapolis, USA)
VC2346	hsp-12.3 (ok3095) IV.	Caenorhabditis Genetics Center (Minneapolis, USA)
VC281	hsp-12.6 (gk156) IV.	Caenorhabditis Genetics Center (Minneapolis, USA)

4.1.8 ENZYMES, STANDARDS AND KITS

Table 4.10: List of Enzymes, Standards and Kits.

Enzyme	Producer
1kb Ladder	Peqlab (Erlangen, Germany)
Pfu DNA polymerase	Promega (Fitchburg, USA)
Pwo DNA polymerase	Roche (Rotkreuz, Schweiz)
Restriction enzymes	Promega/NEB (Fitchburg, USA/Ipswich, USA)
T4 ligase	Promega (Fitchburg, USA)
Taq DNA polymerase	Promega (Fitchburg, USA)
Wizard Miniprep kit	Promega (Fitchburg, USA)
Wizard PCR product purification and gel extraction Kit	Promega (Fitchburg, USA)
Brilliant III Ultra-Fast SYBR Green QRT-PCR Master Mix	Stratagene (Waldbronn, Germany)
Protein-Marker IV	Peqlab (Erlangen, Germany)
LMW marker	Biorad (Munich, Germany)

4.1.9 ANTIBIOTICS

Table 4.11: List of Antibiotics with final used concentrations. Stock solutions were 1000x concentrated.

Antibiotic	used concentration
Ampicillin (in H_2O)	100 µg/µL
Tetracyclin (in EtOH)	12.5 µg/µL
Kanamycin (in H_2O)	50 µg/µL

4.1.10 ANTIBODIES

Table 4.12: Antibodies.

Antibody	Producer
α-Hsp12.1 (polyclonal)	Pineda (Berlin, Germany)
α-Hsp12.6 (polyclonal)	Pineda (Berlin, Germany)
α-rabbit (monoclonal) Peroxidase coupled	Sigma (St. Louis, USA)

4.1.11 PROTEINS

Table 4.13: Proteins, which where not purified in this work and there origin.

Protein	Original Organism	Producer
Citrate synthase	Pork	Dr. Martin Haslbeck
Lysozyme	Chicken egg	Sigma (Massachusetts, USA)
GR-LBDm	Human	Oliver Lorenz, Daniel Rutz
yHsp90	Yeast	Oliver Lorenz, Daniel Rutz
yp23	Yeast	Oliver Lorenz, Daniel Rutz
Sip-1	*C. elegans*	Tilly Fleckenstein

4.1.12 PRIMERS

Table 4.14: Primer for qRT-PCR analyzes.

Primer	Sequence ($5' \rightarrow 3'$)
qHsp12.1-f	TCC ATT TAC AAC TGA CTC GGC GGC TTC
qHsp12.1-r	TGG CAG TGA TTG TGA GAA CTC CGG ATG AG
qHsp12.2-f	TCC GCT ATC GAG GTG ACC GCT GA
qHsp12.2-r	ACG TCA TCT GGA AGT TTG TAG GCA CGG T
qHsp12.3-f	TGT CTG TTG CTA TTG ATC ACG ATC AAA CTG CTA
qHsp12.3-r	TCT TGA TGG TAG CTG GAT CGG TTC CCT
qHsp12.6-f	GGG AGA TGG AGT TGT CAA T
qHsp12.6-r	GCT TCA ATG TGA AGA ATT CCA TGT GAA TCC AAG TTG C
qHsp25-f	AGA GAA ATG TCG GAA CGC CGT ATC GAC G
qHsp25-r	GCC AAT GCG TTC AGA ACA TCA TTC ATC AGC T
qZK1128.7-f	GCC GAT CAC AGT TGC TGA ATA CAT GAA GAC CT
qZK1128.7-r	GCC AAT GCG TTC AGA ACA TCA TTC ATC AGC T
qAct-1-f	AAT CCA AGA GAG GTA TCC TTA
qAct-1-r	GAT GGC GAC ATA CAT GGC
qDaf-21-f	AAG ATG AGG AGG CTG TCG
qDaf-21-r	CAT TGG ACA AGC TCT TGT AGA

4.1.13 PLASMIDS

Table 4.15: Expression and RNAi plasmids used in this work.

Vector	Description	Reference
pET21a	Amp^R, lac Promotor/Operator, T7	Novagen (Wisconsin, USA)
pET28a	Amp^R, lac Promotor/Operator, T7	Novagen (Wisconsin, USA)
pL4440	Amp^R, lac Promotor/Operator, T7, T3	addgene (Massachusetts, USA)
pET21-Hsp12.1	Amp^R, lac Promotor/Operator, T7	Dr. Martin Haslbeck
pET21-Hsp12.2	Amp^R, lac Promotor/Operator, T7	Dr. Martin Haslbeck
pET21-Hsp12.3	Amp^R, lac Promotor/Operator, T7	Dr. Martin Haslbeck
pET21-Hsp12.6	Amp^R, lac Promotor/Operator, T7	Dr. Martin Haslbeck
pET28-Hsp12.6	Amp^R, lac Promotor/Operator, T7	Geneart (Regensburg, Germany)
pET21-Hsp25	Amp^R, lac Promotor/Operator, T7	this work
pET21-ZK1128.7	Amp^R, lac Promotor/Operator, T7	this work
pL4440-Hsp12.1	Amp^R, lac Promotor/Operator, T7, T3	Thermo Scientific (Schwerte, Germany)
pL4440-Hsp12.2	Amp^R, lac Promotor/Operator, T7, T3	Thermo Scientific (Schwerte, Germany)
pL4440-Hsp12.3	Amp^R, lac Promotor/Operator, T7, T3	Thermo Scientific (Schwerte, Germany)
pL4440-Hsp12.6	Amp^R, lac Promotor/Operator, T7, T3	Thermo Scientific (Schwerte, Germany)
pL4440-Hsp25	Amp^R, lac Promotor/Operator, T7, T3	Thermo Scientific (Schwerte, Germany)
pL4440-ZK1128.7	Amp^R, lac Promotor/Operator, T7, T3	Thermo Scientific (Schwerte, Germany)

4.1.14 MEDIA

Besides standard LB_0 media (4.1.1), the following media was used for *E. coli* cultivation.

SOD (pH7.4)	Yeast extract	0.5 %
	Tryptone	2 %
	NaCl	10 mM
	KCl	2.5 mM
	$MgCl_2$ * 6aq	10 mM
	$MgSO_4$ * 7aq	10 mM

For LB_0 plates, 15 g/L Agar Agar were added to LB_0 medium.
The following media were used for *C. elegans* cultivation.

NGM-Agar	Bacto Peptone	2.5 g
	NaCl	3.0 g
	Agar Agar	17.0 g
	Cholesterol (5 mg/mL in EtOH)	1 mL
	H_2O	975 mL
	→ autoclave	
	1 M $CaCl_2$ (sterile)	1 mL
	1 M $MgSO_4$ (sterile)	1 mL
	1 M K-phosphate pH 6 (sterile)	25 mL
	For RNAi plates add additionally	
	1 M IPTG	1 mL
	Amicillin (100 mg/mL in H_2O)	1 mL
	Tetracyclin (12.5 mg/mL in EtOH)	1 mL
M9 Medium	Na_2HPO_4	6.0 g
	KH_2PO_4	3.0 g
	NaCl	5.0 g
	1 M $MgSO_4$	1 mL
	H_2O	1 L
Bleaching Solution	1 M NaOH	20 mL
	Chlorix	20 mL
	H_2O	10 mL

All media and stock solutions were stored in Erlenmeyer flasks, test tubes, or 1 L flasks after pH adjustment. Sterilization was conducted by autoclaving for

20 min to 30 min at 121 °C and 200 kPa. After autoclaving and cooling-down to 60 °C, agar plates were mixed with the respective antibiotics and poured into plastic Petri dishes under sterile conditions. Storage occurred at 4 °C.

4.1.15 BUFFERS

MOLECULAR BIOLOGY

Table 4.17: Buffers used for molecular biology approaches.

TAE (50x)	Tris/acetate pH 8.0	2 M
	EDTA	50 mM
BJ (10x)	Glycerol	50 % (v/v)
	EDTA pH 8.0	10 mM
	Bromphenoleblue	0.2 % (w/v)
	Xylencyanol	0.2 % (w/v)
1% Agarose solution	Agarose	1 g
	TAE (1x)	100 mL
	StainG	1 - 2 µL
dNTP-Mix	dATP	10 mM
	dGTP	10 mM
	dCTP	10 mM
	dTTP	10 mM
TB	PIPES (HEPES) pH 7.5	10 mM
	$CaCl_2$	15 mM
	KCl (adjust pH)	250 mM
	$MnCl_2$	55 mM
Quick Ligation buffer (2x)	Tris/HCl pH 7.6	132 mM
	$MgCl_2$	20 mM
	DTT	2 mM
	ATP	2 mM
	PEG 6000	15 % (v/v)

Protein Chemical Buffers

Table 4.18: Buffers for protein chemical experiments.

SDS running buffer (10x)	Tris/HCl pH 6.8	250 mM
	Glycine	2 M
	SDS	1 % (w/v)
Laemmli sample buffer (5x)	Tris/HCl pH 6.8	312.5 mM
	SDS	10 % (w/v)
	Glycerol	50 % (v/v)
	2-mercaptoethanol	2.5 % (v/v)
	Bromphenolblue	0.05 % (w/v)
Separating gel buffer (4x)	Tris/HCl pH 8.8	250 mM
	SDS	0.8 % (w/v)
Stacking gel buffer (2x)	Tris/HCl pH 6.8	250 mM
	SDS	0.4 % (w/v)
Fairbanks A	Coomassie Brilliant Blue R-250	2.5 g
	Ethanol	250 mL
	Acetic acid	80 mL
	adjust to 1 L with H_2O	
Fairbanks D	Acetic acid	10 % (v/v)
Transfer buffer	Tris/HCl pH 7.5	50 mM
	Glycine	40 mM
	SDS	0.04 % (w/v)
	Methanol	20 % (v/v)
PBS (10x)	KH_2PO_4	15 mM
	Na_2HPO_4	81 mM
	KCl	27 mM
	NaCl	1370 mM
PBS-T	PBS (1x)	

	Tween		0.1 (w/v)
Dialysis and Standard measurement buffer	Na-Phosphate pH 7.5		20 mM
	NaCl		150 mM
CS aggregation buffer	Na-Phosphate pH 7.5		20 mM

Protein Purification Buffers

Table 4.19: Buffers used for protein purifications.

DEAE buffer A	Tris/HCl pH 8	50 mM
	EDTA	5 mM
DEAE buffer B	Tris/HCl pH 8	50 mM
	EDTA	5 mM
	NaCl	1 M
Superdex buffer A	Tris/HCl pH 8	50 mM
	EDTA	5 mM
	NaCl	150 mM
Superdex buffer B	Tris/HCl pH 8	50 mM
	EDTA	5 mM
	NaCl	300 mM

Table 4.20: Standard temperature profile for PCR reactions.

Initial Denaturing	95 °C	3 min
Start PCR cycle		
Denaturing	95 °C	30 s
Annealing	T_m−5 K	30 s
Elongation	72 °C or 68 °C	60 s/1kb
End PCR cycle		
Final Elongation	72 °C or 68 °C	7 min

4.2 METHODS

4.2.1 MOLECULAR BIOLOGY METHODS

PCR and qRT-PCR

polymerase chain reaction Certain DNA fragments can be amplified with the help of polymerase chain reaction (PCR). For the PCR reaction, different polymerases dependent on the aim of the experiment were used. Amplification of genomic DNA fragments was conducted with Pfu or Pwo polymerase; for standard PCR reactions, Taq polymerase was usually used. All primers were designed with respect to melting temperatures between 65 °C to 75 °C. The melting temperature T_m was calculated with ApePlasmid (4.1.3). The standard reaction batch of a PCR reaction is composed as follows:

Template DNA	1 - 5 µL (ca. 50 - 200 ng)
10x reaction buffer	5 µL
dNTP mix	2 µL
Primer 1 (100 pmol/µL)	1 µL
Primer 2 (100 pmol/µL)	1 µL
Polymerase	2.5 units
H_2O	ad 50 µL

PCR reactions were performed in a PCR cycler (4.1.2) with amplification programs adjusted to the respective primer pair, polymerase and fragment length. Typically, thirty cycles were used for amplification (4.20).

quantitative reverse transcriptase pcr Nowadays, quantitative reverse transcriptase PCR (qRT-PCR) is a common method to analyze expression levels on RNA basis. During the reaction, the RNA or mRNA of specific interest is translated with a reverse transcriptase to cDNA. The amount of cDNA is equal to the original mass of RNA. Subsequently, the cDNA is amplified in a standard PCR reaction. After a lag phase, the reaction proceeds exponentially until the quantity and availability of the primer and nucleotides as well as the processivity of polymerases limit the reaction. Since the exit point

Table 4.21: Temperature profile for qRT-PCR measurements.

RT reaction	50 °C	10 min
Denaturing	95 °C	3 min
Start PCR cycle (50x)		
Denaturing	95 °C	20 s
Annealing/Elongation	60 °C	20 s
End PCR cycle		
Denaturing	95 °C	4 min
Cooling	95 °C to 25 °C (−0.3 K/cycle)	30 s
Melting curve	25 °C to 95 °C (0.3 K/cycle)	30 s

of exponential expression is hard to determine, the amplification is directly detected with SYBR Green during the PCR.

SYBR Green is a DNA specific fluorescent cyanine dye. After binding to dsDNA, SYBR Green can be excited with 488 nm and the emitted fluorescence detected at 522 nm.

To assure the quality of a qRT-PCR experiment and the generated results, positive and negative control reactions have to be performed. Positive controls assist in the identification of false negatives that might occur due to sample template quality or PCR inhibitors present in the sample. As positive controls exogenous samples, in this work AlienRNA (Invitrogen), and endogenous controls were used. As endogenous controls (housekeeper genes) Actin (Act-1) and a member of the Hsp90 family from *C. elegans* (Daf-21) were used. Negative controls miss one of the components essential for the reaction, thus no rise in fluorescence was expected. A 'no template' (NTC), 'no reverse transcriptase' (NRTC) and 'no primer control' (NPC) reactions were used for negative controls. NTCs provides means to control for external contamination or other factors, such as dimerizing primers, that can result in non specific increase in fluorescence. The NRTC gives information about genomic DNA contaminations which are amplifiable with the used primer pairs. The third negative control is missing the primers (NPC) and shows unspecific amplification.

All primers were designed to span at least one exon or if possible span exon-exon boundaries. The length of the amplicon of each primer pair was set between 150 - 250 basepairs to allow an optimal performance of SYBR Green. Additionally, all primers were blasted against the *C. elegans* genome to control for their uniqueness. If primers had second binding sites in the genome, it was ensured that the related second primer did not bind nearby in the genome, to guarantee that no contaminating PCR product was amplified. Additionally, all primers were analyzed with respect to secondary structure formation (Primer-BLAST).

qRT-PCR measurements were performed with the Brilliant III Ultra-Fast SYBR Green QRT-PCR Master Mix (Stratagene) in an Mx3000P QPCR System in a one-step reaction, following the temperature profile depicted in table 4.21.

Fluorescence was detected at the end of the Annealing/Elongation step and during the melting curve at the end of each temperature step as triple end point measurement. The detection is conducted with a quartz-tungsten halogen lamp for excitation and a photomultiplier tube for detection of the fluorescence signal. The specific wavelength for detection are defined by dye specific filter sets. The melting curve was used to identify the number of products. Each DNA fragment has its individual melting temperature depending on its nucleotide composition.

All samples contained 10 ng of total RNA, 50 nM of each primer and were formulated according to the mastermix manual [60]. The AlienRNA reactions were prepared according to the manufacturer's manual [59].

For the calculation of total copy numbers of mRNA and the respective fold-changes, Ct-values are used. Ct is the abbreviation of cycle threshold. Basically, in qRT-PCR the numbers of cycles needed for a fixed concentration of the amplicon are used to estimate the different starting concentrations of the templates. The corresponding fluorescence for the fixed amplicon concentration is set as threshold. The required number of cycles to cross this threshold is subsequently defined as Ct-value. The defined threshold has to be in the range, where all performed reaction show comparable increases in fluorescence. This enables the comparison of different samples. For the determination of the Ct-value, the amplification-based threshold method with default settings of the manufacturer's software MXPro is used.

Purification and Storage of DNA

Purification of PCR products, DNA fragments, and plasmid DNA after digestion were performed using the Wizard Plus Gel Extraction Kit (Promega), following the manufacturer's centrifugal protocol. For Minipreps the Wizard Plus SV Minipreps DNA Purification System (Promega) was used. All DNA was stored in sterile, nuclease-free water at −20 °C.

Agarose Gel

To analyze the size of DNA fragments and plasmids, agarose gel electrophoresis was used. After dissolving 1 % (w/v) of agarose by heating in 100 mL 1x TEA buffer, 1 µL to 2 µL of Stain G was added and the solution poured into a flat gel holder. After loading the samples, each gel was run at 120 V for 20 min in case of DNA fragments and plasmid and 1 h in case of digested vectors. If necessary DNA fragments were purified as described above (4.2.1).

RNA Purification and Storage

For preparation of total worm RNA, several NGM plates with nematodes were washed off with H_2O or M9. The worms were centrifuged at 1150 g for one minute and washed three times with 0.1 M sodium chloride. Subsequently, worms were incubated for two hours at 20 °C to ensure digestion of all remaining feeding bacteria. Afterwards, the nematodes were harvested and either frozen in liquid nitrogen for storage purpose or directly used for total RNA preparation.

For RNA extraction, a modified protocol of the SV Total RNA Isolation System from Promega was used. Worm pellets up to a weight of 100 ng were mixed with 175 µL RNA lysis buffer, 10 µL β-mercaptoethanol and five small spatula of glass pearls 0.2 µm in diameter.

Nematodes were disrupted in a MM400 beatmill (Retsch), repeating five times a shaking step at a frequency of 30 Hz for 30 s and a resting delay for 2.5 min. After disruption 350 µL RNA dilution buffer was added and the lysate was centrifuged at 14,000 g for 10 min at room temperature. The supernatant was transferred into a new Eppendorf tube, and mixed with 200 µL 95 % (v/v) ethanol. RNA was further purified as described in the standard centrifugal protocol from Promega.

Purified RNA was frozen with liquid nitrogen and stored at −80 °C for four months at maximum.

Restriction and Ligation

The following protocols were used for DNA digestion and ligation.

RESTRICTION Restriction of DNA plasmids and PCR products was performed by adding 3 units of the certain restriction enzymes to 0.5 µg DNA and 0.1 volumes of 10x restriction buffer to the reaction batch. The reactions were performed according to the producers' manuals.

LIGATION For ligation, digested DNA fragments and vectors were combined in a 3:1 up to 10:1 molar ratio. Each ligation batch contained 10 ng total DNA at maximum in a volume of 20 µL. 1 unit of T4 ligase was added for 1 µg of total DNA. The reaction was either performed in quick ligation buffer (4.17) for 30 min at room temperature or in 10x standard T4 ligase buffer at 4 °C or 14 °C over night, respectively. After ligation, *E. coli* cells were transformed with the total batch as described in (4.2.1).

Sequencing

Plasmid DNA with a concentration ranging from 20 ng/µL to 100 ng/µL was submitted for sequencing to GATC Biotech AG, Cologne, Germany.

Preparation of chemical competent *E. coli* Cells

For DNA transformation, chemical competent *E. coli* cells were produced according to the protocol of Sambrook et al. (2001) or Inoue et al. (1990).

Transformation of *E. coli*

100 ng/µL to 200 ng/µL of chemical competent *E. coli* cells were mixed with 20 ng of plasmid DNA and incubated for 15 min on ice. After a heat step for 45 s at 45 °C, cells were cooled down on ice for 5 min. 700 µL LB_0 were added and the cells incubated at 27 µL for 1 h to let the cells regenerate, the resistance genes transcribed and the antibiotics converting enzymes be synthesized. Cells were pelleted at 3,000 g for 5 min and plated on selective LB plates with glass spheres, 0.5 cm in diameter. Plates were incubated at 37 °C over night.

4.2.2 CULTIVATION AND STORAGE OF *E. COLI*

E. coli was cultivated in a thermostated incubator at 37 °C either on LB_0 plates or in LB_0 liquid media. For selection of strains an appropriate antibiotic was added to the media, hence selecting for cells containing the corresponding resistance genes either on the plasmid or in the genome. Liquid cultures were inoculated with fresh overnight cultures or single colonies from plates. Bacterial growth was monitored at 600 nm ($OD_{600nm} = 1$ corresponding to approx. $8 \cdot 10^8$ cells/ml). For long-term storage, 300 µL 5 % glycerol (sterile) were added to 700 µL of a freshly inoculated culture. Resulting in a 15 % glycerol culture stock, which was frozen using liquid nitrogen and stored at −80 °C.

4.2.3 CULTIVATION AND STORAGE OF *C. ELEGANS*

All *C. elegans* strains were cultivated on NGM plates seeded with a fresh overnight culture of *E. coil* OP50 at 15 °C, 20 °C, or 25 °C. Inoculation occurred via picking adult worms on, transferring synchronized L1 larvae to, chunking of agar pieces from other plates, or transferring 200 µL of a worm cryo culture to fresh NGM plates.

For cryo cultures of *C. elegans*, the nematodes were incubated on NGM plates until exhaustion of the *E. coli* OP50 bacteria lawn. Freshly starved worms were then harvested from plates and mixed with an equal volume of Soft Agar Freezing solution and aliquoted in 1 mL. Soft Agar Freezing cultures were slowly frozen in a Styrofoam box at −80 °C over night and afterwards stored at −80 °C.

4.2.4 *IN VIVO* METHODS

Synchronization of *C. elegans* and Isolation of Eggs

To obtain synchronized nematode populations, worms were chunked on NGM plates and incubated until reproduction started. Nematodes were washed of plates with ddH_2O, collected in 15 mL falcons (4.1.4) and centrifuged at 1150 g for 1 min. The supernatant were removed and 1 volume of nematode pellet mixed gently by inverting with 7 volumes of bleaching solution. The bleaching process was followed visually under a microscope until the number of intact adult nematodes decreased significantly. Worms were centrifuged again and the supernatant aspirated. To remove remaining bleaching solution, the nematode pellet was washed at least three times with 10 volumes of water and two times with M9 buffer (4.1.15). Between each washing step the worms were pelleted by centrifugation (1150 g, 1 min) and the supernatant was removed. After washing 5 volumes of M9 buffer was used to resuspend the egg pellet. For hatching and synchronization of the L1 larvae the nematode eggs were incubated over night at 20 °C with gentle rocking. In case of the isolation of eggs, the egg pellet was directly used for the experiments.

RNAi

Knock-down of certain genes was performed using the feeding approach as RNAi experiment. Therefore, *E. coli* HT115 carrying pL4440 vectors with certain RNAi genes were grown over-night at 37 °C and induced for double stranded mRNA production with 1 mM IPTG the next morning. After 4 h at 37 °C bacteria were seeded on RNAi plates (200 µL per plate of 5 cm in diameter) and synchronized L1 larvae were added (4.2.4). RNAi treated worms were either used for Western Blot analysis, qRT-PCR experiments, Lifespan or thrashing assays.

Lifespan Assay

To analyze the lifespan of different worm stains, 20 synchronized L1 larvae were either placed on a NGM or RNAi plates. After reaching the reproductive state,

the surviving worms were transferred to new plates every second to third day, in order to assure that only the F1 generation was analyzed during that assay.

Thrashing Assay

Thrashing assay of RNAi worms and knockout worms were performed with L1 larvae, which were placed on RNAi plates or NGM plates and incubated at 20 °C until they developed to young adulthood. Young adult worms were picked from plates to a 10 µL drop of M9 (4.1.14). After several minutes of recovery from the transfer, thrashing movements of the individual worms were counted for one minute.

4.2.5 PROTEIN CHEMICAL METHODS

SDS-polyacrylamid Gel Electrophoresis

SDS-polyacrylamid gel electrophoresis (SDS-PAGE) is a discontinuous electrophoresis technique and was performed according to a modified protocol of Laemmli [136]. As standard, gels with 12.5 % (w/v) acrylamid/bis-acrylamid 19:1 for stacking gels and 5 % (w/v) acrylamid/bis-acrylamid for separation gels were used. With tetramethylethylendiamine (TEMED) and 10 % (w/v) ammonium persulfate (APS) the polymerization of each gel section was induced. Samples were mixed with 5x Laemmli buffer and boiled at 95 °C for 5 min prior to loading. Each gel was run at 30 mA constant current for 50 min and subsequently stained with a modified Coomassie staining protocol according to Fairbanks [68]. For molecular weight detection, either a LMW standard from Biorad (4.1.8) or peqlab (4.1.8) was used.

Protein Expression

Protein purification was performed using either the *E. coli* strains BL21 or BL21 p* regarding the expression plasmids. 50 mL cultures with the corresponding antibiotic (4.1.9) to the expression plasmid were grown over night at 37 °C. Expression cultures were inoculated with the over night cultures using a ratio of 1:50 of culture to fresh LB medium with antibiotics and further incubated at 37 °C. When an OD_{600} of $0.5 - 0.8$ was reached, expression was induced by addition of 1 mM IPTG. Expression was carried out over night at 30 °C.

CHROMATOGRAPHY

The following chromatography techniques were used for the purification of soluble and insoluble proteins.

ION-EXCHANGE CHROMATOGRAPHY The principle of separation in ion-exchange chromatography is based on the competitive binding from charged side chains of proteins in the liquid phase to charged chemical linkers in the material of the column bed. Therefore, the binding and elution buffer have to differ in ionic strength and/or in pH to enable best possible binding of the protein to be purified.

In this work the anionic exchange material DEAE ff (GE Healthcare) was used. After equilibration of the column in DEAE buffer A (4.19), proteins in the same buffer were loaded to the column. After application of the proteins, the column was washed with five column volumes to remove not bound or extremely weakly bound proteins. Elution was performed with a linear gradient of NaCl in DEAE buffer B (4.19) up to 500 mM NaCl over at least fifteen column volumes. Washing and elution steps were collected in 10 mL fractions.

SIZE EXCLUSION CHROMATOGRAPHY Separation via gel filtration or size exclusion chromatography is dependent on the retention volume/time of proteins. The retention is defined by the size and shape of the proteins leading to different permeation of the column matrix of well defined pore sizes. In this work Superdex 200 16/60 *prep grade* and Superdex 75 16/60 *prep grade* columns (GE Healthcare) were used with the buffers listed in 4.19. The eluate was collected typically in 1.5 mL fractions.

PURIFICATION OF SOLUBLE PROTEINS

All members of the Hsp12 family from *C. elegans* were purified with a two-step protocol.

After protein expression (s. above) the *E. coli* cells were harvested at 5,000 rpm in a JA-10 rotor (Beckman Coulter, Krefeld, Germany) for 15 min at 4 °C and suspended in buffer A (4.19) taking 5 mL buffer for 1 g of cell pellet (wet weight). Prior to cell lysis, protease inhibitor HP (Serva, Heidelberg, Germany) was added to the cell suspension. Disruption of cells was conducted with the cell disruptor (Constant Systems, Daventry, UK) using 2.3 kbar. To separate the soluble fraction of all cell debris and not lysed cells, the lysate was centrifuged at 18,000 rpm in a JA-25.50 rotor (Beckman Coulter, Krefeld, Germany) for 45 min. Afterwards, the cleared lysate was applied to a DEAE column and eluted as described in 4.2.5.

Table 4.22: Developing steps of Western Blot analysis.

step	time	chemical
blocking	60 min	5 % (w/v) milk powder in PBS-T
wash	three times for 5 s	PBS-T
staining 1	60 min	primary antibody in 1 % (w/v) milk powder in PBS-T
wash	three times for 10 min	PBS-T
staining 2	60 min	secondary antibody in 1 % (w/v) milk powder in PBS-T
wash	three times for 10 min	PBS-T

All fractions containing the protein of interest were combined and concentrated for the subsequent size exclusion chromatography. Only pure protein fraction after gel filtration were pooled, concentrated again and aliquoted in 150 µM fractions.

After each purification step, SDS-PAGE analysis (4.2.5) was performed to identify the fractions which contained the target protein. Proteins were stored at −20 °C or −80 °C depending on their stability.

Western Blot

For western blots SDS-PAGEs were performed as described in (4.2.5). To transfer all proteins from the SDS-PAGE to a membrane, a semi-dry blotting approach was performed according to the manufacturer's protocol.

PVDF or specific PVDF membranes for fluorescence detection were used as membranes . Both types of membranes were activated in methanol prior to western blotting. The transfer of proteins was conducted with 1.5 mA/cm^2 for 60 min.

After blotting, each membrane was developed with a primary and secondary antibody according to the scheme in 4.22.

The signal detection was dependent on the secondary antibody and its coupled detection marker. It was conducted with WesternBright™ECL-Spray Western Blott detection system (advansta, California, USA) and the ImageQuant LAS 400 (GE Healthcare, Munich, Germany).

TCA Precipitation

For trichloroacetic acid (TCA) precipitation of proteins, 50 % (w/v) TCA solution were added to solved proteins to a final concentration of 10 − 15 % (w/v). The mixture was incubated at least for 1 h at −20 °C, thawed and centrifuged

at full speed and 4 °C for 10 min. The supernatant was discarded and the pellet washed with 500 µM acetone and centrifuged as before. The washing step was repeated with 200 µM. The protein pellets were dried with open lid at room temperature for 15 min and solubilized in 1x Laemmli sample buffer for SDS-PAGE analysis.

CHAPERONE ASSAYS

To analyze if the small heat shock proteins studied in this work show chaperone activity, two different model substrates were used to study the suppression of aggregation.

The first model substrate was citrate synthase (CS). Incubation at 43 °C in CS aggregation buffer (4.18) leads to quantitative aggregation after 120 min. After pre-heating of the sHsps at different concentrations at 43 °C, 1 µM CS was added to start the aggregation process.

As second model substrate, lysozyme from chicken egg white was aggregated by reduction via TCEP addition. Lysozyme aggregation was performed at 20 °C for 150 min. Aggregation was started by addition of 500 nM TCEP after temperature equilibration of 5 µM lysozyme in the presence of different concentrations of sHsps.

The measurements were conducted in a Cary 50 UV/VIS spectrophotometer (Agilent, Böblingen, Germany) equipped with a temperature-adjustable cuvette holder at 360 nm in quartz cuvettes for CS aggregation and disposable acryl cuvettes for lysozyme aggregation. After the aggregation process was finished, the insoluble fraction and supernatant was analyzed by SDS-PAGE and Coomassie staining after centrifugation at 10,000 g for 5 min in a table-top centrifuge. The insoluble fraction was washed two times by resuspending it in standard measurement buffer and finally dissolved in 1x Laemmli sample before separation by SDS-PAGE.

4.2.6 BIOPHYSICAL METHODS

THERMOSTABILITY ASSAY

The thermal unfolding of proteins was detected with the thermostability assay (TSA) by the use of the fluorescent dye SYPRO Orange (Invitrogen, California, USA). During the heating procedure the protein unfolds and exposes its hydrophobic residues. SYPRO Orange is a dye which increases its fluorescence upon binding to hydrophobic residues. In this work the TSA was used to measure the stability of proteins at different buffer conditions (s. VERWEIS). All used proteins were diluted to a final concentration of 0.5 mg/mL in 18 µL buffer. Each

sample was then mixed with 2 µL of a 1:100 dilution of the ready-to-use dye provided by Invitrogen (Stadt Land), which leads to a final dilution of 1:1000 of SYPRO Orange. All TSA measurements were conducted in a Mx3000P QPCR System (Agilent, Böblingen, Germany) using the melting curve protocol with a defined heating rate of 0.5 K/min^{-1} between every detection step.

Spectroscopic Methods

ultraviolet (uv)/visible (vis)-spectroscopy Absorption describes a physical process where electrons are lifted from their electronic ground state to an excited state by light of a certain wavelength. All functional groups in molecules which are responsible for absorption, are named chromophores. In proteins especially the absorption of the aromatic amino acids tryptophan, tyrosine, and phenylalanine are used to determine the concentration of protein solutions. With the Lambert-Beer law the concentration can be calculated from the absorbance at 280 nm (4.1).

$$A_{280nm} = log\frac{I_0}{I_1} = \epsilon_{280nm} \cdot c \cdot d \rightarrow c = \frac{A_{280nm}}{\epsilon_{280nm} \cdot d} \tag{4.1}$$

A_{280nm} is the absorbance at 280 nm, I_0 stands for incident light intensity, I_1 for the transmitted light intensity, ϵ_{280nm} for the molar extinction coefficient at 280 nm, c for the concentration of the analyzed solution, and d for the path length of the used cuvette.

Theoretical extinction coefficients were calculated from the amino acid sequence with the Protparam tool (4.4). All concentrations were determined with a Cary 50 UV/VIS spectrophotometer (Varian) and corrected for the buffer absorbance.

circular dichroism (cd)-spectroscopy Unsymmetrical molecules, for example the peptide backbone and the amino acids except Glycine, are able to depolarize light. This effect is called circular dichroism (CD) and utilized in CD-spectroscopy. Chrioptical characteristics of the backbone are defined by the secondary structure. For aromatic amino acids the characteristics depend on the asymmetric environment in the natively folded protein. The far-UV CD spectrum (FUV) represents the sum of all signals originating from different secondary structure elements (4.23).

All CD measurements were conducted in a Jasco J-715 or a J-710 CD spectropolarimeter equipped with a PTC 343 Peltier element. Standard FUV spectra were measured between 280 nm and 190 nm, with a scan speed of 20 nm/min, a data pitch of 0.1 s, a band width of 1 nm and a response time of 4 s with sixteen accumulations. All samples were measured at 20 °C in a plate cuvette with a path length of 0.2 nm and a concentration of 0.2 mg/mm. All spectra were buf-

Table 4.23: Signals of secondary structure elements.

secondary structure	CD signal
β-sheet	maximum at 196 nm, minimum at 218 nm
α-helix	maximum at 192 nm, minima at 209 nm and at 222 nm
random coil	minimum at 195 nm, maximum at 212 nm

fer corrected and normalized with respect to the mean residual weight ellipticity Θ_{MRW} (4.2).

$$\Theta_{MRW} = \frac{\Theta \cdot 100}{d \cdot c \cdot N_{aa}} \tag{4.2}$$

Θ stands for the obtained ellipticity (mdeg), d for the path length (mm), c for the concentration (mM), and N_{aa} is the number of amino acids.

Near UV-spectra (NUV) were measured with the same device parameters from 340 nm to 250 nm in a cuvette with 5 mm path length at concentrations of 0.5 mg/mL.

Thermal stability transitions were conducted in a 1 mm closable cuvette at 220 nm from 10 °C to 90 °C and reverse, with a heating rate of 0.25 K/min^{-1}.

Chemical stabilities were determined by mixing 10 µM of protein with increasing amounts of Guanidinum chloride and incubated over night at 15 °C. After incubation the ellipticity of each sample was measured at 220 nm in a time dependent approach for 50 s.

Analytical Ultracentrifugation

Analytical Ultracentrifugation (AUC) allows to analyze the behavior of macromolecules, such as proteins and their complexes, in a gravitational field (up to 300,000 g). As a result of AUC measurements, the sedimentation coefficient (s-value), the molar mass M, and the shape of the analyzed molecules (frictional ratio, f/f_0) are detectable. Since the range of rotational speeds of an analytical ultracentrifuge is quite large (3,000-60,000 rpm), small molecules like polypeptides, but also huge macromolecule structures up to cells and organelles can be analyzed.

Basically two standard procedures in analytical ultracentrifugation are distinguished. First, the sedimentation velocity experiment and second, the sedimentation equilibrium experiment. S-values and oligomerization states are mainly detected by sedimentation velocity experiments. Information about the shape, molecular weights and interacting systems are often analyzed by equilibrium experiments.

Hereafter, the focus is laid on sedimentation velocity experiments, which were used in this work.

Sedimentation velocity experiments are non-equilibrium experiments. At the beginning of the sedimentation all sample cells are filled homogeneously with the protein solution to be analyzed. The induction of a gravitational field forces molecules to sediment and a boundary between solvent and macromolecule containing solution is formed. The sedimentation occurs with a constant velocity (4.5), because there is a balance of gravitational (4.3) and frictional force (4.4).

$$F_G = m \cdot a = \frac{M(1 - \overline{v}\rho)}{N_A} \cdot \omega^2 r \tag{4.3}$$

$$F_R = v \cdot f \tag{4.4}$$

$$v = \frac{M(1 - \overline{v}\rho)}{N_A \cdot f} \cdot \omega^2 r = s \cdot \omega^2 \cdot r \tag{4.5}$$

With m mass of sedimenting particle, a centrifugal acceleration, M molar mass of the sedimentation particle, $\overline{v}$ partial specific volume of the sedimenting particle , ρ density of the solvent, N_A Avogadro's number, f frictional coefficient of the particle , ω angular velocity, r distance to the rotor center, and s sedimentation coefficient of the particle.

The gravitational force is dependent on the molar mass, the partial specific volume and the density. The frictional force depends on the frictional coefficient, which is determined by the shape of the particle and the viscosity η of the solvent. According to this, the composition of the buffer has an influence on the sedimentation behavior of all analyzed macromolecules. According to equation 4.6, the influences of different buffer conditions on the s-value can be corrected to sedimentation in water at 20 °C ($s_{20,W}$).

$$s_{20,W} = s_{T,b} \frac{\eta_{T,b}(1 - \overline{v}_{20,W}\rho_{20,W})}{\eta_{20,W}(1 - \overline{v}_{T,b}\rho_{T,b})} \tag{4.6}$$

$20,W$ describes the standard conditions 20 °C and water as solvent. T is the temperature and the index b stands for the solvent used for the measurement.

The sedimentation coefficient is assigned by the speed of movement of the boundary between solvent and sedimenting macromolecules:

$$s = \frac{1}{\omega^2} \cdot \frac{\partial ln\overline{x}}{\partial t} \tag{4.7}$$

where $\overline{x}$ describes the position of the boundary.

The entire description of the sedimentation process in sector shaped cells as used in sedimentation velocity experiments is given by Lamm's differential equation (4.8).

$$\frac{dc}{dt} = D\left(\frac{\partial^2 c}{\partial r^2} - \frac{1}{r}\cdot\frac{\partial c}{\partial r}\right) - s\cdot\omega^2\cdot\left(r\cdot\frac{\partial c}{\partial r} - 2c\right) \tag{4.8}$$

D stands for the diffusion coefficient, ω for the angular velocity, r for the distance to the rotor center, and s for the sedimentation coefficient.

The sedimentation coefficient (s-value) depends on the molar mass, the partial specific volume of the macromolecule and the density of the solvent (4.9)

$$s = \frac{M(1-\overline{v}\cdot\rho)}{N_A\cdot f} \tag{4.9}$$

Through the frictional coefficient f the shape of the molecule can be indexed. Therefore, a quotient of the frictional coefficient f of the molecule and the coefficient f_0 of a sphere with same volume as the molecule is build. This quotient is called Perrin factor or frictional ratio and is inherently larger than 1. For global proteins the Perrin factor typically is around 1.3. The larger the Perrin-factor, the more the shape of the molecule differs from a sphere.

All sedimentation velocity experiments were conducted in an Optima XL-A equipped with absorbance and interference optics (Beckman Coulter, Krefeld, Germany) or a Proteomelab XL-A (Beckman Coulter, Krefeld, Germany) equipped with a fluorescence detection system from Aviv (New Jersey, USA). Samples were loaded in quartz- or sapphire-capped double sector centerpieces for absorbance and fluorescent or interference detection, respectively. For absorbance and interference measurements, a centerpiece was filled with the sample and its matching reference in the reference channel. Fluorescence detection does not need buffer correction, allowing all sectors to be filled with samples. Absorption was detected either at 280 nm or 230 nm for low protein concentration, interference detection was conducted at 645 nm and the fluorescence was detected with a excitation wavelength of 488 nm. All measurements were performed at 20 °C.

The analysis of obtained sedimentation profiles was performed with SEDFIT from Peter Schuck (4.1.3) and DCDTPLUS from John Philo (4.1.3).

APPENDIX

5

5.1 PURIFICATION OF THE HSP12-FAMILY

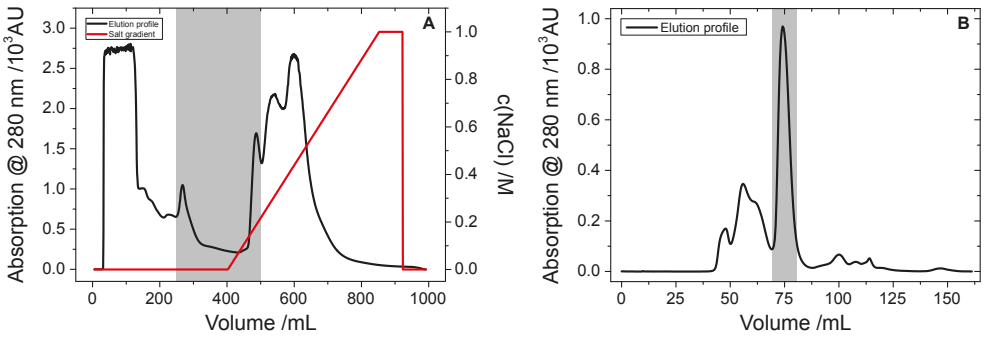

Figure 5.1: Representative elution profiles of the purification of the Hsp12 proteins. Depicted are the elution profile of the DEAE ff column of a purification of Hsp12.1 (panel A) and the corresponding elution profile of the gelfiltration column (panel B). The applied sodium chloride gradient is shown in red in panel A. The gray areas reflect the fraction pooled for concentration and gel filtration in the case of the DEAE ff purification step and the fraction pooled for full length mass and far-UV CD analyses in the case of the gelfiltration column.

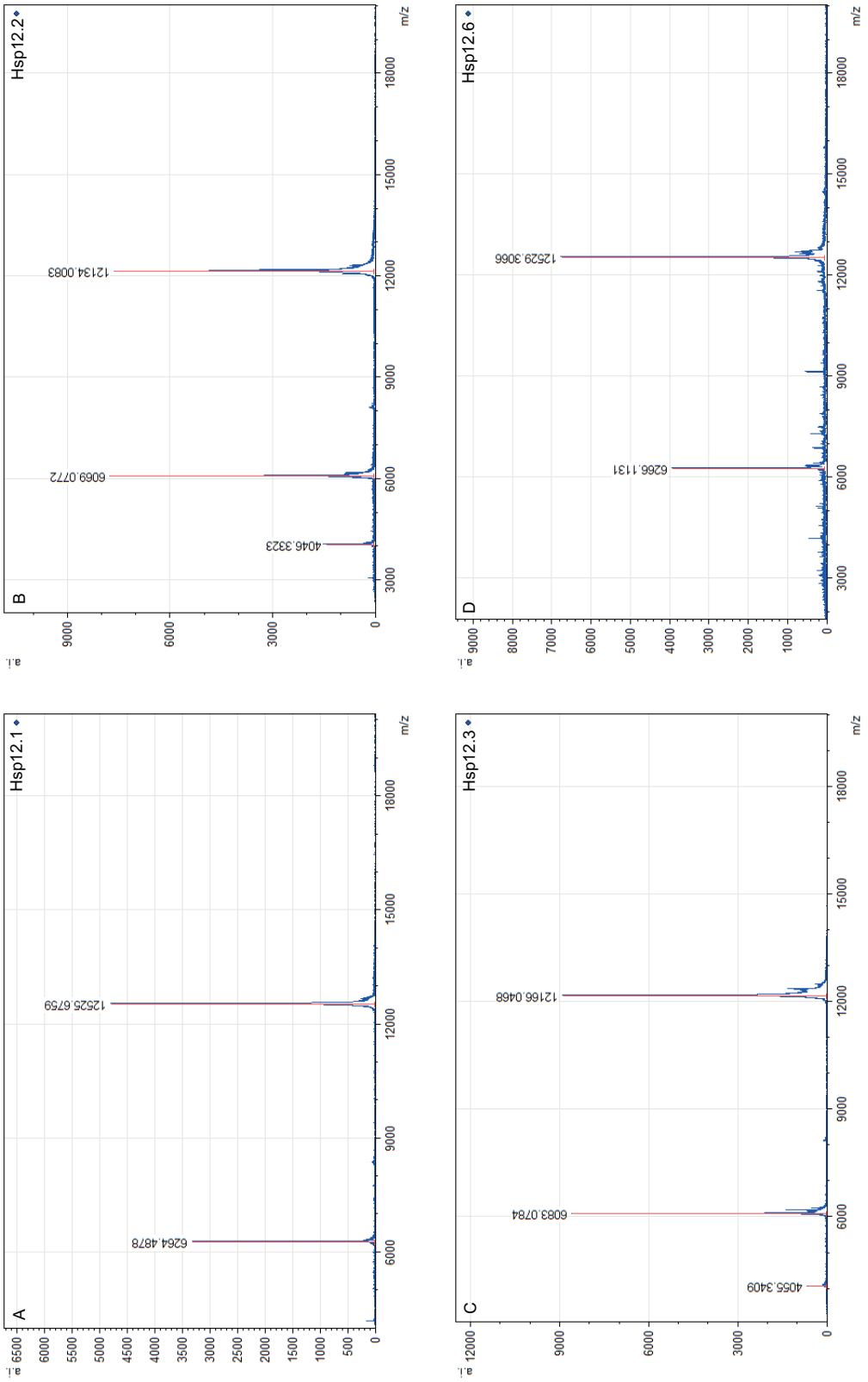

Figure 5.2: Representative full length mass analyses of the purified Hsp12 proteins. A: Hsp12.1, B: Hsp12.2, C: Hsp12.3, and D: Hsp12.6. All spectra show the M^+ peak at an approximately correct mass of the analyzed protein and the corresponding M^{2+}.

5.2 QRT-PCR EXPERIMENT SETUP

Table 5.1: Ct-values of the primer pairs used in qRT-PCR measurements at different primer concentrations tested. Shown are the normal reaction, No template control (NTC), and the corresponding differences of cycles. With decreasing amount of primers present in the reaction the Ct-value of the NTCs are increasing. This corresponds to a reduction of primer dimers.

Primer pair for	Concentration	Average Ct-value of the Reaction	Average Ct-value of the NTC	Difference of Ct-value
Hsp12.1	200 nM	19.68 ± 0.31	21.15 ± 1.00	1.47
	75 nM	18.39 ± 0.08	19.57 ± 0.93	1.18
	50 nM	27.32 ± 0.06	29.41 ± 0.05	2.09
Hsp12.2	200 nM	25.40 ± 0.10	28.04 ± 1.04	2.65
	75 nM	24.20 ± 0.04	28.18 ± 0.57	3.99
	50 nM	21.19 ± 0.26	33.41 ± 0.22	12.02
Hsp12.3	200 nM	24.40 ± 1.04	30.01 ± 0.93	5.61
	75 nM	22.63 ± 0.80	29.33 ± 1.11	6.70
	50 nM	27.56 ± 0.21	33.34 ± 0.22	5.78
Hsp12.6	200 nM	22.55 ± 0.28	23.64 ± 0.55	1.10
	75 nM	26.02 ± 0.60	32.47 ± 1.51	6.45
	50 nM	28.00 ± 0.28	34.36 ± 0.27	6.38
Hsp25	200 nM	29.88 ± 2.67	31.98 ± 0.95	2.10
	75 nM	26.02 ± 0.60	32.47 ± 1.51	6.45
	50 nM	24.88 ± 0.28	35.29 ± 0.41	10.41
ZK1128.7	200 nM	24.46 ± 0.27	29.24 ± 0.51	4.78
	75 nM	22.44 ± 0.38	27.98 ± 0.05	5.54
	50 nM	26.56 ± 0.22	34.29 ± 0.20	7.75
Act-1	50 nM	18.44 ± 0.31	39.74 ± 0.48	21.30
Daf-21	50 nM	19.37 ± 0.36	35.88 ± 0.50	26.51

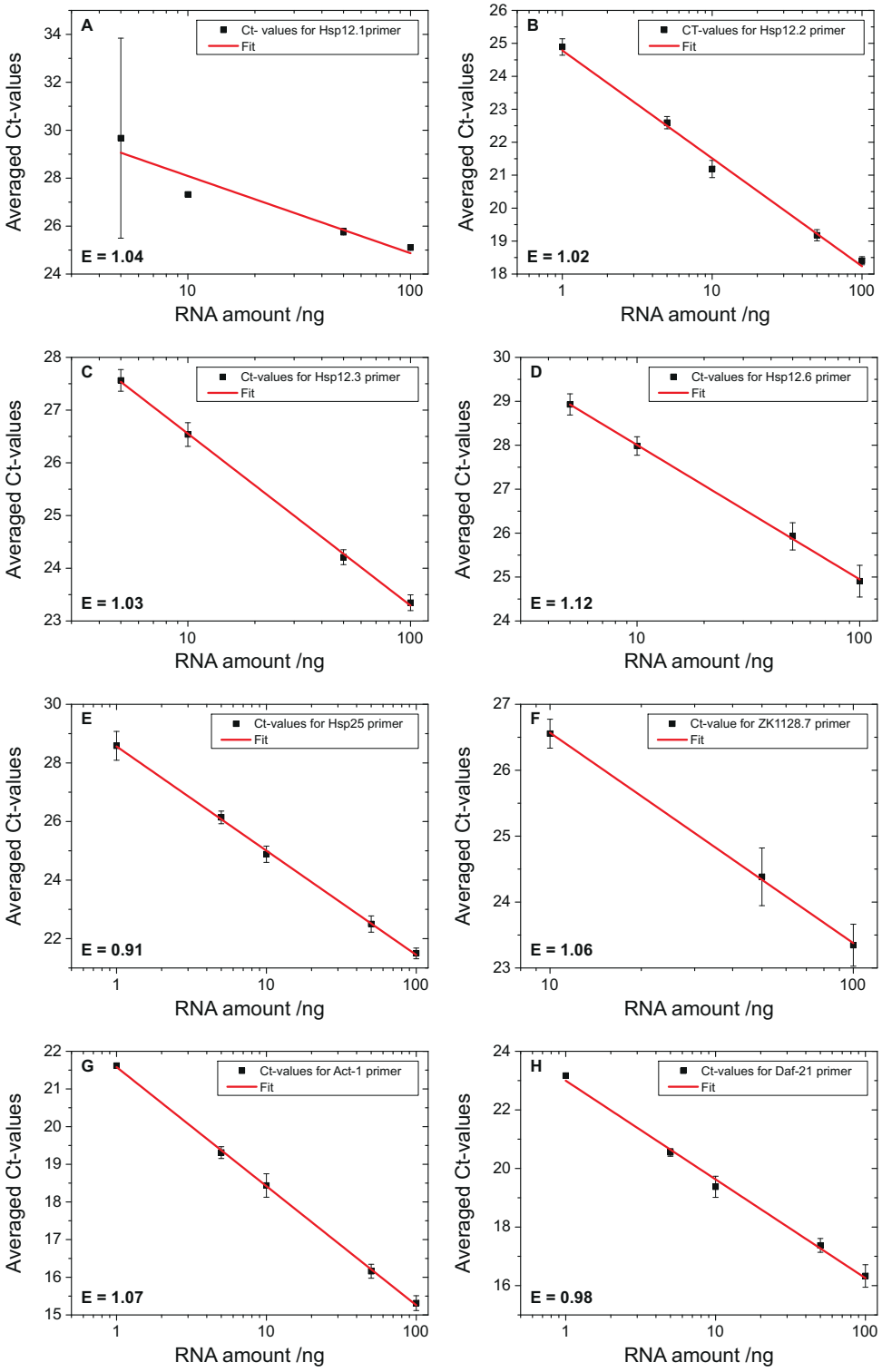

Figure 5.3: Efficiency determination of the primer pairs used in the qRT-PCR experiments. From A to H primer pairs for Hsp12.1, Hsp12.2, Hsp12.3, Hsp12.6, Hsp25, ZK1128.7, Act-1, and Daf-21 are depicted.

LIST OF PUPLICATIONS 6

1. Drazic, A. et al. *Role of cysteines in the stability and DNA-binding acitivity of hypochlorite-specific transcription factor YjiE* (accepted, PlosOne).

2. Kayser, J. et al. *Small heat shock proteins control intermediate lament network structure* (submitted to BJ, May 2013).

3. Huang, B. et al. *Scalable production of full-length normal and mutant huntingtin in human cells and its biochemical characterization* (submitted to JBS, May 2013).

4. Lorenz, O. et al. *Modulation of the conformational cycle of the chaperone Hsp90 by a stringent clientprotein* (in progress, submission to Cell).

5. Krause, M. et al. *Comparative analyses of C. elegans' Hsp12-family* (in progress).

6. Krause, M. et al. *The phenotype of Hsp12.6* (in progress).

7. Drazic, A. et al. *Interplay between oligomerization and activation of HypT* (in progress).

8. Fleckenstein, T. et al. *pH-dependency of Sip-1* (in progress).

9. Rehn, A. et al. *p23 chimaera and Hsp90* (in progress).

BIBLIOGRAPHY

[1] B. D. Ackley, S. H. Kang, J. R. Crew, C. Suh, Y. Jin, and J. M. Kramer. The basement membrane components nidogen and type xviii collagen regulate organization of neuromuscular junctions in caenorhabditis elegans. *J Neurosci*, 23(9):3577–87, 2003.

[2] E. Ahrman, W. Lambert, J. A. Aquilina, C. V. Robinson, and C. S. Emanuelsson. Chemical cross-linking of the chloroplast localized small heat-shock protein, hsp21, and the model substrate citrate synthase. *Protein Sci*, 16(7):1464–78, 2007.

[3] M. M. Ali, S. M. Roe, C. K. Vaughan, P. Meyer, B. Panaretou, P. W. Piper, C. Prodromou, and L. H. Pearl. Crystal structure of an hsp90-nucleotide-p23/sba1 closed chaperone complex. *Nature*, 440(7087):1013–7, 2006.

[4] L. Almeida-Souza, S. Goethals, V. de Winter, I. Dierick, R. Gallardo, J. Van Durme, J. Irobi, J. Gettemans, F. Rousseau, J. Schymkowitz, V. Timmerman, and S. Janssens. Increased monomerization of mutant hspb1 leads to protein hyperactivity in charcot-marie-tooth neuropathy. *J Biol Chem*, 285(17):12778–86, 2010.

[5] S. F. Altschul, W. Gish, W. Miller, E. W. Myers, and D. J. Lipman. Basic local alignment search tool. *J Mol Biol*, 215(3):403–10, 1990.

[6] Z. Altun and D. Hall. Introduction, 2009.

[7] C. B. Anfinsen, E. Haber, M. Sela, and J. White, F. H. The kinetics of formation of native ribonuclease during oxidation of the reduced polypeptide chain. *Proc Natl Acad Sci U S A*, 47:1309–14, 1961.

[8] I. Antoshechkin and P. W. Sternberg. The versatile worm: genetic and genomic resources for caenorhabditis elegans research. *Nat Rev Genet*, 8(7):518–32, 2007.

[9] C. Bagneris, O. A. Bateman, C. E. Naylor, N. Cronin, W. C. Boelens, N. H. Keep, and C. Slingsby. Crystal structures of alpha-crystallin domain dimers of alphab-crystallin and hsp20. *J Mol Biol*, 392(5):1242–52, 2009.

[10] U. Baschant and J. Tuckermann. The role of the glucocorticoid receptor in inflammation and immunity. *J Steroid Biochem Mol Biol*, 120(2-3):69–75, 2010.

[11] E. Basha, K. L. Friedrich, and E. Vierling. The n-terminal arm of small heat shock proteins is important for both chaperone activity and substrate specificity. *J Biol Chem*, 281(52):39943–52, 2006.

[12] E. Basha, G. J. Lee, L. A. Breci, A. C. Hausrath, N. R. Buan, K. C. Giese, and E. Vierling. The identity of proteins associated with a small heat shock protein during heat stress in vivo indicates that these chaperones protect a wide range of cellular functions. *J Biol Chem*, 279(9):7566–75, 2004.

[13] E. Basha, H. O'Neill, and E. Vierling. Small heat shock proteins and alpha-crystallins: dynamic proteins with flexible functions. *Trends Biochem Sci*, 37(3):106–17, 2012.

[14] R. Baumeister, E. Schaffitzel, and M. Hertweck. Endocrine signaling in caenorhabditis elegans controls stress response and longevity. *J Endocrinol*, 190(2):191–202, 2006.

[15] A. Bepperling, F. Alte, T. Kriehuber, N. Braun, S. Weinkauf, M. Groll, M. Haslbeck, and J. Buchner. Alternative bacterial two-component small heat shock protein systems. *Proc Natl Acad Sci U S A*, 109(50):20407–12, 2012.

[16] V. Berry, P. Francis, M. A. Reddy, D. Collyer, E. Vithana, I. MacKay, G. Dawson, A. H. Carey, A. Moore, S. S. Bhattacharya, and R. A. Quinlan. Alpha-b crystallin gene (cryab) mutation causes dominant congenital posterior polar cataract in humans. *Am J Hum Genet*, 69(5):1141–5, 2001.

[17] F. A. Bettelheim. Syneretic response to pressure in ocular lens. *J Theor Biol*, 197(2):277–80, 1999.

[18] S. G. Bhagyalaxmi, P. Srinivas, K. A. Barton, K. R. Kumar, M. Vidyavathi, J. M. Petrash, G. Bhanuprakash Reddy, and T. Padma. A novel mutation (f71l) in alphaa-crystallin with defective chaperone-like function associated with age-related cataract. *Biochim Biophys Acta*, 1792(10):974–81, 2009.

[19] D. A. Birnby, E. M. Link, J. J. Vowels, H. Tian, P. L. Colacurcio, and J. H. Thomas. A transmembrane guanylyl cyclase (daf-11) and hsp90 (daf-21) regulate a common set of chemosensory behaviors in caenorhabditis elegans. *Genetics*, 155(1):85–104, 2000.

[20] M. P. Bova, L. L. Ding, J. Horwitz, and B. K. Fung. Subunit exchange of alphaa-crystallin. *J Biol Chem*, 272(47):29511–7, 1997.

[21] M. P. Bova, Q. Huang, L. Ding, and J. Horwitz. Subunit exchange, conformational stability, and chaperone-like function of the small heat shock protein 16.5 from methanococcus jannaschii. *J Biol Chem*, 277(41):38468–75, 2002.

[22] M. P. Bova, H. S. McHaourab, Y. Han, and B. K. Fung. Subunit exchange of small heat shock proteins. analysis of oligomer formation of alphaa-crystallin and hsp27 by fluorescence resonance energy transfer and site-directed truncations. *J Biol Chem*, 275(2):1035–42, 2000.

[23] B. Bowerman. Cell signaling. wnt moves beyond the canon. *Science*, 320(5874):327–8, 2008.

[24] J. P. Brady, D. Garland, Y. Duglas-Tabor, J. Robison, W. G., A. Groome, and E. F. Wawrousek. Targeted disruption of the mouse alpha a-crystallin gene induces cataract and cytoplasmic inclusion bodies containing the small heat shock protein alpha b-crystallin. *Proc Natl Acad Sci U S A*, 94(3):884–9, 1997.

[25] N. Braun, M. Zacharias, J. Peschek, A. Kastenmüller, J. Zou, M. Hanzlik, M. Haslbeck, J. Rappsilber, J. Buchner, and S. Weinkauf. Multiple molecular architectures of the eye lens chaperone αb-crystallin elucidated by a triple hybrid approach. *Proc Natl Acad Sci U S A*, 108(51):20491–6, 2011.

[26] S. Brenner. The genetics of behaviour. *Br Med Bull*, 29(3):269–71, 1973.

[27] J. Buchner. Supervising the fold: functional principles of molecular chaperones. *FASEB J*, 10(1):10–9, 1996.

[28] J. Buchner, M. Ehrnsperger, M. Gaestel, and S. Walke. Purification and characterization of small heat shock proteins. *Methods Enzymol*, 290:339–49, 1998.

[29] S. D. Buckingham and D. B. Sattelle. Fast, automated measurement of nematode swimming (thrashing) without morphometry. *BMC Neurosci*, 10:84, 2009.

[30] O. V. Bukach, A. S. Seit-Nebi, S. B. Marston, and N. B. Gusev. Some properties of human small heat shock protein hsp20 (hspb6). *Eur J Biochem*, 271(2):291–302, 2004.

[31] K. Burkewitz, K. Choe, E. Lee, A. Deonarine, and K. Strange. Characterization of the proteostasis roles of glycerol accumulation, protein degradation and protein synthesis during osmotic stress in *C. elegans*. *PlosOne*, 7:1–14, 2012.

[32] A. Calixto, D. Chelur, I. Topalidou, X. Chen, and M. Chalfie. Enhanced neuronal rnai in c. elegans using sid-1. *Nat Methods*, 7(7):554–9, 2010.

[33] E. P. Candido. The small heat shock proteins of the nematode caenorhabditis elegans: structure, regulation and biology. *Prog Mol Subcell Biol*, 28:61–78, 2002.

[34] S. Capponi, A. Geroldi, P. Fossa, M. Grandis, P. Ciotti, R. Gulli, A. Schenone, P. Mandich, and E. Bellone. Hspb1 and hspb8 in inherited neuropathies: study of an italian cohort of dhmn and cmt2 patients. *J Peripher Nerv Syst*, 16(4):287–94, 2011.

[35] G. J. Caspers, J. A. Leunissen, and W. W. de Jong. The expanding small heat-shock protein family, and structure predictions of the conserved "alpha-crystallin domain". *J Mol Evol*, 40(3):238–48, 1995.

[36] M. G. Catlett and K. B. Kaplan. Sgt1p is a unique co-chaperone that acts as a client adaptor to link hsp90 to skp1p. *J Biol Chem*, 281(44):33739–48, 2006.

[37] D. P. Chandler, C. A. Wagnon, and J. Bolton, H. Reverse transcriptase (rt) inhibition of pcr at low concentrations of template and its implications for quantitative rt-pcr. *Appl Environ Microbiol*, 64(2):669–77, 1998.

[38] J. Chen, M. J. Feige, T. M. Franzmann, A. Bepperling, and J. Buchner. Regions outside the alpha-crystallin domain of the small heat shock protein hsp26 are required for its dimerization. *J Mol Biol*, 398(1):122–31, 2010.

[39] Q. Chen, J. Ma, M. Yan, M. E. Mothobi, Y. Liu, and F. Zheng. A novel mutation in cryab associated with autosomal dominant congenital nuclear cataract in a chinese family. *Mol Vis*, 15:1359–65, 2009.

[40] G. Cheng, E. Basha, V. H. Wysocki, and E. Vierling. Insights into small heat shock protein and substrate structure during chaperone action derived from hydrogen/deuterium exchange and mass spectrometry. *J Biol Chem*, 283(39):26634–42, 2008.

[41] J. I. Clark and P. J. Muchowski. Small heat-shock proteins and their potential role in human disease. *Curr Opin Struct Biol*, 10(1):52–9, 2000.

[42] L. A. Compton and J. Johnson, W. C. Analysis of protein circular dichroism spectra for secondary structure using a simple matrix multiplication. *Anal Biochem*, 155(1):155–67, 1986.

[43] T. Czechowski, M. Stitt, T. Altmann, M. K. Udvardi, and W. R. Scheible. Genome-wide identification and testing of superior reference genes for transcript normalization in arabidopsis. *Plant Physiol*, 139(1):5–17, 2005.

[44] P. N. Datskevich, V. V. Nefedova, M. V. Sudnitsyna, and N. B. Gusev. Mutations of small heat shock proteins and human congenital diseases. *Biochemistry (Mosc)*, 77(13):1500–14, 2012.

[45] W. W. de Jong, G. J. Caspers, and J. A. Leunissen. Genealogy of the alpha-crystallin–small heat-shock protein superfamily. *Int J Biol Macromol*, 22(3-4):151–62, 1998.

[46] N. de Miguel, N. Braun, A. Bepperling, T. Kriehuber, A. Kastenmuller, J. Buchner, S. O. Angel, and M. Haslbeck. Structural and functional diversity in the family of small heat shock proteins from the parasite toxoplasma gondii. *Biochim Biophys Acta*, 1793(11):1738–48, 2009.

[47] M. R. Del Bigio, A. E. Chudley, H. B. Sarnat, C. Campbell, S. Goobie, B. N. Chodirker, and D. Selcen. Infantile muscular dystrophy in canadian aboriginals is an alphab-crystallinopathy. *Ann Neurol*, 69(5):866–71, 2011.

[48] S. P. Delbecq, S. Jehle, and R. Klevit. Binding determinants of the small heat shock protein, alphab-crystallin: recognition of the 'ixi' motif. *EMBO J*, 31(24):4587–94, 2012.

[49] S. P. Delbecq and R. E. Klevit. One size does not fit all: the oligomeric states of alphab crystallin. *FEBS Lett*, 587(8):1073–80, 2013.

[50] M. Denis, S. Cuthill, A. C. Wikstrom, L. Poellinger, and J. A. Gustafsson. Association of the dioxin receptor with the mr 90,000 heat shock protein: a structural kinship with the glucocorticoid receptor. *Biochem Biophys Res Commun*, 155(2):801–7, 1988.

[51] R. R. Devi, W. Yao, P. Vijayalakshmi, Y. V. Sergeev, P. Sundaresan, and J. F. Hejtmancik. Crystallin gene mutations in indian families with inherited pediatric cataract. *Mol Vis*, 14:1157–70, 2008.

[52] K. Dheda, J. F. Huggett, S. A. Bustin, M. A. Johnson, G. Rook, and A. Zumla. Validation of housekeeping genes for normalizing rna expression in real-time pcr. *Biotechniques*, 37(1):112–4, 116, 118–9, 2004.

[53] K. A. Dill and H. S. Chan. From levinthal to pathways to funnels. *Nat Struct Biol*, 4(1):10–9, 1997.

[54] L. Ding and E. P. Candido. Association of several small heat-shock proteins with reproductive tissues in the nematode caenorhabditis elegans. *Biochem J*, 351(Pt 1):13–7, 2000.

[55] L. Ding and E. P. Candido. Hsp25, a small heat shock protein associated with dense bodies and m-lines of body wall muscle in caenorhabditis elegans. *J Biol Chem*, 275(13):9510–7, 2000.

[56] L. Ding and E. P. Candido. Hsp43, a small heat-shock protein localized to specific cells of the vulva and spermatheca in the nematode caenorhabditis elegans. *Biochem J*, 349(Pt 2):409–12, 2000.

[57] K. Dittmar, J. B. Lim, L. Caruccio, M. Bettinotti, and D. Stroncek. Assessment of the relative number of copies of the gene encoding human neutrophil antigen-2a(hna-2a), cd177, and a homologous pseudogene by quantitative real-time pcr. *Immunohematology*, 19(4):122–6, 2003.

[58] K. D. Dittmar, K. A. Hutchison, J. K. Owens-Grillo, and W. B. Pratt. Reconstitution of the steroid receptor.hsp90 heterocomplex assembly system of rabbit reticulocyte lysate. *J Biol Chem*, 271(22):12833–9, 1996.

[59] S. P. Division. *Alien Reference RNA QRT-PCR Detection Kit, Revision A*.

[60] S. P. Division. *Brilliant III Ultra-Fast QPCR Master Mix, Revision B*.

[61] I. V. Dudich, V. P. Zav'yalov, W. Pfeil, M. Gaestel, G. A. Zav'yalova, A. I. Denesyuk, and T. Korpela. Dimer structure as a minimum cooperative subunit of small heat-shock proteins. *Biochim Biophys Acta*, 1253(2):163–8, 1995.

[62] M. Ehrnsperger, S. Graber, M. Gaestel, and J. Buchner. Binding of non-native protein to hsp25 during heat shock creates a reservoir of folding intermediates for reactivation. *EMBO J*, 16(2):221–9, 1997.

[63] M. Ehrnsperger, C. Hergersberg, U. Wienhues, A. Nichtl, and J. Buchner. Stabilization of proteins and peptides in diagnostic immunological assays by the molecular chaperone hsp25. *Anal Biochem*, 259(2):218–25, 1998.

[64] J. Ellis. Proteins as molecular chaperones. *Nature*, 328(6129):378–9, 1987.

[65] R. J. Ellis, S. M. van der Vies, and S. M. Hemmingsen. The molecular chaperone concept. *Biochem Soc Symp*, 55:145–53, 1989.

[66] O. V. Evgrafov, I. Mersiyanova, J. Irobi, L. Van Den Bosch, I. Dierick, C. L. Leung, O. Schagina, N. Verpoorten, K. Van Impe, V. Fedotov, E. Dadali, M. Auer-Grumbach, C. Windpassinger, K. Wagner, Z. Mitrovic, D. Hilton-Jones, K. Talbot, J. J. Martin, N. Vasserman, S. Tverskaya, A. Polyakov, R. K. Liem, J. Gettemans, W. Robberecht, P. De Jonghe, and V. Timmerman. Mutant small heat-shock protein 27 causes axonal charcot-marie-tooth disease and distal hereditary motor neuropathy. *Nat Genet*, 36(6):602–6, 2004.

[67] P. P. Fagerholm, B. T. Philipson, and B. Lindstrom. Normal human lens - the distribution of protein. *Exp Eye Res*, 33(6):615–20, 1981.

[68] G. Fairbanks, T. L. Steck, and D. F. Wallach. Electrophoretic analysis of the major polypeptides of the human erythrocyte membrane. *Biochemistry*, 10(13):2606–17, 1971.

[69] C. E. Finch and G. Ruvkun. The genetics of aging. *Annu Rev Genomics Hum Genet*, 2:435–62, 2001.

[70] A. L. Fink. Natively unfolded proteins. *Curr Opin Struct Biol*, 15(1):35–41, 2005.

[71] T. Fleckenstein. *ongoing thesis*. PhD thesis, TUM, Faculty of Chemistry, unpublished.

[72] K. M. Forrest, S. Al-Sarraj, C. Sewry, S. Buk, S. V. Tan, M. Pitt, A. Durward, M. McDougall, M. Irving, M. G. Hanna, E. Matthews, A. Sarkozy, J. Hudson, R. Barresi, K. Bushby, H. Jungbluth, and E. Wraige. Infantile onset myofibrillar myopathy due to recessive cryab mutations. *Neuromuscul Disord*, 21(1):37–40, 2011.

[73] E. Freire, A. Schon, B. M. Hutchins, and R. K. Brown. Chemical denaturation as a tool in the formulation optimization of biologics. *Drug Discov Today*, 2013.

[74] K. L. Friedrich, K. C. Giese, N. R. Buan, and E. Vierling. Interactions between small heat shock protein subunits and substrate in small heat shock protein-substrate complexes. *J Biol Chem*, 279(2):1080–9, 2004.

[75] A. M. Gaiser, C. J. Kaiser, V. Haslbeck, and K. Richter. Downregulation of the hsp90 system causes defects in muscle cells of caenorhabditis elegans. *PLoS One*, 6(9):e25485, 2011.

[76] L. R. Garcia, P. Mehta, and P. W. Sternberg. Regulation of distinct muscle behaviors controls the c. elegans male's copulatory spicules during mating. *Cell*, 107(6):777–88, 2001.

[77] B. J. Gentil and L. Cooper. Molecular basis of axonal dysfunction and traffic impairments in cmt. *Brain Res Bull*, 88(5):444–53, 2012.

[78] C. Georgopoulos and W. J. Welch. Role of the major heat shock proteins as molecular chaperones. *Annu Rev Cell Biol*, 9:601–34, 1993.

[79] J. G. Ghosh, J. Shenoy, A. K., and J. I. Clark. Interactions between important regulatory proteins and human alphab crystallin. *Biochemistry*, 46(21):6308–17, 2007.

[80] M. E. Goldberg, R. Rudolph, and R. Jaenicke. A kinetic study of the competition between renaturation and aggregation during the refolding of denatured-reduced egg white lysozyme. *Biochemistry*, 30(11):2790–7, 1991.

[81] P. Goloubinoff, A. Mogk, A. P. Zvi, T. Tomoyasu, and B. Bukau. Sequential mechanism of solubilization and refolding of stable protein aggregates by a bichaperone network. *Proc Natl Acad Sci U S A*, 96(24):13732–7, 1999.

[82] J. Graw, N. Klopp, T. Illig, M. N. Preising, and B. Lorenz. Congenital cataract and macular hypoplasia in humans associated with a de novo mutation in cryaa and compound heterozygous mutations in p. *Graefes Arch Clin Exp Ophthalmol*, 244(8):912–9, 2006.

[83] F. Gu, W. Luo, X. Li, Z. Wang, S. Lu, M. Zhang, B. Zhao, S. Zhu, S. Feng, Y. B. Yan, S. Huang, and X. Ma. A novel mutation in alphaa-crystallin (cryaa) caused autosomal dominant congenital cataract in a large chinese family. *Hum Mutat*, 29(5):769, 2008.

[84] D. A. Haley, J. Horwitz, and P. L. Stewart. The small heat-shock protein, alphab-crystallin, has a variable quaternary structure. *J Mol Biol*, 277(1):27–35, 1998.

[85] Y. Hanazono, K. Takeda, T. Oka, T. Abe, T. Tomonari, N. Akiyama, Y. Aikawa, M. Yohda, and K. Miki. Nonequivalence observed for the 16-meric structure of a small heat shock protein, sphsp16.0, from schizosaccharomyces pombe. *Structure*, 21(2):220–8, 2013.

[86] L. Hansen, W. Yao, H. Eiberg, K. W. Kjaer, K. Baggesen, J. F. Hejtmancik, and T. Rosenberg. Genetic heterogeneity in microcornea-cataract: five novel mutations in cryaa, crygd, and gja8. *Invest Ophthalmol Vis Sci*, 48(9):3937–44, 2007.

[87] F. U. Hartl, A. Bracher, and M. Hayer-Hartl. Molecular chaperones in protein folding and proteostasis. *Nature*, 475(7356):324–32, 2011.

[88] F. U. Hartl and M. Hayer-Hartl. Molecular chaperones in the cytosol: from nascent chain to folded protein. *Science*, 295(5561):1852–8, 2002.

[89] M. Haslbeck, T. Franzmann, D. Weinfurtner, and J. Buchner. Some like it hot: the structure and function of small heat-shock proteins. *Nat Struct Mol Biol*, 12(10):842–6, 2005.

[90] M. Haslbeck, A. Ignatiou, H. Saibil, S. Helmich, E. Frenzl, T. Stromer, and J. Buchner. A domain in the n-terminal part of hsp26 is essential for chaperone function and oligomerization. *J Mol Biol*, 343(2):445–55, 2004.

[91] M. Haslbeck, A. Kastenmuller, J. Buchner, S. Weinkauf, and N. Braun. Structural dynamics of archaeal small heat shock proteins. *J Mol Biol*, 378(2):362–74, 2008.

[92] M. Haslbeck, S. Walke, T. Stromer, M. Ehrnsperger, H. E. White, S. Chen, H. R. Saibil, and J. Buchner. Hsp26: a temperature-regulated chaperone. *EMBO J*, 18(23):6744–51, 1999.

[93] M. Hessling, K. Richter, and J. Buchner. Dissection of the atp-induced conformational cycle of the molecular chaperone hsp90. *Nat Struct Mol Biol*, 16(3):287–93, 2009.

[94] G. R. Hilton, H. Lioe, F. Stengel, A. J. Baldwin, and J. L. Benesch. Small heat-shock proteins: Paramedics of the cell. *Top Curr Chem*, 2012.

[95] J. Hodgkin. Sex determination. right gene, wrong chromosome. *Nature*, 336(6201):712, 1988.

[96] J. Hodgkin, H. R. Horvitz, and S. Brenner. Nondisjunction mutants of the nematode caenorhabditis elegans. *Genetics*, 91(1):67–94, 1979.

[97] I. Hope. *C. elegans - A practical approach*. The practical approach series. 1999.

[98] H. R. Horvitz, S. Brenner, J. Hodgkin, and R. K. Herman. A uniform genetic nomenclature for the nematode caenorhabditis elegans. *Mol Gen Genet*, 175(2):129–33, 1979.

[99] J. Horwitz. Alpha-crystallin. *Exp Eye Res*, 76(2):145–53, 2003.

[100] J. Horwitz, M. Bova, Q. L. Huang, L. Ding, O. Yaron, and S. Lowman. Mutation of alpha b-crystallin: effects on chaperone-like activity. *Int J Biol Macromol*, 22(3-4):263–9, 1998.

[101] H. Houlden, M. Laura, F. Wavrant-De Vrieze, J. Blake, N. Wood, and M. M. Reilly. Mutations in the hsp27 (hspb1) gene cause dominant, recessive, and sporadic distal hmn/cmt type 2. *Neurology*, 71(21):1660–8, 2008.

[102] A. L. Hsu, C. T. Murphy, and C. Kenyon. Regulation of aging and age-related disease by daf-16 and heat-shock factor. *Science*, 300(5622):1142–5, 2003.

[103] Y. Ikeda, A. Abe, C. Ishida, K. Takahashi, K. Hayasaka, and M. Yamada. A clinical phenotype of distal hereditary motor neuronopathy type ii with a novel hspb1 mutation. *J Neurol Sci*, 277(1-2):9–12, 2009.

[104] N. Inagaki, T. Hayashi, T. Arimura, Y. Koga, M. Takahashi, H. Shibata, K. Teraoka, T. Chikamori, A. Yamashina, and A. Kimura. Alpha b-crystallin mutation in dilated cardiomyopathy. *Biochem Biophys Res Commun*, 342(2):379–86, 2006.

[105] J. Irobi, K. Van Impe, P. Seeman, A. Jordanova, I. Dierick, N. Verpoorten, A. Michalik, E. De Vriendt, A. Jacobs, V. Van Gerwen, K. Vennekens, R. Mazanec, I. Tournev, D. Hilton-Jones, K. Talbot, I. Kremensky, L. Van Den Bosch, W. Robberecht, J. Van Vandekerckhove, C. Van Broeckhoven, J. Gettemans, P. De Jonghe, and V. Timmerman. Hot-spot residue in small heat-shock protein 22 causes distal motor neuropathy. *Nat Genet*, 36(6):597–601, 2004.

[106] U. Jakob, M. Gaestel, K. Engel, and J. Buchner. Small heat shock proteins are molecular chaperones. *J Biol Chem*, 268(3):1517–20, 1993.

[107] U. Jakob, W. Muse, M. Eser, and J. C. Bardwell. Chaperone activity with a redox switch. *Cell*, 96(3):341–52, 1999.

[108] P. A. James, J. Rankin, and K. Talbot. Asymmetrical late onset motor neuropathy associated with a novel mutation in the small heat shock protein hspb1 (hsp27). *J Neurol Neurosurg Psychiatry*, 79(4):461–3, 2008.

[109] N. Jaya, V. Garcia, and E. Vierling. Substrate binding site flexibility of the small heat shock protein molecular chaperones. *Proc Natl Acad Sci U S A*, 106(37):15604–9, 2009.

[110] S. Jehle, P. Rajagopal, B. Bardiaux, S. Markovic, R. Kuhne, J. R. Stout, V. A. Higman, R. E. Klevit, B. J. van Rossum, and H. Oschkinat. Solid-state nmr and saxs studies provide a structural basis for the activation of alphab-crystallin oligomers. *Nat Struct Mol Biol*, 17(9):1037–42, 2010.

[111] S. Jehle, B. van Rossum, J. R. Stout, S. M. Noguchi, K. Falber, K. Rehbein, H. Oschkinat, R. E. Klevit, and P. Rajagopal. alphab-crystallin: a hybrid solid-state/solution-state nmr investigation reveals structural aspects of the heterogeneous oligomer. *J Mol Biol*, 385(5):1481–97, 2009.

[112] S. Jehle, B. S. Vollmar, B. Bardiaux, K. K. Dove, P. Rajagopal, T. Gonen, H. Oschkinat, and R. E. Klevit. N-terminal domain of alphab-crystallin provides a conformational switch for multimerization and structural heterogeneity. *Proc Natl Acad Sci U S A*, 108(16):6409–14, 2011.

[113] D. Jones, R. H. Russnak, R. J. Kay, and E. P. Candido. Structure, expression, and evolution of a heat shock gene locus in caenorhabditis elegans

that is flanked by repetitive elements. *J Biol Chem*, 261(26):12006–15, 1986.

[114] T. Kaletta and M. O. Hengartner. Finding function in novel targets: C. elegans as a model organism. *Nat Rev Drug Discov*, 5(5):387–98, 2006.

[115] H. H. Kampinga and E. A. Craig. The hsp70 chaperone machinery: J proteins as drivers of functional specificity. *Nat Rev Mol Cell Biol*, 11(8):579–92, 2010.

[116] G. Kappe, W. C. Boelens, and W. W. de Jong. Why proteins without an alpha-crystallin domain should not be included in the human small heat shock protein family hspb. *Cell Stress Chaperones*, 15(4):457–61, 2010.

[117] S. M. Kelly, T. J. Jess, and N. C. Price. How to study proteins by circular dichroism. *Biochim Biophys Acta*, 1751(2):119–39, 2005.

[118] C. K. Kennaway, J. L. Benesch, U. Gohlke, L. Wang, C. V. Robinson, E. V. Orlova, H. R. Saibil, and N. H. Keep. Dodecameric structure of the small heat shock protein acr1 from mycobacterium tuberculosis. *J Biol Chem*, 280(39):33419–25, 2005.

[119] C. Kenyon, J. Chang, E. Gensch, A. Rudner, and R. Tabtiang. A c. elegans mutant that lives twice as long as wild type. *Nature*, 366(6454):461–4, 1993.

[120] A. O. Khan, L. Abu Safieh, and F. S. Alkuraya. Later retinal degeneration following childhood surgical aphakia in a family with recessive cryab mutation (p.r56w). *Ophthalmic Genet*, 31(1):30–6, 2010.

[121] T. Kiefhaber, R. Rudolph, H. H. Kohler, and J. Buchner. Protein aggregation in vitro and in vivo: a quantitative model of the kinetic competition between folding and aggregation. *Biotechnology (N Y)*, 9(9):825–9, 1991.

[122] K. Kijima, C. Numakura, T. Goto, T. Takahashi, T. Otagiri, K. Umetsu, and K. Hayasaka. Small heat shock protein 27 mutation in a japanese patient with distal hereditary motor neuropathy. *J Hum Genet*, 50(9):473–6, 2005.

[123] K. K. Kim, R. Kim, and S. H. Kim. Crystal structure of a small heat-shock protein. *Nature*, 394(6693):595–9, 1998.

[124] P. S. Kim and R. L. Baldwin. Specific intermediates in the folding reactions of small proteins and the mechanism of protein folding. *Annu Rev Biochem*, 51:459–89, 1982.

[125] B. P. Kokke, W. C. Boelens, and W. W. de Jong. The lack of chaperonelike activity of caenorhabditis elegans hsp12.2 cannot be restored by domain swapping with human alphab-crystallin. *Cell Stress Chaperones*, 6(4):360–7, 2001.

[126] B. P. Kokke, M. R. Leroux, E. P. Candido, W. C. Boelens, and W. W. de Jong. Caenorhabditis elegans small heat-shock proteins hsp12.2 and hsp12.3 form tetramers and have no chaperone-like activity. *FEBS Lett*, 433(3):228–32, 1998.

[127] S. J. Kolb, P. J. Snyder, E. J. Poi, E. A. Renard, A. Bartlett, S. Gu, S. Sutton, W. D. Arnold, M. L. Freimer, V. H. Lawson, J. T. Kissel, and T. W. Prior. Mutant small heat shock protein b3 causes motor neuropathy: utility of a candidate gene approach. *Neurology*, 74(6):502–6, 2010.

[128] H. Kosano, B. Stensgard, M. C. Charlesworth, N. McMahon, and D. Toft. The assembly of progesterone receptor-hsp90 complexes using purified proteins. *J Biol Chem*, 273(49):32973–9, 1998.

[129] S. Kostenko and U. Moens. Heat shock protein 27 phosphorylation: kinases, phosphatases, functions and pathology. *Cell Mol Life Sci*, 66(20):3289–307, 2009.

[130] H. A. Koteiche and H. S. McHaourab. Folding pattern of the alpha-crystallin domain in alphaa-crystallin determined by site-directed spin labeling. *J Mol Biol*, 294(2):561–77, 1999.

[131] N. Kourtis, V. Nikoletopoulou, and N. Tavernarakis. Small heat-shock proteins protect from heat-stroke-associated neurodegeneration. *Nature*, 490(7419):213–8, 2012.

[132] M. Krause, M. Wild, B. Rosenzweig, and D. Hirsh. Wild-type and mutant actin genes in caenorhabditis elegans. *J Mol Biol*, 208(3):381–92, 1989.

[133] T. Kriehuber. *Hsp26 etc.* PhD thesis, TUM, Faculty of Chemistry, 2012.

[134] T. Kriehuber, T. Rattei, T. Weinmaier, A. Bepperling, M. Haslbeck, and J. Buchner. Independent evolution of the core domain and its flanking sequences in small heat shock proteins. *FASEB J*, 24(10):3633–42, 2010.

[135] C. Kumsta, M. Thamsen, and U. Jakob. Effects of oxidative stress on behavior, physiology, and the redox thiol proteome of caenorhabditis elegans. *Antioxid Redox Signal*, 14(6):1023–37, 2011.

[136] U. K. Laemmli. Cleavage of structural proteins during the assembly of the head of bacteriophage t4. *Nature*, 227(5259):680–5, 1970.

[137] A. Laganowsky, J. L. Benesch, M. Landau, L. Ding, M. R. Sawaya, D. Cascio, Q. Huang, C. V. Robinson, J. Horwitz, and D. Eisenberg. Crystal structures of truncated alphaa and alphab crystallins reveal structural mechanisms of polydispersity important for eye lens function. *Protein Sci*, 19(5):1031–43, 2010.

[138] G. J. Lee, A. M. Roseman, H. R. Saibil, and E. Vierling. A small heat shock protein stably binds heat-denatured model substrates and can maintain a substrate in a folding-competent state. *EMBO J*, 16(3):659–71, 1997.

[139] M. R. Leroux and E. P. Candido. Subunit characterization of the caenorhabditis elegans chaperonin containing tcp-1 and expression pattern of the gene encoding cct-1. *Biochem Biophys Res Commun*, 241(3):687–92, 1997.

[140] M. R. Leroux, B. J. Ma, G. Batelier, R. Melki, and E. P. Candido. Unique structural features of a novel class of small heat shock proteins. *J Biol Chem*, 272(19):12847–53, 1997.

[141] M. C. Leung, P. L. Williams, A. Benedetto, C. Au, K. J. Helmcke, M. Aschner, and J. N. Meyer. Caenorhabditis elegans: an emerging model in biomedical and environmental toxicology. *Toxicol Sci*, 106(1):5–28, 2008.

[142] H. Li, C. Li, Q. Lu, T. Su, T. Ke, D. W. Li, M. Yuan, J. Liu, X. Ren, Z. Zhang, S. Zeng, Q. K. Wang, and M. Liu. Cataract mutation p20s of alphab-crystallin impairs chaperone activity of alphaa-crystallin and induces apoptosis of human lens epithelial cells. *Biochim Biophys Acta*, 1782(5):303–9, 2008.

[143] J. Li and J. Buchner. Structure, function and regulation of the hsp90 machinery. *Biomed J*, 36(3):106–17, 2013.

[144] J. Li, J. Soroka, and J. Buchner. The hsp90 chaperone machinery: conformational dynamics and regulation by co-chaperones. *Biochim Biophys Acta*, 1823(3):624–35, 2012.

[145] K. P. Lin, B. W. Soong, C. C. Yang, L. W. Huang, M. H. Chang, I. H. Lee, A. Antonellis, and Y. C. Lee. The mutational spectrum in a cohort of charcot-marie-tooth disease type 2 among the han chinese in taiwan. *PLoS One*, 6(12):e29393, 2011.

[146] B. Linder, Z. Jin, J. H. Freedman, and C. S. Rubin. Molecular characterization of a novel, developmentally regulated small embryonic chaperone from caenorhabditis elegans. *J Biol Chem*, 271(47):30158–66, 1996.

[147] R. A. Lindner, J. A. Carver, M. Ehrnsperger, J. Buchner, G. Esposito, J. Behlke, G. Lutsch, A. Kotlyarov, and M. Gaestel. Mouse hsp25, a small shock protein. the role of its c-terminal extension in oligomerization and chaperone action. *Eur J Biochem*, 267(7):1923–32, 2000.

[148] R. Lints and D. Hall. Male introduction, 2009.

[149] M. Litt, P. Kramer, D. M. LaMorticella, W. Murphey, E. W. Lovrien, and R. G. Weleber. Autosomal dominant congenital cataract associated with a missense mutation in the human alpha crystallin gene cryaa. *Hum Mol Genet*, 7(3):471–4, 1998.

[150] K. S. Liu and P. W. Sternberg. Sensory regulation of male mating behavior in caenorhabditis elegans. *Neuron*, 14(1):79–89, 1995.

[151] Y. Liu, X. Zhang, L. Luo, M. Wu, R. Zeng, G. Cheng, B. Hu, B. Liu, J. J. Liang, and F. Shang. A novel alphab-crystallin mutation associated with autosomal dominant congenital lamellar cataract. *Invest Ophthalmol Vis Sci*, 47(3):1069–75, 2006.

[152] O. Lorenz. *ongoing thesis*. PhD thesis, TUM, Faculty of Chemistry, unpublished.

[153] M. Luigetti, G. M. Fabrizi, F. Madia, M. Ferrarini, A. Conte, A. Del Grande, G. Tasca, P. A. Tonali, and M. Sabatelli. A novel hspb1 mutation in an italian patient with cmt2/dhmn phenotype. *J Neurol Sci*, 298(1-2):114–7, 2010.

[154] D. S. Mackay, U. P. Andley, and A. Shiels. Cell death triggered by a novel mutation in the alphaa-crystallin gene underlies autosomal dominant cataract linked to chromosome 21q. *Eur J Hum Genet*, 11(10):784–93, 2003.

[155] P. Mandich, M. Grandis, A. Varese, A. Geroldi, M. Acquaviva, P. Ciotti, R. Gulli, L. Doria-Lamba, G. M. Fabrizi, G. Giribaldi, A. Pizzuti, A. Schenone, and E. Bellone. Severe neuropathy after diphtheria-tetanus-pertussis vaccination in a child carrying a novel frame-shift mutation in the small heat-shock protein 27 gene. *J Child Neurol*, 25(1):107–9, 2010.

[156] A. Martin, T. A. Baker, and R. T. Sauer. Rebuilt aaa + motors reveal operating principles for atp-fuelled machines. *Nature*, 437(7062):1115–20, 2005.

[157] M. Matuszewska, D. Kuczynska-Wisnik, E. Laskowska, and K. Liberek. The small heat shock protein ibpa of escherichia coli cooperates with ibpb in stabilization of thermally aggregated proteins in a disaggregation competent state. *J Biol Chem*, 280(13):12292–8, 2005.

[158] M. P. Mayer and B. Bukau. Hsp70 chaperones: cellular functions and molecular mechanism. *Cell Mol Life Sci*, 62(6):670–84, 2005.

[159] J. J. McElwee, E. Schuster, E. Blanc, J. H. Thomas, and D. Gems. Shared transcriptional signature in caenorhabditis elegans dauer larvae and long-lived daf-2 mutants implicates detoxification system in longevity assurance. *J Biol Chem*, 279(43):44533–43, 2004.

[160] H. S. McHaourab, E. K. Dodson, and H. A. Koteiche. Mechanism of chaperone function in small heat shock proteins. two-mode binding of the excited states of t4 lysozyme mutants by alphaa-crystallin. *J Biol Chem*, 277(43):40557–66, 2002.

[161] H. S. McHaourab, J. A. Godar, and P. L. Stewart. Structure and mechanism of protein stability sensors: chaperone activity of small heat shock proteins. *Biochemistry*, 48(18):3828–37, 2009.

[162] J. F. Morley and R. I. Morimoto. Regulation of longevity in caenorhabditis elegans by heat shock factor and molecular chaperones. *Mol Biol Cell*, 15(2):657–64, 2004.

[163] A. M. Morris, T. M. Treweek, J. A. Aquilina, J. A. Carver, and M. J. Walker. Glutamic acid residues in the c-terminal extension of small heat shock protein 25 are critical for structural and functional integrity. *FEBS J*, 275(23):5885–98, 2008.

[164] E. R. Morris and M. S. Searle. Overview of protein folding mechanisms: experimental and theoretical approaches to probing energy landscapes. *Curr Protoc Protein Sci*, Chapter 28:Unit 28 2 1–22, 2012.

[165] P. J. Murphy, Y. Morishima, H. Chen, M. D. Galigniana, J. F. Mansfield, J. Simons, S. S., and W. B. Pratt. Visualization and mechanism of assembly of a glucocorticoid receptor.hsp70 complex that is primed for subsequent hsp90-dependent opening of the steroid binding cleft. *J Biol Chem*, 278(37):34764–73, 2003.

[166] F. Narberhaus. Alpha-crystallin-type heat shock proteins: socializing minichaperones in the context of a multichaperone network. *Microbiol Mol Biol Rev*, 66(1):64–93; table of contents, 2002.

[167] P. Nicolaou, R. Knoll, K. Haghighi, G. C. Fan, n. Dorn, G. W., G. Hasenfub, and E. G. Kranias. Human mutation in the anti-apoptotic heat shock protein 20 abrogates its cardioprotective effects. *J Biol Chem*, 283(48):33465–71, 2008.

[168] N. Norhave, D. Spurgeon, C. Svendsen, and N. Cedergreen. How does growth temperature affect cadmium toxicity measured on different life history traits in the soil nematode *Caenorhabditis elegans*? *Environ Toxicol Chem*, 4:787–793, 2012.

[169] M. D. Perng, S. F. Wen, I. P. van den, A. R. Prescott, and R. A. Quinlan. Desmin aggregate formation by r120g alphab-crystallin is caused by altered filament interactions and is dependent upon network status in cells. *Mol Biol Cell*, 15(5):2335–46, 2004.

[170] J. Peschek. *Structural and functional principles of the small Heat shock protein a-crystallin*. PhD thesis, TUM, Faculty of Chemistry, 2012.

[171] J. Peschek, N. Braun, T. M. Franzmann, Y. Georgalis, M. Haslbeck, S. Weinkauf, and J. Buchner. The eye lens chaperone alpha-crystallin forms defined globular assemblies. *Proc Natl Acad Sci U S A*, 106(32):13272–7, 2009.

[172] M. Pfaffl, A. Tichopád, C. Prgomet, and T. Neuvians. Determination of stable housekeeping genes, differentially regulated target genes and sample integrity: Bestkeeper – excel-based tool using pair-wise correlations. *Biotechnology Letters*, 26:509–515, 2004.

[173] D. Picard, B. Khursheed, M. J. Garabedian, M. G. Fortin, S. Lindquist, and K. R. Yamamoto. Reduced levels of hsp90 compromise steroid receptor action in vivo. *Nature*, 348(6297):166–8, 1990.

[174] A. Pilotto, N. Marziliano, M. Pasotti, M. Grasso, A. M. Costante, and E. Arbustini. alphab-crystallin mutation in dilated cardiomyopathies: low prevalence in a consecutive series of 200 unrelated probands. *Biochem Biophys Res Commun*, 346(4):1115–7, 2006.

[175] V. Prahlad, T. Cornelius, and R. I. Morimoto. Regulation of the cellular heat shock response in caenorhabditis elegans by thermosensory neurons. *Science*, 320(5877):811–4, 2008.

[176] V. Prahlad, D. Pilgrim, and E. B. Goodwin. Roles for mating and environment in c. elegans sex determination. *Science*, 302(5647):1046–9, 2003.

[177] E. Pras, M. Frydman, E. Levy-Nissenbaum, T. Bakhan, J. Raz, E. I. Assia, B. Goldman, and E. Pras. A nonsense mutation (w9x) in cryaa causes autosomal recessive cataract in an inbred jewish persian family. *Invest Ophthalmol Vis Sci*, 41(11):3511–5, 2000.

[178] W. B. Pratt, Y. Morishima, and Y. Osawa. The hsp90 chaperone machinery regulates signaling by modulating ligand binding clefts. *J Biol Chem*, 283(34):22885–9, 2008.

[179] W. B. Pratt and D. O. Toft. Regulation of signaling protein function and trafficking by the hsp90/hsp70-based chaperone machinery. *Exp Biol Med (Maywood)*, 228(2):111–33, 2003.

[180] C. Prodromou, B. Panaretou, S. Chohan, G. Siligardi, R. O'Brien, J. E. Ladbury, S. M. Roe, P. W. Piper, and L. H. Pearl. The atpase cycle of hsp90 drives a molecular 'clamp' via transient dimerization of the n-terminal domains. *EMBO J*, 19(16):4383–92, 2000.

[181] C. Prodromou, G. Siligardi, R. O'Brien, D. N. Woolfson, L. Regan, B. Panaretou, J. E. Ladbury, P. W. Piper, and L. H. Pearl. Regulation of hsp90 atpase activity by tetratricopeptide repeat (tpr)-domain co-chaperones. *EMBO J*, 18(3):754–62, 1999.

[182] P. Reilich, B. Schoser, N. Schramm, S. Krause, J. Schessl, W. Kress, J. Muller-Hocker, M. C. Walter, and H. Lochmuller. The p.g154s mutation of the alpha-b crystallin gene (cryab) causes late-onset distal myopathy. *Neuromuscul Disord*, 20(4):255–9, 2010.

[183] M. Retzlaff, F. Hagn, L. Mitschke, M. Hessling, F. Gugel, H. Kessler, K. Richter, and J. Buchner. Asymmetric activation of the hsp90 dimer by its cochaperone aha1. *Mol Cell*, 37(3):344–54, 2010.

[184] K. Richter and J. Buchner. Hsp90: chaperoning signal transduction. *J Cell Physiol*, 188(3):281–90, 2001.

[185] K. Richter, M. Haslbeck, and J. Buchner. The heat shock response: life on the verge of death. *Mol Cell*, 40(2):253–66, 2010.

[186] K. Richter, J. Soroka, L. Skalniak, A. Leskovar, M. Hessling, J. Reinstein, and J. Buchner. Conserved conformational changes in the atpase cycle of human hsp90. *J Biol Chem*, 283(26):17757–65, 2008.

[187] A. Rohl, J. Rohrberg, and J. Buchner. The chaperone hsp90: changing partners for demanding clients. *Trends Biochem Sci*, 38(5):253–62, 2013.

[188] A. K. Rose, S. G. Shaw, M. A. Prendergast, and H. J. Little. The importance of glucocorticoids in alcohol dependence and neurotoxicity. *Alcohol Clin Exp Res*, 34(12):2011–8, 2010.

[189] A. M. Rossor, G. L. Davidson, J. Blake, J. M. Polke, S. M. Murphy, H. Houlden, A. Innes, B. Kalmar, L. Greensmith, and M. M. Reilly. A novel p.glu175x premature stop mutation in the c-terminal end of hsp27 is a cause of cmt2. *J Peripher Nerv Syst*, 17(2):201–5, 2012.

[190] R. H. Russnak and E. P. Candido. Locus encoding a family of small heat shock genes in caenorhabditis elegans: two genes duplicated to form a 3.8-kilobase inverted repeat. *Mol Cell Biol*, 5(6):1268–78, 1985.

[191] R. H. Russnak, D. Jones, and E. P. Candido. Cloning and analysis of cdna sequences coding for two 16 kilodalton heat shock proteins (hsps) in caenorhabditis elegans: homology with the small hsps of drosophila. *Nucleic Acids Res*, 11(10):3187–205, 1983.

[192] S. Sacconi, L. Feasson, J. C. Antoine, C. Pecheux, R. Bernard, A. M. Cobo, A. Casarin, L. Salviati, C. Desnuelle, and A. Urtizberea. A novel cryab mutation resulting in multisystemic disease. *Neuromuscul Disord*, 22(1):66–72, 2012.

[193] L. A. Safieh, A. O. Khan, and F. S. Alkuraya. Identification of a novel cryab mutation associated with autosomal recessive juvenile cataract in a saudi family. *Mol Vis*, 15:980–4, 2009.

[194] S. T. Santhiya, T. Soker, N. Klopp, T. Illig, M. V. Prakash, B. Selvaraj, P. M. Gopinath, and J. Graw. Identification of a novel, putative cataract-causing allele in cryaa (g98r) in an indian family. *Mol Vis*, 12:768–73, 2006.

[195] E. C. Schirmer, J. R. Glover, M. A. Singer, and S. Lindquist. Hsp100/clp proteins: a common mechanism explains diverse functions. *Trends Biochem Sci*, 21(8):289–96, 1996.

[196] F. Schmid. *Protein structure: A practical approach.*, volume 1. Oxford University Press, 1989.

[197] J. A. Schriefer. Diethylstilbesterol- and pregnancy-induced changes in rat neurointermediate lobe oxytocin, arginine vasopressin, methionine enkephalin and dynorphin. *Neuroendocrinology*, 54(3):185–91, 1991.

[198] P. Schuck. Size-distribution analysis of macromolecules by sedimentation velocity ultracentrifugation and lamm equation modeling. *Biophys J*, 78(3):1606–19, 2000.

[199] P. Schuck. Analytical ultracentrifugation as a tool for studying protein interactions. *Biophys Rev*, 5(2):159–171, 2013.

[200] P. Schuck, M. A. Perugini, N. R. Gonzales, G. J. Howlett, and D. Schubert. Size-distribution analysis of proteins by analytical ultracentrifugation: strategies and application to model systems. *Biophys J*, 82(2):1096–111, 2002.

[201] D. Selcen. Myofibrillar myopathies. *Neuromuscul Disord*, 21(3):161–71, 2011.

[202] D. Selcen and A. G. Engel. Myofibrillar myopathy caused by novel dominant negative alpha b-crystallin mutations. *Ann Neurol*, 54(6):804–10, 2003.

[203] J. Shim, S. H. Im, and J. Lee. Tissue-specific expression, heat inducibility, and biological roles of two hsp16 genes in caenorhabditis elegans. *FEBS Lett*, 537(1-3):139–45, 2003.

[204] T. P. Snutch and D. L. Baillie. Alterations in the pattern of gene expression following heat shock in the nematode caenorhabditis elegans. *Can J Biochem Cell Biol*, 61(6):480–7, 1983.

[205] N. Sreerama and R. W. Woody. Estimation of protein secondary structure from circular dichroism spectra: comparison of contin, selcon, and cdsstr methods with an expanded reference set. *Anal Biochem*, 287(2):252–60, 2000.

[206] P. A. Srere. Citrate-condensing enzyme-oxalacetate binary complex. studies on its physical and chemical properties. *J Biol Chem*, 241(9):2157–65, 1966.

[207] L. F. Stancato, Y. H. Chow, K. A. Hutchison, G. H. Perdew, R. Jove, and W. B. Pratt. Raf exists in a native heterocomplex with hsp90 and p50 that can be reconstituted in a cell-free system. *J Biol Chem*, 268(29):21711–6, 1993.

[208] G. J. Stege, G. C. Li, L. Li, H. H. Kampinga, and A. W. Konings. On the role of hsp72 in heat-induced intranuclear protein aggregation. *Int J Hyperthermia*, 10(5):659–74, 1994.

[209] T. Stromer, M. Ehrnsperger, M. Gaestel, and J. Buchner. Analysis of the interaction of small heat shock proteins with unfolding proteins. *J Biol Chem*, 278(20):18015–21, 2003.

[210] T. Stromer, E. Fischer, K. Richter, M. Haslbeck, and J. Buchner. Analysis of the regulation of the molecular chaperone hsp26 by temperature-induced dissociation: the n-terminal domail is important for oligomer assembly and the binding of unfolding proteins. *J Biol Chem*, 279(12):11222–8, 2004.

[211] J. Sulston. *Cell lineage*, chapter 5, pages 123–155. 1988.

[212] J. Sulston and H. Horvitz. Post-embryonic cell lineages of the nematode, caenorhabditis elegans. *Developmental Biology*, 56:110–156, 1977.

[213] J. E. Sulston, D. G. Albertson, and J. N. Thomson. The caenorhabditis elegans male: postembryonic development of nongonadal structures. *Dev Biol*, 78(2):542–76, 1980.

[214] T. X. Sun, B. K. Das, and J. J. Liang. Conformational and functional differences between recombinant human lens alphaa- and alphab-crystallin. *J Biol Chem*, 272(10):6220–5, 1997.

[215] W. Sun, X. Xiao, S. Li, X. Guo, and Q. Zhang. Mutation analysis of 12 genes in chinese families with congenital cataracts. *Mol Vis*, 17:2197–206, 2011.

[216] Y. Sun and T. H. MacRae. Small heat shock proteins: molecular structure and chaperone function. *Cell Mol Life Sci*, 62(21):2460–76, 2005.

[217] M. Taipale, D. F. Jarosz, and S. Lindquist. Hsp90 at the hub of protein homeostasis: emerging mechanistic insights. *Nat Rev Mol Cell Biol*, 11(7):515–28, 2010.

[218] M. Taipale, I. Krykbaeva, M. Koeva, C. Kayatekin, K. D. Westover, G. I. Karras, and S. Lindquist. Quantitative analysis of hsp90-client interactions reveals principles of substrate recognition. *Cell*, 150(5):987–1001, 2012.

[219] C. Tanford, r. Buckley, C. E., P. K. De, and E. P. Lively. Effect of ethylene glycol on the conformation of gama-globulin and beta-lactoglobulin. *J Biol Chem*, 237:1168–71, 1962.

[220] B. S. Tang, G. H. Zhao, W. Luo, K. Xia, F. Cai, Q. Pan, R. X. Zhang, F. F. Zhang, X. M. Liu, B. Chen, C. Zhang, L. Shen, H. Jiang, Z. G. Long, and H. P. Dai. Small heat-shock protein 22 mutated in autosomal dominant charcot-marie-tooth disease type 2l. *Hum Genet*, 116(3):222–4, 2005.

[221] R. P. Taylor and I. J. Benjamin. Small heat shock proteins: a new classification scheme in mammals. *J Mol Cell Cardiol*, 38(3):433–44, 2005.

[222] L. Timmons, D. L. Court, and A. Fire. Ingestion of bacterially expressed dsrnas can produce specific and potent genetic interference in caenorhabditis elegans. *Gene*, 263(1-2):103–12, 2001.

[223] M. K. Udvardi, T. Czechowski, and W. R. Scheible. Eleven golden rules of quantitative rt-pcr. *Plant Cell*, 20(7):1736–7, 2008.

[224] C. Urbanke, G. Witte, and U. Curth. Sedimentation velocity method in the analytical ultracentrifuge for the study of protein-protein interactions. *Methods Mol Biol*, 305:101–14, 2005.

[225] F. A. van de Klundert, R. H. Smulders, M. L. Gijsen, R. A. Lindner, R. Jaenicke, J. A. Carver, and W. W. de Jong. The mammalian small heat-shock protein hsp20 forms dimers and is a poor chaperone. *Eur J Biochem*, 258(3):1014–21, 1998.

[226] A. van der Straten, C. Rommel, B. Dickson, and E. Hafen. The heat shock protein 83 (hsp83) is required for raf-mediated signalling in drosophila. *EMBO J*, 16(8):1961–9, 1997.

[227] R. Van Montfort, C. Slingsby, and E. Vierling. Structure and function of the small heat shock protein/alpha-crystallin family of molecular chaperones. *Adv Protein Chem*, 59:105–56, 2001.

[228] R. Van Montfort, C. Slingsby, and E. Vierling. Structure and function of the small heat shock protein/alpha-crystallin family of molecular chaperones. *Adv Protein Chem*, 59:105–56, 2001.

[229] R. L. van Montfort, E. Basha, K. L. Friedrich, C. Slingsby, and E. Vierling. Crystal structure and assembly of a eukaryotic small heat shock protein. *Nat Struct Biol*, 8(12):1025–30, 2001.

[230] R. L. van Montfort, E. Basha, K. L. Friedrich, C. Slingsby, and E. Vierling. Crystal structure and assembly of a eukaryotic small heat shock protein. *Nat Struct Biol*, 8(12):1025–30, 2001.

[231] W. A. Van Voorhies. Production of sperm reduces nematode lifespan. *Nature*, 360(6403):456–8, 1992.

[232] J. Vandesompele, K. De Preter, F. Pattyn, B. Poppe, N. Van Roy, A. De Paepe, and F. Speleman. Accurate normalization of real-time quantitative rt-pcr data by geometric averaging of multiple internal control genes. *Genome Biol*, 3(7):RESEARCH0034, 2002.

[233] S. Vandevyver, L. Dejager, and C. Libert. On the trail of the glucocorticoid receptor: into the nucleus and back. *Traffic*, 13(3):364–74, 2012.

[234] S. Vandevyver, L. Dejager, J. Tuckermann, and C. Libert. New insights into the anti-inflammatory mechanisms of glucocorticoids: an emerging role for glucocorticoid-receptor-mediated transactivation. *Endocrinology*, 154(3):993–1007, 2013.

[235] C. K. Vaughan, U. Gohlke, F. Sobott, V. M. Good, M. M. Ali, C. Prodromou, C. V. Robinson, H. R. Saibil, and L. H. Pearl. Structure of an hsp90-cdc37-cdk4 complex. *Mol Cell*, 23(5):697–707, 2006.

[236] P. Vicart, A. Caron, P. Guicheney, Z. Li, M. C. Prevost, A. Faure, D. Chateau, F. Chapon, F. Tome, J. M. Dupret, D. Paulin, and M. Fardeau. A missense mutation in the alphab-crystallin chaperone gene causes a desmin-related myopathy. *Nat Genet*, 20(1):92–5, 1998.

[237] S. K. Wandinger, K. Richter, and J. Buchner. The hsp90 chaperone machinery. *J Biol Chem*, 283(27):18473–7, 2008.

[238] D. Wang, P. Liu, and X. Xing. Pre-treatment with mild uv irradiation increases the resistance of nematode caenorhabditis elegans to toxicity on locomotion behaviors from metal exposure. *Environ Toxicol Pharmacol*, 29(3):213–22, 2010.

[239] S. Ward and J. S. Carrel. Fertilization and sperm competition in the nematode caenorhabditis elegans. *Dev Biol*, 73(2):304–21, 1979.

[240] D. M. Weinfurtner. *Strukturelle und funktionelle Charakterisierung einer Familie kleiner Hitzeschockproteine*. PhD thesis, TUM, Faculty of Chemistry, 2008.

[241] S. Welker, B. Rudolph, E. Frenzel, F. Hagn, G. Liebisch, G. Schmitz, J. Scheuring, A. Kerth, A. Blume, S. Weinkauf, M. Haslbeck, H. Kessler, and J. Buchner. Hsp12 is an intrinsically unstructured stress protein that folds upon membrane association and modulates membrane function. *Mol Cell*, 39(4):507–20, 2010.

[242] D. B. Wetlaufer. Nucleation, rapid folding, and globular intrachain regions in proteins. *Proc Natl Acad Sci U S A*, 70(3):697–701, 1973.

[243] H. E. White, E. V. Orlova, S. Chen, L. Wang, A. Ignatiou, B. Gowen, T. Stromer, T. M. Franzmann, M. Haslbeck, J. Buchner, and H. R. Saibil. Multiple distinct assemblies reveal conformational flexibility in the small heat shock protein hsp26. *Structure*, 14(7):1197–204, 2006.

[244] J. White. *The Anatomy*, chapter 4, pages 81–122. 1988.

[245] L. Whitmore and B. A. Wallace. Dichroweb, an online server for protein secondary structure analyses from circular dichroism spectroscopic data. *Nucleic Acids Res*, 32(Web Server issue):W668–73, 2004.

[246] J. D. Willett, N. Podugu, G. Sudama, J. J. Kopecky, and J. Isbister. Applications of cold temperature stress to age fractionate caenorhabditis elegans: a simple inexpensive technique. *J Gerontol A Biol Sci Med Sci*, 65(5):457–67, 2010.

[247] J. H. Willis, E. Munro, R. Lyczak, and B. Bowerman. Conditional dominant mutations in the caenorhabditis elegans gene act-2 identify cytoplasmic and muscle roles for a redundant actin isoform. *Mol Biol Cell*, 17(3):1051–64, 2006.

[248] S. Witt. *Protein chaperones and protection from neurodegenerative diseases*. John Wiley & Sons, 2011.

[249] J. C. Young, W. M. Obermann, and F. U. Hartl. Specific binding of tetratricopeptide repeat proteins to the c-terminal 12-kda domain of hsp90. *J Biol Chem*, 273(29):18007–10, 1998.

[250] Y. Zhang, D. Chen, M. A. Smith, B. Zhang, and X. Pan. Selection of reliable reference genes in caenorhabditis elegans for analysis of nanotoxicity. *PLoS One*, 7(3):e31849, 2012.

[251] Y. L. Zhao and D. Y. Wang. Formation and regulation of adaptive response in nematode caenorhabditis elegans. *Oxid Med Cell Longev*, 2012:564093, 2012.

DANKSAGUNG

An erster Stelle möchte ich mich bei meinem Doktorvater Prof. Johannes Buchner für die Betreuung meiner Doktorarbeit bedanken. Durch produktives Feedback und viele Freiräume wurde mir die Möglichkeit gegeben, weitestgehend eigenständig mein Thema zu bearbeiten. Außerdem möchte ich mich bei Dr. Martin Haslbeck für sein ständig offenes Ohr und Hilfe während der gesamten Arbeit bedanken. Frau Hilber und Frau Rubinstein für die organisatorische Hilfe in Bezug auf alle bürokratischen Dinge.

Ich danke allen Doktoranden des Lehrstuhls für Biotechnologie, die mir während meiner Doktorarbeit durch viele reflektierende Gespräche, fachlichen Austausch und private Aktivitäten die Zeit unvergesslich gemacht haben. Besonders zu nennen sind Julia, Adrian, Alina, Vroni, Oli, Daniel, Christoph, Danae, Lars und Moritz. Außdem möchte ich mich noch bei meiner WG und den Chorfreunden Andi, Gitta, Thomas, Bernhard, Felix, Steffi und Matthias bedanken.

Schließlich möchte ich mich bei meiner Familie bedanken. Zuerst bei meinen Eltern, die mich immer in Allem unterstützen. Sie haben mir mein Studium ermöglicht und damit grundlegend zum Gelingen dieser Arbeit beigetragen. Bei meinen Schwestern, die beide auf sehr individuelle Weise zum Gelingen dieser Doktorarbeit beigetragen haben. Meinem Onkel Claus gilt ein grosses Dankeschön, da er immer viel Spaßhatte, mich an die Grenzen meines Wissens zu treiben. Dadurch konnte ich unglaublich viel lernen.

Und Nic, der mir immer den Rücken stärkt und vor allem in den stressigen Zeiten frei gehalten hat.

Vielen, vielen Dank an euch alle.

DECLARATION

I hereby declare that this thesis was performed and written on my own and that references and resources used within this work have been explicitly indicated. This work was not submitted to any other board of examiners. Parts of this work will be published in scientific journals.

Munich, 3rd September 2013

Maike Krause